Summer 2020

Magnetic control of transport of particles and droplets in low Reynolds number shear flows

Jie Zhang

MAGNETIC CONTROL OF TRANSPORT OF PARTICLES AND DROPLETS IN LOW REYNOLDS NUMBER SHEAR FLOWS

by

JIE ZHANG

A DISSERTATION

Presented to the Graduate Faculty of the

MISSOURI UNIVERSITY OF SCIENCE AND TECHNOLOGY

In Partial Fulfillment of the Requirements for the Degree

DOCTOR OF PHILOSOPHY

in

MECHANICAL ENGINEERING

2020

Approved by:

Cheng Wang, Advisor
K. M. Isaac
Kelly Homan
K. Chandrashekhara
Xiaoming He

PUBLICATION DISSERTATION OPTION

This dissertation consists of the following five articles which have been published as follows:

Paper I, found on pages 9-24 is a conference paper published in the proceedings of COMSOL conference 2017 Boston in Boston, Massachusetts.

Paper II, found on pages 25-53 have been published in Magnetochemistry.

Paper III, found on pages 54-89 have been published in Microfluidics and Nanofluidics.

Paper IV, found on pages 90-116 have been published in Journal of Micromechanics and Microengineering.

Paper IV, found on pages 117-138 have been published in Soft Matter.

ABSTRACT

Magnetic particles and droplets have been used in a wide range applications including biomedicine, biological analysis and chemical reaction. The manipulation of magnetic microparticles or microdroplets in microscale fluid environments is one of the most critical processes in the systems and platforms based on microfluidic technology. The conventional methods are based on magnetic forces to manipulate magnetic particles or droplets in a viscous fluid.

In contrast to conventional magnetic separation method, several recent experimental and theoretical studies have demonstrated a different way to manipulate magnetic non-spherical particles by using a uniform magnetic field in the microchannel. However, the fundamental mechanism behind this method is not fully understood. In this research, we aims to use numerical and experimental methods to explore and investigate manipulation of microparticles and microdroplets in the microfluidics by using a uniform magnetic field. In the first part, rotational dynamics of elliptical particles in a simple shear flow is numerically investigated; then, lateral migration of elliptical particles in a plane Poiseuille flow is numerically investigated; The third part compares the rotational dynamics of paramagnetic and ferromagnetic elliptical particles particles in a simple shear flow; in the fourth part, particle-particle interactions and relative motions of a pair of magnetic elliptical particles in a quiescent flow are numerically investigated; magnetic separation of magnetic microdroplets by the uniform magnetic field is proposed in the fifth part.

The methods demonstrated in this research not only develop numerical and experimental way to understand the fundamental transport properties of magnetic particles and droplets in microscale fluid environments, but also provide a simple and efficient method for the separation of microdroplets in microfluidic device, which can impact biomedical and bio-medicine technologies.

ACKNOWLEDGMENTS

I would like to express my sincere gratitude to my advisor, Dr. Cheng Wang, for his insightful guidance and patience during my graduate study at Missouri University of Science and Technology. He is always open to meet when I need to have a discussion with him. His professional and diligent attitude to do research makes me not only a better researcher but also a better person. Furthermore, I gratefully acknowledges the Department of Mechanical and Aerospace Engineering at Missouri University of Science and Technology for providing financial support during my graduate study.

I would also like to express my thanks to all my dissertation committee members, Dr. K. M. Isaac, Dr. Kelly Homan, Dr. K. Chandrashekhara, and Dr. Xiaoming He. They gave me valuable suggestions and comments, which was very helpful for me to complete this dissertation.

I am very thankful to my research group members, Dr. Ran Zhou, Mr. Christopher Sobecki, and Mr. Md. Rifat Hassan for their support in life and insightful discussions in research. I would also like to thank my friends, Mr. Junji Huang, Dr. Chao Zhang, Mr. Wenyu Liao, and Dr. Wei Wang for their support and help during my study in Rolla.

Ultimately, I would like to express special thanks to my parents for their love, understanding, supports and encouragement during my study in the United States.

TABLE OF CONTENTS

Page

LIST OF ILLUSTRATIONS

LIST OF TABLES

SECTION

1. INTRODUCTION

Magnetic particles have been used in a vast number of applications including biomedicine (Pankhurst *et al.*, 2003), biological analysis, and chemical catalysis (Gijs *et al.*, 2009; Pamme, 2012). The separation of magnetic microparticles and nanoparticles in microscale fluid environments is one of the most important processes in the systems and platforms based on microfluidic technology (Pamme, 2006, 2012). A magnetic field is a powerful tool to separate magnetic particles or magnetically labelled cells, antigens, and enzymes (Gijs, 2004; Pamme, 2006; Suwa and Watarai, 2011). Most magnetic separation methods are based on magnetophoresis, which manipulates magnetic particles in a viscous fluid by using magnetic forces. To generate the magnetic force, it requires both magnetic particles and a spatially non-uniform field (magnetic field gradient) (Pamme, 2006). There are two different types of magnetophoresis: one is called negative magnetophoresis – manipulating diamagnetic particles in a magnetic fluid such as ferrofluids (Bucak *et al.*, 2011; Winkleman *et al.*, 2007; Zhou *et al.*, 2016; Zhou and Xuan, 2016); the other one is called positive magnetophoresis – separating paramagnetic or ferromagnetic particles in a non-magnetic fluid such as water (Chen *et al.*, 2015; Zborowski *et al.*, 1999).

In contrast to conventional magnetophoresis, several recent experimental and theoretical studies (Matsunaga *et al.*, 2017a,b; Zhou *et al.*, 2017a,b) have demonstrated a different way to manipulate magnetic non-spherical particles by a uniform magnetic field in the microchannel. The uniform magnetic field does not generate a magnetic force, but instead generates non-zero magnetic torques due to the non-spherical particle shape. When coupled with particle-wall hydrodynamic interaction (Gavze and Shapiro, 1997; Leal, 1980), the uniform magnetic field alters the rotational dynamics of non-spherical particles, and

consequently controls the lateral migration of particles. Experiments preformed by Zhou et al. (Zhou *et al.*, 2017a,b) have demonstrated that a weak uniform magnetic field can separate paramagnetic particles in a microchannel pressure-driven flow. The magnetic torque broke the symmetry of the particle rotation. Due to the particle-wall hydrodynamic interaction, the particles migrated laterally towards or away from the wall depending on the direction of magnetic field. Matsunaga et al. (Matsunaga *et al.*, 2017a,b) proposed a far-field theory and used the boundary element method to demonstrate that a strong uniform magnetic field can separate the ferromagnetic particles in both simple shear flow near the wall and Poiseuille flow between two walls. In this method, ferromagnetic particles are pinned at steady angles and the lateral migration results from particle-wall hydrodynamic interactions as well.

Due to its importance to science and engineering, the dynamics of non-spherical particles in flows have been a subject of extensive theoretical, numerical and experimental investigations. For example, the pioneering work includes Jeffery's theory (Jeffery, 1922) and experimental studies by Mason's group (Goldsmith and Mason, 1961; Trevelyan and Mason, 1951). With the advancement of computing capabilities, numerical simulations have been increasingly employed to study the motion of both spherical and non-spherical particles in a variety of shear flows, including plane Couette and Poiseuille flows. Feng et al. (Feng *et al.*, 1994) reported a direction numerical simulation (DNS) based on the finite element method (FEM) to study the lateral migration of the neutrally and non-neutrally buoyant circular particle in plane Couette and Poiseuille flows. The simulation results agree qualitatively with the results of perturbation theories and experimental data. Gavze and Shapiro (Gavze and Shapiro, 1997) used a boundary integral equation method to investigate the effect of particle shape on forces and velocities acting on the particle near the wall in a shear flow. Pan's group proposed a distributed Lagrange-multiplier-based fictitious domain method (DLM) to investigate the motion of multiple neutrally buoyant circular cylinders and elliptical cylinders in shear flow (Huang *et al.*, 2015; Pan *et al.*, 2013) and plane Poiseuille flow (Chen *et al.*, 2012; Pan and Glowinski, 2002). Yang et al. (Yang

et al., 2005) reported two methods, the arbitrary Lagrangian-Eulerian (ALE) method and the distributed Lagrange-multiplier-based fictitious domain method (DLM), to study the migration of a single neutrally buoyant rigid sphere in tube Poiseuille flow. Ai et al. (Ai *et al.*, 2009b) investigated some key factors on pressure-driven transport of particles in a symmetric converging-diverging microchannel by the ALE finite-element method. Lee et al. (Lee *et al.*, 2009a,b) used the same method as Gavze and Shapiro (Gavze and Shapiro, 1997) to study the particle transport behaviour with different size, shape and material properties in the plane Couette flow.

In addition to a single magnetic particle, high density magnetic microparticles or nanoparticles immersed in non-magnetic fluid tend to form chains, clusters or columns under an external magnetic field. The suspension consisting of high density magnetic microparticles or nanoparticles is called as magnetorheological fluids (MRFs) (De Vicente *et al.*, 2011). The MRFs are smart materials which show various rheological properties, such as yield stress and apparent viscosity. The values of these rheological properties are increased to several orders of magnitude under the appropriately applied magnetic field. Due to their remarkable properties and the quick response to the magnetic field, MRFs are the good candidates for a vast number of industrial and medical applications, such as magnetorheological rotor damper, brakes, clutches, valves and cancer therapeutic (Bica *et al.*, 2013; Rabinow, 1948; Sheng *et al.*, 1999). Recently, the experimental (Anupama *et al.*, 2018; Bell *et al.*, 2008, 2007; Bombard *et al.*, 2014; de Vicente *et al.*, 2010; Dong *et al.*, 2015; Jiang *et al.*, 2011; López-López *et al.*, 2009, 2007; Morillas *et al.*, 2015; Ngatu *et al.*, 2008; Sedlacik *et al.*, 2013) and theoretical (Bossis *et al.*, 2015; De Vicente *et al.*, 2009; Kuzhir *et al.*, 2009) investigations reported that the MRFs with non-spherical particles have stronger magnetorheological properties and better sedimentation stability compared to those with spherical particles.

Furthermore, droplet microfluidics has emerged as a powerful technology on a lab-on-a-chip platform for high-throughput screening of chemical and biological assays (Du *et al.*, 2016; Guo *et al.*, 2012; Shembekar *et al.*, 2016). Dispersed in a continuous phase, individual droplets often encapsulate chemical or biological samples (e.g., cells, DNA, proteins, and bacteria), serve as miniaturized reactors, and allow biological and chemical reactions inside individual micro-droplets (Shang *et al.*, 2017). The large surface to volume ratio leads to significantly enhanced mass and heat transfer and bio-/chemical reactions. Moreover, the high-throughput nature enables a vast number of assays in parallel, thereby drastically improving accuracy of the results. Manipulation, e.g., sorting, of the droplets based on their contents or properties is a often a critical step in the chemical or biological assay. Droplets can be sorted by passive or active methods. Passive methods are based on hydrodynamic features, such as geometry and fluid properties, to manipulation the droplets (Bowman *et al.*, 2012; Hatch *et al.*, 2013; Kadivar *et al.*, 2013; Tan *et al.*, 2004, 2008; Tan and Lee, 2005). For passive methods to be effective, a complex geometry is usually employed or a particular fluid such as viscoelastic fluid is used as a buffer, which places some limitations on lab-on-a-chip applications. Active methods employ external fields (Xi *et al.*, 2017), such as electric (Agresti *et al.*, 2010; Ahn *et al.*, 2009, 2011, 2006; de Ruiter *et al.*, 2014; Eastburn *et al.*, 2015; Guo *et al.*, 2010; Link *et al.*, 2006; Niu *et al.*, 2007; Rao *et al.*, 2015a,b; Sciambi and Abate, 2014, 2015), acoustic (Lee *et al.*, 2012; Leibacher *et al.*, 2015; Li *et al.*, 2013; Nam *et al.*, 2012; Petersson *et al.*, 2005; Schmid *et al.*, 2014), or magnetic forces (Brouzes *et al.*, 2015; Kim *et al.*, 2014; Li *et al.*, 2016; Lombardi and Dittrich, 2011; Nguyen *et al.*, 2006; Surenjav *et al.*, 2009; Teste *et al.*, 2015; Zhang *et al.*, 2011, 2009), to manipulate droplets. Among the various active methods, magnetic methods have several distinctive advantages such as low or no heat generation, simple implementation and contactless control, and thus, have received increasing attention over the last few years (Huang *et al.*, 2017).

The objective of this doctoral research is to explore and investigate manipulation of microparticles and microdroplets in the microfluidics by using a uniform magnetic field. This approach will have many advantages over the traditional force-based techniques, including simple implementation, feasibility of scaling up, and large reach distance. Specifically, I develop direct numerical models and use experiments to understand the fundamental transport properties of particles and droplets, thus enabling novel applications, e.g., efficient magnetic separation methods, which can impact biomedical and bio-medicine technologies.

2. ORGANIZATION OF DISSERTATION

In this study, many technical developments have been achieved. Due to the page limit, only five major developments are presented in this dissertation. The first four papers are based on numerical simulations to investigate dynamics of magnetic microparticles, while the fifth paper is based on experimental method to study lateral migration of magnetic microdroplets. Specifically, Paper I focuses on rotational dynamics of elliptical particles in a simple shear flow. Paper II studies lateral migration of elliptical particles in a plane Poiseuille flow. Paper III compares translational and rotational dynamics of paramagnetic and ferromagnetic elliptical particles in both simple shear and pressure-driven flows. Paper IV investigates particle-particle interactions and relative motions of a pair of magnetic elliptical particles in a quiescent flow. Paper V proposes a novel method to magnetically separate magnetic droplets from non-magnetic droplets by using a uniform magnetic field.

All five papers share a same research topic: manipulation of microparticles and microdroplets by using a uniform magnetic field, while each of them has a different focus.

Paper I presents direct numerical simulation to investigate the rotational dynamics of elliptical particles in a simple shear flow under the uniform magnetic field. The present of magnetic field breaks the symmetry of particle rotation and alters the period of rotation. The effects of direction and strength of magnetic field, and aspect ratio of particle on particle rotation are numerically investigated.

Based on findings in Paper I, the lateral migration of elliptical paramagnetic particles in a plane Poiseuille flow is investigated in Paper II. The particle shown to exhibit negligible lateral migration in the absence of a magnetic field. When the magnetic field is applied, the particle migrates laterally. The effects of direction and strength of magnetic field on the direction and velocity of particle lateral migration are numerically studied. By investigating a wide range of parameters, our direct numerical simulations yield a comprehensive

understanding of the particle migration mechanism. An empirical scaling relationship is proposed to relate the lateral migration distance to the asymmetry of the rotational velocity and lateral oscillation amplitude.

Paper III compares the rotational dynamics of paramagnetic and ferromagnetic elliptical particles in a simple shear flow. The results shown that paramagnetic and ferromagnetic particles exhibit markedly different rotational dynamics under a uniform magnetic field, which are in good agree with theoretical predication. The numerical investigation further reveals drastically different lateral migration behaviors of paramagnetic and ferromagnetic particles in a wall bounded simple shear flow under a uniform magnetic field. These two kinds of particles can thus be separated by combining a shear flow and a uniform magnetic field. We also study the lateral migration of paramagnetic and ferromagnetic particles in a pressure-driven flow (a more practical flow configuration in microfluidics), and observe similar lateral migration behaviors. These findings demonstrate a simple but useful way to manipulate non-spherical microparticles in microfluidic devices.

To understand the fundamental mechanism of particle-particle interactions of a pair of magnetic non-spherical particles, Paper IV proposes a fluid-structure interaction model with a full consideration of particle-fluid-magnetic field interaction. The results show that the particles spend much more time for the global reorientation than for the local magneto-orientation. The effects of initial particle position and aspect ratio on relative motion of particles are numerically investigated. The particle-particle interactions and relative motions of a pair of elliptical particles in this study provide insights on the particle alignment and chaining processes under uniform magnetic fields, which are closely related to the response of magneto-rheological fluids to magnetic fields.

In addition to numerical works, a simple and effective mechanism that can achieve the separation of magnetic droplets in microfluidic flow under a uniform magnetic field is demonstrated. In this method, the combination of the uniform magnetic field and the

pressure-driven flow in a microchannel lends to the lateral migration of magnetic droplets. Using high-speed imaging and numerical methods, the effects of magnetic field strength and direction, and interfacial tension on the lateral migration of droplets are investigated.

PAPER

I. STUDY OF ROTATION OF ELLIPSOIDAL PARTICLES IN COMBINED SIMPLE SHEAR FLOW AND MAGNETIC FIELDS

Jie Zhang, Cheng Wang

Department of Mechanical & Aerospace Engineering

Missouri University of Science and Technology

Rolla, Missouri 65409

Tel: 573–341–4636, Fax: 573–341–4607

Email: wancheng@mst.edu

ABSTRACT

Jeffery's theory describes the periodic rotation of ellipsoidal particles in a simple shear flow at vanishing Reynolds number limit. In this paper, we present direct numerical simulations, implemented by using the arbitrary Lagrangian-Eulerian (ALE) method, to study the motion of ellipsoidal paramagnetic particles in a simple shear flow subjected to a uniform magnetic field. We investigated the effect of several parameters, including magnetic field strength, direction of magnetic field, and particle aspect ratio, on rotation period and asymmetry of particle rotation. Without a magnetic field, the simulation results are in good agreement with Jeffery's theory. When a magnetic field is applied perpendicular to the flow direction, the rotational period became longer, and the magnetic field breaks the symmetry of rotational motion of the ellipsoidal particle. As the magnetic field strength increases

to a large enough value, the particle could not perform a complete rotation and reaches a steady angle. With other different directions of the magnetic field, the period of rotation and asymmetry of the angular dynamics is also modified.

Keywords: microfluidics; magnetic field; microparticle; Jeffory orbits

1. INTRODUCTION

Non-spherical microparticles are widely encountered in industrial, environmental and biological fluids: for example wood fibers in the paper-making industry (Alava and Niskanen, 2006), suspensions in complex fluids (Larson, 1999), and various micron-sized biological objects (Young, 2006). In biology and bioengineering, shape is one of the most important physical attributes of biological relevant particles (Mitragotri and Lahann, 2009; Young, 2006). It plays an important role in various applications of biomedicine and biology, such as diagnosis of diseases (Anstey *et al.*, 2009), drug delivery (Champion *et al.*, 2007) and cell synchronization (Valero *et al.*, 2011). Because biological particles are often suspended in fluid environments, it is critical to understand the fundamental transport behaviors of non-spherical particles suspended in fluids. Over the last few decades there have been comprehensive theoretical and experimental investigations about the motion of ellipsoidal particle in a simple shear flow (Jeffery, 1922; Leal, 1980; Saffman, 1956; Taylor, 1923).

Jeffery firstly studies the motion of ellipsoidal particle immersed in a simple shear viscous flow (Jeffery, 1922). The periodic motion of particle is so called Jeffery orbits. The rotation period of a prolate spheroid with an aspect ratio AR (major semi-axis length/minor semi-axis length) in a simple shear flow $\mathbf{U} = (\dot{\gamma}y, 0, 0)$ is given by

$$T = \frac{2\pi}{\dot{\gamma}(AR + 1/AR)}.$$

The angle between the particle's major axis and the z-axis, θ, and the angle between the y-axis and xy-projection of the particle axis, ϕ, are shown in Figure 1, which are given by

$$tan\theta = \frac{C \cdot AR}{\sqrt{AR^2 cos^2\phi + sin^2\phi}},$$

$$tan\phi = ARtan(2\pi\frac{t}{T}),$$

where C is the orbit constant determined by the initial orientation of the particle. For $C = \infty$ ($\theta = 90°$), the particle just rotates in xy-plane, which means that ϕ only depends on the particle aspect ratio and the flow shear rate.

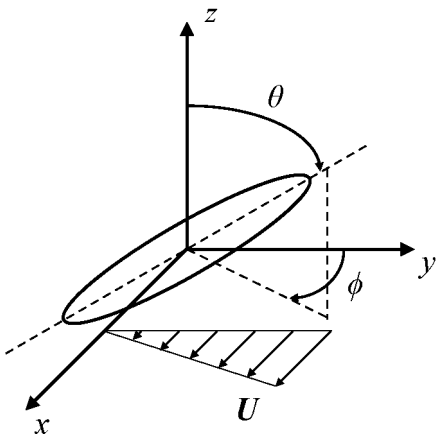

Figure 1. Schematic of an ellipsoidal particle in a simple shear flow.

In this paper, a 2D fluid-structure interaction (FSI) model is created to study the effect of magnetic field and particle aspect ratio on the period of rotation and symmetry of ellipsoidal paramagnetic particles. The paper is organized as follows. In Section 2, the simulation method, including mathematical model, COMSOL setting and material properties, is presented. In Section 3, we first compare the rotational period obtained from the simulation to Jeffery's theory. Then we present the results and discussion about the effect of the strength and direction of magnetic field and particle aspect ratio on particle. In Section 4, the main conclusions of this study are summarized.

2. SIMULATION METHOD

2.1. MATHEMATICAL MODEL

We consider an ellipsoidal particle immersed in a simple shear viscous flow in a Newtonian fluid with density ρ_f and dynamic viscosity η_f as shown in Figure 2. The center of the particle, coinciding with the origin of Cartesian coordinate system, is located in the center of a square computational domain. The particle aspect ratio is $AR = a/b$, where a and b are the major and minor semi-axis lengths of particles, respectively. The length of the computational domain is L. The rotation angle of particle is defined as ϕ between the major axis of the particle and y axis. The shear flow is $u = \dot{\gamma} y$, where $\dot{\gamma}$ is the shear rate of flow. A uniform magnetic field, $\mathbf{H_0}$, is imposed at an arbitrary direction, denoted by α.

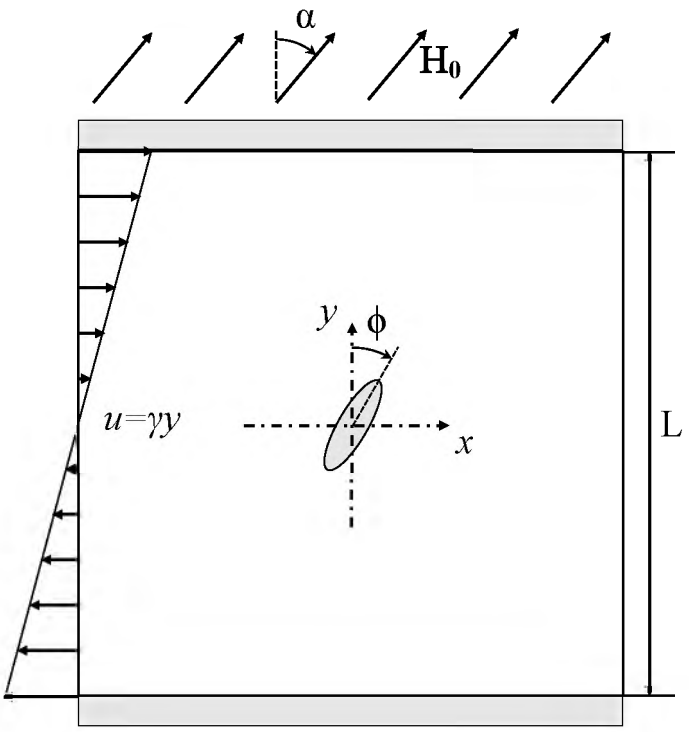

Figure 2. An ellipsoidal particle suspended in a simple shear flow and under a magnetic field $\mathbf{H_0}$, which is directed at an angle α.

The Jeffery orbits are obtained with the assumption of Stokes flow, i.e., zero Reynolds number and no fluid inertia. Therefore, the flow field, $\boldsymbol{u}$, is governed by the continuity equation and Stokes equation:

$$\nabla \cdot \boldsymbol{u} = 0; \tag{1}$$

$$\rho_p \frac{\partial \boldsymbol{u}}{\partial t} = \nabla \cdot [-p\boldsymbol{I} + \eta_f(\nabla \boldsymbol{u} + (\nabla \boldsymbol{u})^T)], \tag{2}$$

where p is the pressure. To have a simple shear flow, the velocities of top and bottom walls are set to have the same magnitude but opposite directions. The periodic flow conditions are set to the left and right boundaries of the computational domain. No-slip condition is set on the particle surface, so the fluid velocities on the particle surface are given as:

$$\boldsymbol{u} = \boldsymbol{U_p} + \boldsymbol{\omega_p} \times (\boldsymbol{x_s} - \boldsymbol{x_p}), \tag{3}$$

where $\boldsymbol{U_p}$ and $\boldsymbol{\omega_p}$ are the translational and rotational velocities of particle, respectively. $\boldsymbol{x_s}$ and $\boldsymbol{x_p}$ are the position vectors of the surface and the center of the particle. The hydrodynamic force and torque acting on the particle are expressed as:

$$\boldsymbol{F}_H = \int (\boldsymbol{\tau}_H \cdot \boldsymbol{n}) dS, \tag{4}$$

$$\boldsymbol{T}_H = \int [\boldsymbol{\tau}_H \times (\boldsymbol{x_s} - \boldsymbol{x_p}) \cdot \boldsymbol{n}] dS, \tag{5}$$

where

$$\boldsymbol{\tau}_H = -p\boldsymbol{I} + \eta_f(\nabla \boldsymbol{u} + (\nabla \boldsymbol{u})^T)$$

is the hydrodynamic stress tensor on the surface of particle.

The governing equations of the uniform magnetic field are given as:

$$\boldsymbol{H} = -\nabla V_m, \tag{6}$$

$$\nabla \cdot \boldsymbol{H} = 0, \tag{7}$$

where V_m is the magnetic potential. The magnetic potential difference to generate the magnetic field is set on the top and bottom wall. Magnetic insulation boundary condition is applied on the left and the right boundaries of the computational domain. Since the magnetic field is uniform, the force acting on the particle is zero. The magnetic torque acting on particle is expressed as:

$$\mathbf{T}_m = \mu_0 V_p \chi_p \mathbf{H}^- \times \mathbf{H}, \tag{8}$$

where $\mathbf{H}^-$ and $\mathbf{H}$ are the magnetic fields inside and outside the particle, respectively, χ_p is the magnetic susceptibility of the particle, μ_0 is the magnetic permeability of the vacuum, and V_p is the volume of particle. The translation and rotation of particle are governed by Newton's second law and Euler's equation:

$$m_p \frac{d\mathbf{U}_p}{dt} = \mathbf{F}_h, \tag{9}$$

$$I_p \frac{d\omega_p}{dt} = \mathbf{T}_h + \mathbf{T}_m, \tag{10}$$

where m_p and I_p are the mass and the moment of inertia of the particle. The angular velocity of particle $\boldsymbol{\omega_p} = \boldsymbol{\omega_h} + \boldsymbol{\omega_m}$ is the angular velocity produced by hydrodynamic torque and $\boldsymbol{\omega_m}$ is the angular velocity produced by magnetic torque. At each time step, the position of center $\mathbf{C}_p(t) = (X_p, Y_p)$ and orientation $\phi_p(t) = \phi(t)$ of the particle are expressed as:

$$\boldsymbol{C}_p(t) = \boldsymbol{C}_p(0) + \int_0^t \boldsymbol{U}_p(s) ds, \tag{11}$$

$$\phi_p(t) = \phi_p(0) + \int_0^t \omega_p(s) ds, \tag{12}$$

where $\boldsymbol{C}_p(0)$ and $\phi_p(0)$ are the initial position and orientation of the particle.

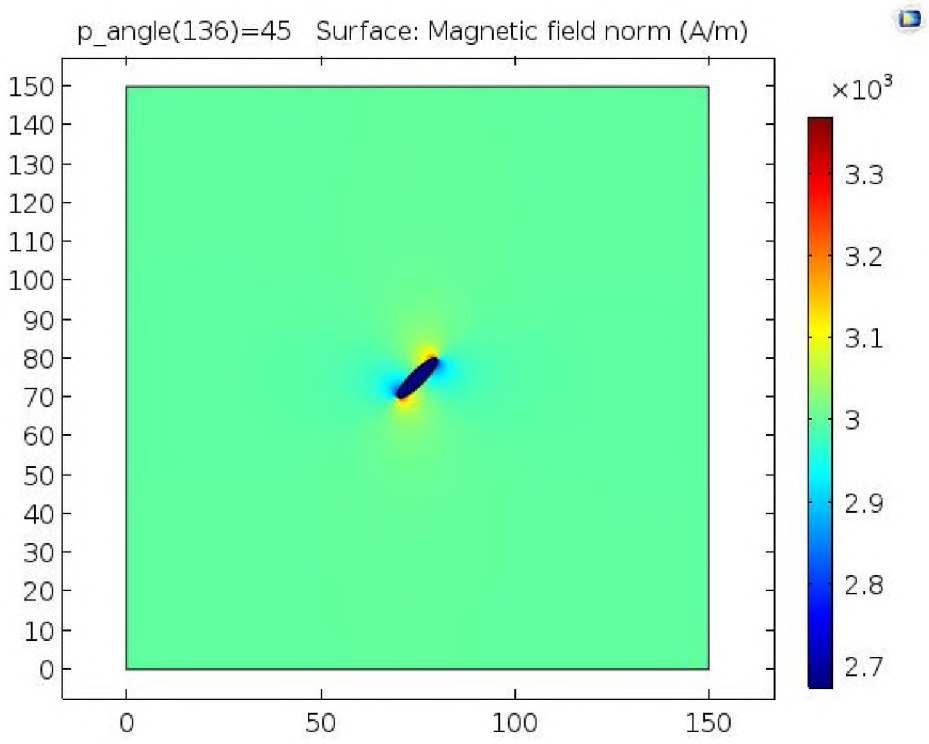

Figure 3. Magnetic field around the particle under the uniform magnetic field of H_0 = 3000 A/m at ϕ = 45°.

2.2. COMOL SETTINGS

To calculate the magnetic torque acting on the particle, the magnetic field around the ellipsoidal particle is first computed by the AC/DC module in COMSOL Multiphysics software. Figure 3 shows the magnetic field around the particle in the computational domain under the magnetic field of H_0 = 3000 A/m, directed at α = 0°. Stationary Solver with Parametric Sweep analysis are used to calculate the magnetic field inside and outside of the particle at different rotation angle ϕ. Due to the symmetry of ellipsoidal particle, the simulation was conducted at ϕ from -90° to 90° with an angle step of 1°.

Creeping Flow component is used to compute the flow field around the ellipsoidal particle. The top and bottom walls are set as moving wall condition with velocities at 1.5 mm/s and -1.5 mm/s respectively. Hence, the corresponding shear rate is 200 s^{-1}. The

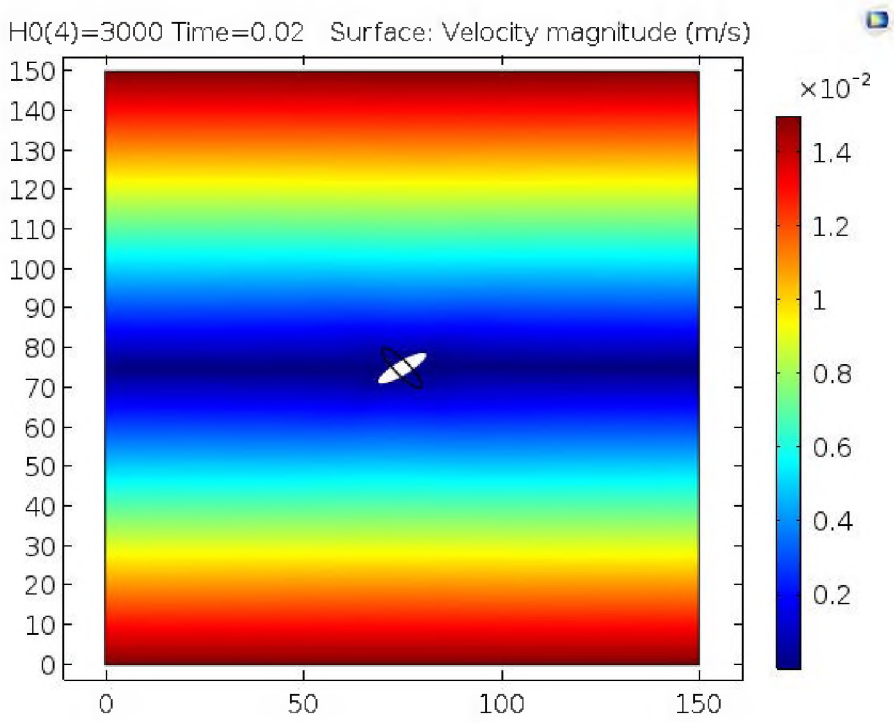

Figure 4. Velocity field in a simple shear flow at a shear rate of $\dot{\gamma} = 200s^{-1}$.

left and right boundaries are set as periodic flow conditions with zero pressure difference. No-slip boundary condition is set on the surface of particle, so the particle wall is set as a moving wall with fluid velocity of u as defined in Equation 3.

The translational and rotational motion of the particle is determined by solving ordinary differential equations (ODEs) in Global ODEs and DAEs component. Equation 9-12 are used in Global Equations to calculate translational and rotational velocities, and the position and orientation of the particle at each time step.

Moving Mesh component is used to describe the deforming mesh at the particle-fluid boundaries. Automatic Remeshing is enabled to re-initialize the mesh when the mesh quality below a threshold value, in this case, 0.2.

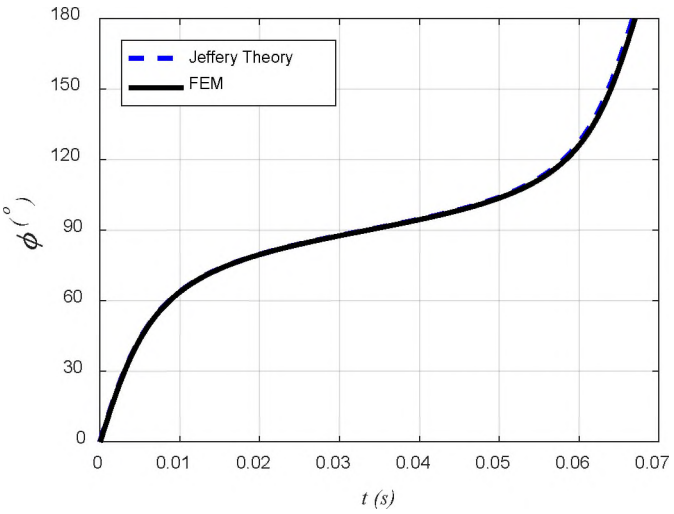

Figure 5. Comparison of the period between Jeffery's theory and the FEM simulation.

2.3. MATERIAL PROPERTIES

In this study, the fluid and particles in the simulations are water and polystyrene particles respectively. The density and dynamic viscosity of water are 1000 kg/m^3 and 1.002×10^{-3} Pa·s respectively. The magnetic susceptibilities of fluid and particle are 0 and 0.26 respectively. The density of particle is 1100 kg/m^3. The particles used in the simulation have varying aspect ratios, but have the same volume, which is equivalent to a 7 μm-diameter sphere.

3. RESULTS AND DISCUSSION

3.1. VALIDATION OF NUMERICAL METHOD

We first compare the results of our simulation to Jeffery's theory. Figure 5 shows the period of rotation of Jeffery's theory and our simulation for particle aspect ratio AR = 4 without an applied magnetic field. The theoretical period of Jeffery orbit is 0.06675 s; the period in this simulation is 0.0670 s. The relative error is 0.37%, suggesting that

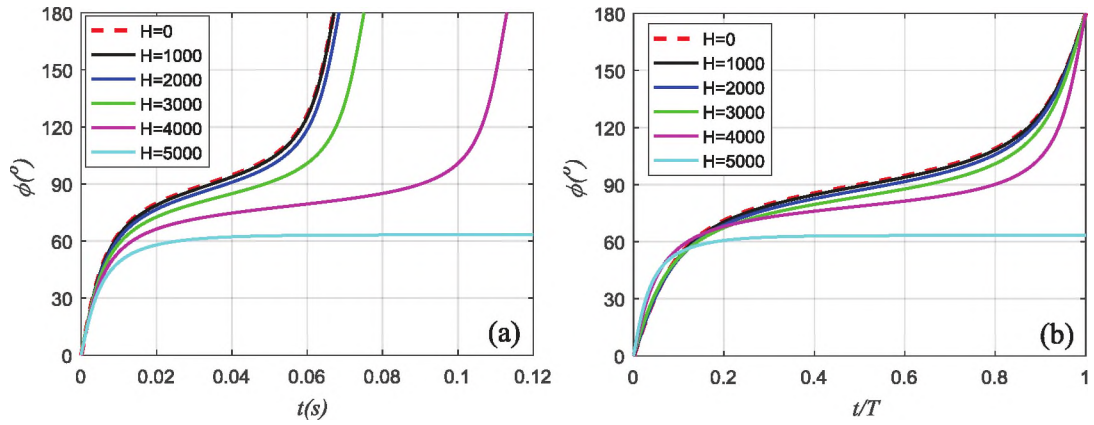

Figure 6. The effect of magnetic field strength H_0 (A/m) on the rotation period and asymmetry of the particle rotation. The magnetic field is applied at angle strength ($\alpha = 0°$).

this simulation has a remarkable agreement with the theory. Therefore, this simulation method has been validated to be sufficiently accurate to study the periodic rotation of particle immersed in the simple shear flow.

3.2. THE EFFECT OF MAGNETIC FIELD STRENGTH

In this section, we investigate the effect of magnetic field strength on the period and asymmetry of rotation of particle for aspect ratio $AR = 4$. Figure 6a shows that the angle of rotation, ϕ, corresponding to rotation time, t, with different magnetic field strength at the direction $\alpha = 0°$. It is shown that the rotation period increases with increasing magnetic field strength. Interestingly, as the magnetic field strength increases to a large enough value, the particle could not perform a complete rotation and reaches a steady angle. In this case, when the magnetic field strength is 5000 A/m, the rotation angle stays at 63.28°. Figure 6b shows that that the angle of rotation, ϕ, corresponding to the dimensionless rotation time, t/T, with different magnetic field strength at the direction $\alpha = 0°$, where T is the rotation period obtained in Figure 6a. We defined a ratio parameter $\tau = T_1/T$ to characterize the symmetry and asymmetry of particle rotation as shown in Figure 6b, where T_1 is the time the particle rotating from $\phi = 0°$ to $\phi = 90°$. So the time the particle rotation from $\phi = 90°$

to $\phi = 180°, T_2 = T - T_1$. When magnetic field strength is 0 A/m, the curve is axisymmetric to (t/T, ϕ) = (0.5, 90°), where $\tau = 0.5$. It is consistent with Jeffery's theory. However, when magnetic field strength is 1000 A/m, the symmetry is broken, and $\tau > 0.5$. As the magnetic field strength increases, τ become larger and larger, which means the asymmetry of rotation becomes more pronounced.

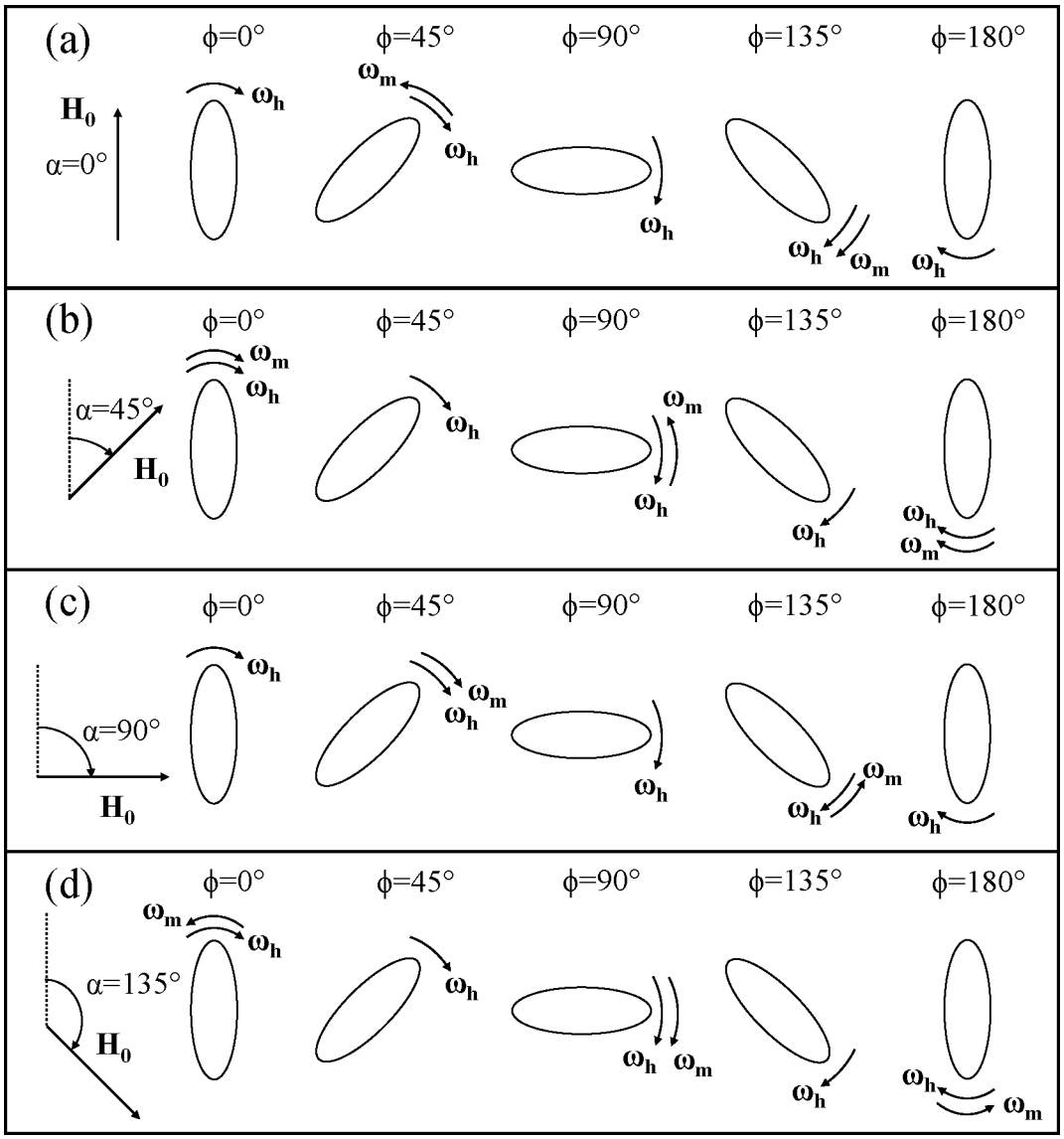

Figure 7. Illustration of particle rotation in the combined flow and magnetic fields.

The rotation behavior of the particle during one period in the combined flow and magnetic fields at $\alpha = 0°$ is illustrated in Figure 7a. Without the magnetic field applied, only the hydrodynamic torque acts on the particle and rotates in the clockwise direction. When the magnetic field is applied at $\alpha = 0°$, the angular velocity produced by magnetic torque, ω_m, rotates in counterclockwise direction from $\phi = 0°$ to $\phi = 90°$, which is the opposite to the angular velocity produced by hydrodynamic torque, ω_h; while ω_m rotates in clockwise direction from $\phi = 90°$ to $\phi = 180°$, which is the same as ω_h. Therefore, the particle will rotate slower, and spend more time from $\phi = 0°$ to $\phi = 90°$, while less time from $\phi = 90°$ to $\phi = 180°$, that is, $T_1 > T_2$. That is the reason why $\tau > 0.5$ when a magnetic field is applied. The larger the magnetic field strength, the larger τ. When the magnetic field strength increases to a large enough value, ω_m will be equal to ω_h in a certain angle between $\phi = 0°$ and $\phi = 90°$ and the particle will stop rotating. For magnetic field directed at other directions, the effect is illustrated in Figure 7b-d, and will be discussed further in the next section.

3.3. THE EFFECT OF THE DIRECTION OF MAGNETIC FIELD

In this section, the effect of the direction of magnetic field on the period and asymmetry of rotation of particle for aspect ratio $AR = 4$ is investigated. Figure 8a shows that the angle of rotation corresponding to rotation time with different direction of magnetic field at strength $H_0 = 2000$ A/m. The results show that the period of rotation at $\alpha = 45°$ become longer than the period at $\alpha = 0°$, while the period of rotation at $\alpha = 135°$ become shorter than the period at $\alpha = 0°$. The periods of rotation are almost the same at $\alpha = 90°$ and $\alpha = 0°$. The angle of rotation corresponding to the dimensionless time with different direction of magnetic field at strength $H_0 = 2000$ A/m is shown in Figure 8b. As we can see, $\tau > 0.5$ when $\alpha = 0°$, while $\tau < 0.5$ when $\alpha = 90°$. $\tau = 0.5$ when $\alpha = 45°$ and $135°$. The rotation behaviors of one period in the combined flow and magnetic fields at the different direction are shown in Figure 7. As we discussed before, the particle spend more time from

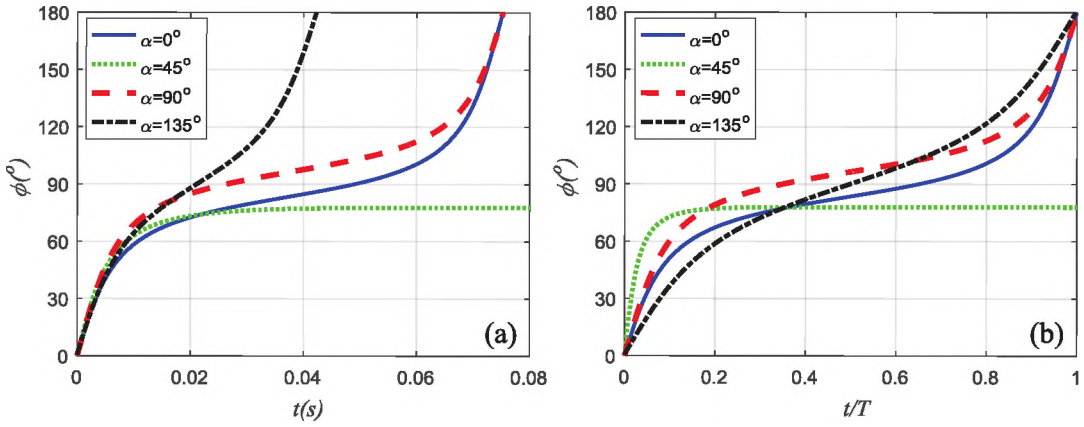

Figure 8. The effect of the direction of magnetic field at a fixed strength (H_0 = 2000 A/m) on the rotational period and asymmetry of particle rotation.

$\phi = 0°$ to $\phi = 90°$, while less time from $\phi = 90°$ to $\phi = 180°$ at $\alpha = 0°$. For $\alpha = 90°$, ω_m and ω_h have the same direction from $\phi = 0°$ to $\phi = 90°$, while have the opposite direction from $\phi = 90°$ to $\phi = 180°$ shown in Figure 7b. It means that the particle spends less time from $\phi = 0°$ to $\phi = 90°$, while more time from $\phi = 90°$ to $\phi = 180°$ at $\alpha = 0°$, that is, $T_1 < T_2$ and $\tau < 0.5$. For $\alpha = 45°$,ω_m and ω_h have the same direction from $\phi = 0°$ to $\phi = 45°$ and $\phi = 135°$ to $\phi = 180°$, while have the opposite direction from $\phi = 45°$ to $\phi = 135°$ shown in Figure 7c. Due the symmetry of flow field and particle, the time spending from $\phi = 0°$ to $\phi = 45°$ and $\phi = 135°$ to $\phi = 180°$ are equal. At the same time, the time spending from $\phi = 45°$ to $\phi = 90°$ and $\phi = 90°$ to $\phi = 135°$ are equal. So $T_1 = T_2$ and $\tau = 0.5$. The similar reason can explain the rotation behavior at $\alpha = 135°$ shown in Figure 7d.

3.4. THE EFFECT OF PARTICLE ASPECT RATIO

In this section, we study the effect of particle aspect ratio on the period and asymmetry of rotation of particle. Figure 9a shows that the angle of rotation corresponding to rotation time with different particle aspect ratio at H_0 = 2000 A/m and $\alpha = 0°$. As particle aspect ratio increases, the period of rotation increases, agreeing well with the trend predicted by Jeffery's theory. Figure 9b shows the angle of rotation corresponding to the dimensionless

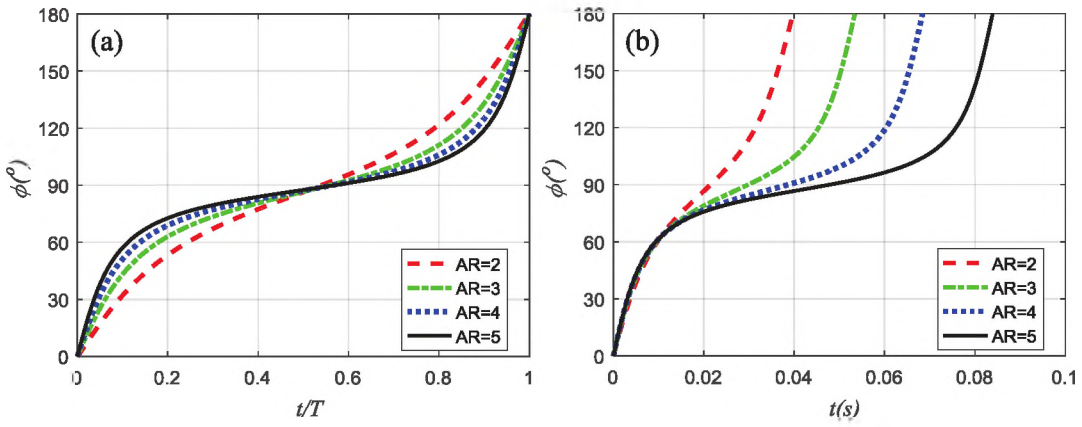

Figure 9. The effect of particle aspect ratio on the rotational period and asymmetry of particle rotation at (H_0 = 2000A/m, α = 0°).

time with different particle aspect ratio at H_0 = 2000 A/m and α = 0°. It is shown that τ is always larger than 0.5 for different particle aspect ratio, which is consistent with what we discussed before. When aspect ratio increases, there is a slight increase for τ, which means that particle aspect ratio has only a marginal effect on the asymmetry of rotation of particle.

4. CONCLUSIONS

The motion of ellipsoidal particles in a simple shear flow subjected to a uniform magnetic field is numerically investigated by a multiphysics model that couples magnetic field, flow field and rigid body motions. The magnetic field strength has a significant effect on the period and asymmetry of rotation of particle. As the magnetic field strength increases, the rotation period of particle increases and the asymmetry of rotation becomes more pronounced. When the magnetic field strength increases to a large enough value, the particle could not perform a complete rotation and reaches a steady angle. Further, the direction of magnetic field modifies both the period and asymmetry of rotation of particle. Placed at 45°, the direction of magnetic field shortens the period of rotation, while at 135° it increases the period. The symmetry of particle rotation is preserved for magnetic fields placed at 45° and 135°. The magnetic field, when directed at 0° and 90°, causes the asymmetry of rotation.

For particle aspect ratio, the results show that it changes the period of rotation of particle, which is consistent with Jeffery's theory, but has a subtle effect on the asymmetry of particle rotation.

ACKNOWLEDGMENTS

The authors gratefully acknowledge the financial support from the Department of Mechanical and Aerospace Engineering at Missouri University of Science and Technology.

REFERENCES

Alava, M. and Niskanen, K., 'The physics of paper,' Reports on progress in physics, 2006, **69**(3), p. 669.

Anstey, N. M., Russell, B., Yeo, T. W., and Price, R. N., 'The pathophysiology of vivax malaria,' Trends in parasitology, 2009, **25**(5), pp. 220–227.

Champion, J. A., Katare, Y. K., and Mitragotri, S., 'Particle shape: a new design parameter for micro-and nanoscale drug delivery carriers,' Journal of controlled release, 2007, **121**(1-2), pp. 3–9.

Jeffery, G. B., 'The motion of ellipsoidal particles immersed in a viscous fluid,' Proceedings of the Royal Society of London A: Mathematical, Physical and Engineering Sciences, 1922, **102**(715), pp. 161–179.

Larson, R. G., *The structure and rheology of complex fluids*, volume 150, Oxford university press New York, 1999.

Leal, L., 'Particle motions in a viscous fluid,' Annual Review of Fluid Mechanics, 1980, **12**(1), pp. 435–476.

Mitragotri, S. and Lahann, J., 'Physical approaches to biomaterial design,' Nature materials, 2009, **8**(1), p. 15.

Saffman, P., 'On the motion of small spheroidal particles in a viscous liquid,' Journal of Fluid Mechanics, 1956, **1**(5), pp. 540–553.

Taylor, G. I., 'The motion of ellipsoidal particles in a viscous fluid,' Proceedings of the Royal Society of London. Series A, Containing Papers of a Mathematical and Physical Character, 1923, **103**(720), pp. 58–61.

Valero, A., Braschler, T., Rauch, A., Demierre, N., Barral, Y., and Renaud, P., 'Tracking and synchronization of the yeast cell cycle using dielectrophoretic opacity,' Lab on a Chip, 2011, **11**(10), pp. 1754–1760.

Young, K. D., 'The selective value of bacterial shape,' Microbiol. Mol. Biol. Rev., 2006, **70**(3), pp. 660–703.

II. NUMERICAL STUDY OF LATERAL MIGRATION OF ELLIPTICAL MAGNETIC MICROPARTICLES IN MICROCHANNELS IN UNIFORM MAGNETIC FIELDS

Jie Zhang, Cheng Wang

Department of Mechanical & Aerospace Engineering

Missouri University of Science and Technology

Rolla, Missouri 65409

Tel: 573–341–4636, Fax: 573–341–4607

Email: wancheng@mst.edu

ABSTRACT

This work reports numerical investigation of lateral migration of a paramagnetic microparticle of an elliptic shape in a plane Poiseuille flow of a Newtonian fluid under a uniform magnetic field by direct numerical simulation (DNS). A finite element method (FEM) based on the arbitrary Lagrangian-Eulerian (ALE) approach is used to study the effects of strength and direction of the magnetic field, particle-wall separation distance and particle shape on the lateral migration. The particle is shown to exhibit negligible lateral migration in the absence of a magnetic field. When the magnetic field is applied, the particle migrates laterally. The migration direction depends on the direction of the external magnetic field, which controls the symmetry property of the particle rotational velocity. The magnitude of net lateral migration velocity over a π cycle is increased with the magnetic field strength when the particle is able to execute complete rotations, expect for $\alpha = 45°$ and 135°. By investigating a wide range of parameters, our direct numerical simulations yield a comprehensive understanding of the particle migration mechanism. Based on the numerical data, an empirical scaling relationship is proposed to relate the lateral migration distance

to the asymmetry of the rotational velocity and lateral oscillation amplitude. The scaling relationship provides useful guidelines on design of devices to manipulate nonspherical micro-particles, which have important applications in lab-on-a-chip technology, biology and biomedical engineering.

Keywords: microparticles; magnetic field; direct numerical simulation; particle separation

1. INTRODUCTION

For decades, magnetic fields have been widely used to separate microscale and nanoscale magnetic particles suspended in fluids in various industrial, biological and biomedical applications, such as mineral purification (Yavuz *et al.*, 2009), cell separation (Hejazian *et al.*, 2015), and targeted drug delivery (Arruebo *et al.*, 2007). The underlying principle in these applications is magnetophoresis – the motion of particles due to magnetic forces. The generation of magnetic forces requires both a magnetic particle and a spatially non-uniform magnetic field (or non-zero magnetic field gradients) (Pamme, 2006).

Recent experiments have demonstrated a non-conventional strategy to manipulate magnetic particles by combining a magnetic torque, non-spherical shapes and shear flows (Zhou *et al.*, 2017a,b). Different from traditional techniques based on forces, this torque-based method only requires a uniform magnetic field. As a result, there is no magnetic force, and thus, the method may be better described as “force-free magnetophoresis". Here, the lateral migration of non-spherical particles stems from the coupling of the magnetic field, flow field and particle-wall hydrodynamic interactions. While earlier experiments provide the first observations of this unique phenomenon, it remains difficult to conduct well-controlled experimental studies. On the other hand, numerical simulations are powerful tools to carry out systematic investigations to gain insights on various factors that influence the particle transport behaviours.

Due to its importance to science and engineering, the dynamics of non-spherical particles in flows have been a subject of extensive theoretical, numerical and experimental investigations. For example, the pioneering work includes Jeffery's theory (Jeffery, 1922) and experimental studies by Mason's group (Goldsmith and Mason, 1961; Trevelyan and Mason, 1951). With the advancement of computing capabilities, numerical simulations have been increasingly employed to study the motion of both spherical and non-spherical particles in a variety of shear flows, including plane Couette and Poiseuille flows. Feng et al. (Feng *et al.*, 1994) reported a direction numerical simulation (DNS) based on the finite element method (FEM) to study the lateral migration of the neutrally and non-neutrally buoyant circular particle in plane Couette and Poiseuille flows. The simulation results agree qualitatively with the results of perturbation theories and experimental data. Gavze and Shapiro (Gavze and Shapiro, 1997) used a boundary integral equation method to investigate the effect of particle shape on forces and velocities acting on the particle near the wall in a shear flow. Pan's group proposed a distributed Lagrange-multiplier-based fictitious domain method (DLM) to investigate the motion of multiple neutrally buoyant circular cylinders and elliptical cylinders in shear flow (Huang *et al.*, 2015; Pan *et al.*, 2013) and plane Poiseuille flow (Chen *et al.*, 2012; Pan and Glowinski, 2002). Yang et al. (Yang *et al.*, 2005) reported two methods, the arbitrary Lagrangian-Eulerian (ALE) method and the distributed Lagrange-multiplier-based fictitious domain method (DLM), to study the migration of a single neutrally buoyant rigid sphere in tube Poiseuille flow. Ai et al. (Ai *et al.*, 2009b) investigated some key factors on pressure-driven transport of particles in a symmetric converging-diverging microchannel by the ALE finite-element method. Lee et al. (Lee *et al.*, 2009a,b) used the same method as Gavze and Shapiro (Gavze and Shapiro, 1997) to study the particle transport behaviour with different size, shape and material properties in the plane Couette flow.

Motions of magnetic particles have been numerically investigated due to their close relevance to biomedical separations (Gijs *et al.*, 2009) and magnetically assisted drug delivery (Martinez *et al.*, 2013). Smistrup et al. (Smistrup *et al.*, 2005) used numerical simulations to study magnetic separation of magnetic beads in the microchannel under the magnetic field of microfabricated electro-magnets. Their simulation results agree qualitatively with the experimental data. Sinha et al. (Sinha *et al.*, 2007) numerically investigated the motion of magnetic microbeads in the microchannel under a non-uniform magnetic field. More recently, shape-dependent drag force and magnetization are exploited to separate non-magnetic particles and biological cells in a ferrofluid (Chen *et al.*, 2017; Zhou and Xuan, 2016). In prior works, the particles are often treated as point masses while the effect of hydrodynamic interactions resulting from particle shape and finite size are not directly considered.

Our previous work focused experimentally on lateral migration when the particle is undergoing rotational motion (Zhou *et al.*, 2017a,b). The work by Matsunaga et al. is mainly concerned lateral migration that occurred when particle is not rotating (Matsunaga *et al.*, 2017a,b). The work by Cao et al. numerically studied the rotation and lateral migration of particles for both scenarios including weak and strong field strengths (Cao *et al.*, 2018). The present work studies the effects of strength and direction of the magnetic field strength, initial particle position, particle aspect ratio, and particularly proposes a scaling relationship between the symmetry properties of the particle's rotational velocity, and the magnitude of lateral oscillation in the absence of a magnetic field. By implementing an ALE method in the COMSOL FEM solver, our direct numerical simulations couple and simultaneously solve the flow field, magnetic field, and particle motions. The magnetic torque, hydrodynamic torque as well as hydrodynamic force are computed and used to determine the translational and rotational motions of the particle via Newton's second law and Euler's law. After validating the numerical model with Jeffery's theory, systematic numerical simulations are

carried out to understand the roles of key factors, including the strength and direction of the magnetic field, particle aspect ratio, and initial particle-wall separation distance, on the lateral migration of the particle.

2. SIMULATION METHOD

2.1. MATHEMATICAL MODEL

We consider a prolate elliptical particle immersed in a plane Poiseuille flow of an incompressible Newtonian fluid with density ρ_f and dynamic viscosity η_f as shown in Figure 1. The computational domain, Ω, is surrounded by the boundary, ABCD, and particle surface, Γ. The width and length of the computational domain are W and L, respectively. The particle aspect ratio is $AR = a/b$, where a and b are the major and minor semi-axis lengths of the particle, respectively. The particle-wall separation distance, y_p, is defined as the vertical distance between the particle center and the x axis. The orientation of the particle, ϕ, is defined as the angle between the major axis of the particle and positive y axis. A uniform magnetic field, $\mathbf{H}_0$, is imposed at an arbitrary direction, denoted by α, as shown in Figure 1.

The flow field, $\mathbf{u}$, is governed by the continuity equation and Navier-Stokes (NS) equations for an incompressible and Newtonian flow:

$$\nabla \cdot \mathbf{u} = 0, \tag{1}$$

$$\rho_f \left[\frac{\partial \mathbf{u}}{\partial t} + (\mathbf{u} \cdot \nabla)\,\mathbf{u} \right] = -\nabla p + \nabla \cdot \eta_f \left(\nabla \mathbf{u} + (\nabla \mathbf{u})^T \right), \tag{2}$$

where p is the pressure and t is the time.

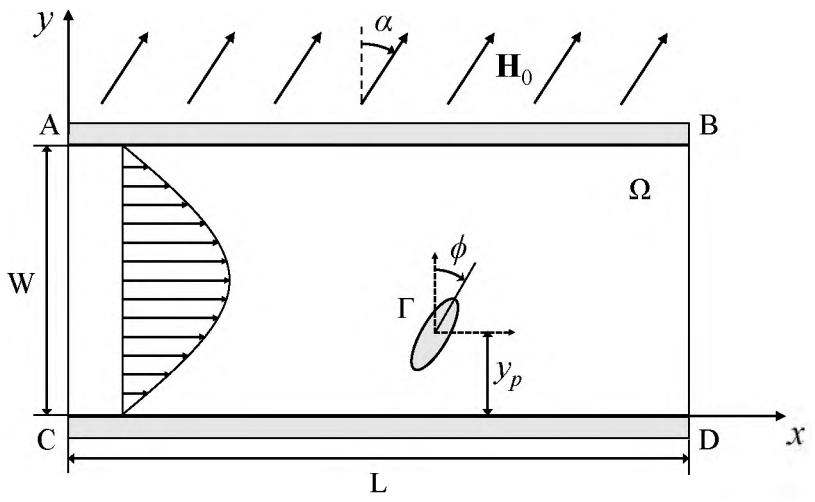

Figure 1. Schematic view of the numerical model of an elliptical particle suspended in a plane Poiseuille flow under the influence of a uniform magnetic field $\mathbf{H}_0$. The fluid and particle domains are Ω and Γ, respectively. The orientation angle of the particle is denoted by ϕ. The particle-wall separation distance is denoted by y_p.

To obtain a fully developed laminar flow profile, the laminar inflow is at the inlet AC. The zero normal pressure condition is set to the outlet BD. No-slip condition is applied on channel walls AB and CD. No-slip condition also applies on the particle surface, so the fluid velocities on the particle surface are given as:

$$\mathbf{u} = \mathbf{U}_p + \boldsymbol{\omega}_p \times (\mathbf{x}_s - \mathbf{x}_p), \tag{3}$$

where $\mathbf{U}_p$ and $\boldsymbol{\omega}_p$ are translational and rotational velocities of particle, respectively. $\mathbf{x}_s$ and $\mathbf{x}_p$ are the position vectors of the surface and the center of the particle. The hydrodynamic force and torque acting on the particle are expressed as:

$$\mathbf{F}_h = \int (\boldsymbol{\tau}_h \cdot \mathbf{n}) dS, \tag{4}$$

$$\mathbf{T}_h = \int (\boldsymbol{\tau}_h \times (\mathbf{x}_s - \mathbf{x}_p) \cdot \mathbf{n}) dS, \tag{5}$$

where $\boldsymbol{\tau}_h = \eta_f \left(\nabla \mathbf{u} + (\nabla \mathbf{u})^T\right)$ is the hydrodynamic stress tensor.

The governing equations of the magnetic field are given as:

$$\nabla \times \mathbf{H} = 0, \tag{6}$$

$$\nabla \cdot \mathbf{B} = 0, \tag{7}$$

where $\mathbf{H}$ and $\mathbf{B}$ are the magnetic field strength and the magnetic flux density, respectively. To obtain a uniform magnetic field, the magnetic scalar potential difference is set to AB and CD. A zero magnetic potential $V_m = 0$ is set to AB and a magnetic potential $V_m = V_{m0}$ is set to CD. The magnetic insulation condition is set at AC and BD. Since the magnetic field is uniform and the particle is paramagnetic, the force acting on the particle is zero. Assuming the magnetic particle is homogeneous, isotropic, and linearly magnetizable, the magnetic torque acting on particle is expressed as (Stratton, 2007):

$$\mathbf{T}_m = \mu_0 V_p \chi_p \mathbf{H}^- \times \mathbf{H}_0, \tag{8}$$

where $\mathbf{H}^-$ and $\mathbf{H}_0$ are the magnetic fields inside and outside the particle, respectively, χ_p is the magnetic susceptibility of the particle, μ_0 is the magnetic permeability of the vacuum, and V_p is the volume of particle.

The translation and rotation of the particle are governed by Newton's second law and Euler's equation:

$$m_p \frac{d\mathbf{U}_p}{dt} = \mathbf{F}_h, \tag{9}$$

$$I_p \frac{d\omega_p}{dt} = \mathbf{T}_h + \mathbf{T}_m, \tag{10}$$

where m_p and I_p are the mass and the moment of inertia of the particle. Since the particle rotation is in the xy plane, only the z-component of ω_p, $\mathbf{T}_h$ and $\mathbf{T}_m$ are necessary to calculate the rotational velocity, and $\omega_p = \omega_p \hat{k}$.

The position of center $\mathbf{C}_p(t) = (x_p, y_p)$ and orientation ϕ_p of particle are given by:

$$\boldsymbol{C}_p(t) = \boldsymbol{C}_p(0) + \int_0^t \boldsymbol{U}_p(s)ds, \tag{11}$$

$$\phi_p(t) = \phi_p(0) + \int_0^t \omega_p(s)ds, \tag{12}$$

where $\boldsymbol{C}_p(0)$ and $\phi_p(0)$ are the initial position and orientation of the particle.

The position and orientation of the particle will affect the magnetic and flow fields around the particle, and successively alter the magnetic torque and hydrodynamic force and torque acting on the particle. Therefore, we use direct numerical simulation (DNS) based on the finite element method (FEM) and arbitrary Lagrangian-Eulerian(ALE) method to account such coupling among the particle, fluid flow, and magnetic fields. Similar method has been successfully achieved by Hu et al. (Hu *et al.*, 2001) and Ai et al (Ai *et al.*, 2009a,b; Ai and Qian, 2010; Ai *et al.*, 2014). Numerical models are implemented by using a commercial FEM solver COMSOL Multiphysics. First, we use the stationary solver for parametric sweep analysis to simulate the magnetic field inside and outside of the particle, and calculate the magnetic torque acting on the particle. Then, a two-way coupling fluid-particle interaction model is solved by using a time-dependent solver, where the magnetic torque is imported into the model as a variable. Quadratic triangular elements are generated in the simulations. Fine mesh around the particle and finer mesh around the tip of the particle are created to accurately calculate the hydrodynamic force and torque acting on the particle.

2.2. MATERIAL PROPERTIES USED IN SIMULATIONS

In this study, the fluid and particles in the simulations are water and magnetite-doped polystyrene particle, respectively. The density and dynamic viscosity of water are 1000 kg/m^3 and 1.002×10^{-3} Pa·s, respectively. The magnetic susceptibility of particle is $\chi_p = 0.26$ according to previous studies (Zhou *et al.*, 2017a,b), whereas the fluid is a non-magnetic

fluid. The density of the particle is 1100 kg/m^3. The particles used in the simulation have varying aspect ratios, but all have the same volume, which is equal to the volume of a 7 μm-diameter circular particle. The width and length of the computational domain are W = 800 μm and L = 50 μm, respectively. Inlet flow velocity is 2.5 mm/s, so Re = 0.125.

Table 1. Six meshes for grid independence analysis

	Domain elements	Boundary elements on particle surface
Mesh 1	6184	56
Mesh 2	7794	68
Mesh 3	8281	92
Mesh 4	11608	116
Mesh 5	12359	152
Mesh 6	13079	184

2.3. GRID INDEPENDENCE ANALYSIS

Grid independence analysis is presented to determine the appropriate meshes for a fast and accurate numerical simulation.The results of six different meshes in a plane Poiseuille flow in the absence of the magnetic field are shown in Table 1 and Figure 2. As can be seen, the numerical results are good enough when the domain element number is larger than 11,600 and the boundary element number on the particle surface is larger than 120. So in the paper, we used about 12,000 elements in the computational domain Ω in Figure 1, and about 150 elements on the particle surface Γ, which could give reasonably accurate results.

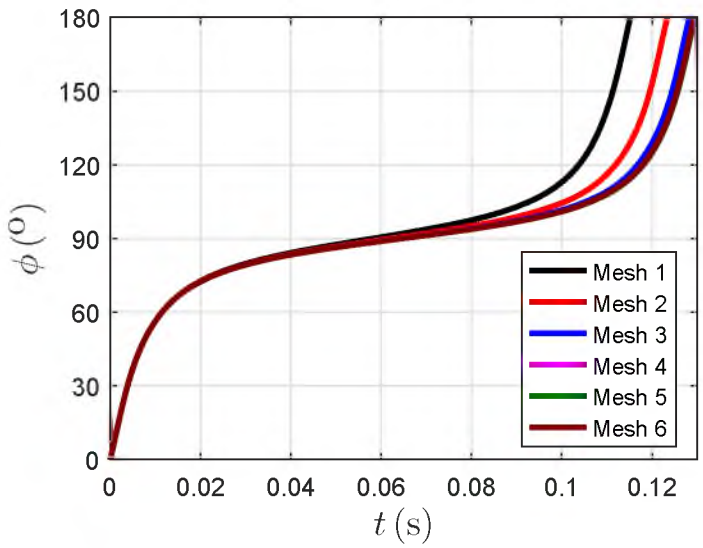

Figure 2. Grid independence analysis: particle orientation as a function of time, for $AR = 4$, $y_{p0} = 12$ μm

3. RESULTS AND DISCUSSION

3.1. VALIDATION OF NUMERICAL METHOD

To validate our numerical method, we first compare the results of our simulation to Jeffery's theory, which describes the periodic rotation of an axisymmetric ellipsoidal particle in a simple shear flow (Jeffery, 1922). The period of the particle rotating from 0° to 360° is $T^J = 2\pi/\dot{\gamma}(AR + 1/AR)$, where $\dot{\gamma}$ is the shear rate. Due to the fore-aft symmetry of the particle, here we define T_0^J as the period of rotation from 0° to 180°, i.e., $T_0^J = T^J/2$. Figure 3 shows the particle rotation predicted by Jeffery's theory and our simulation for a particle having $AR = 4$ in a simple shear flow with shear rate $\dot{\gamma} = 200$ s^{-1} in the absence of a magnetic field. The theoretical value of T_0^J from the Jeffery theory is 0.0668 s, while the period obtained in our FEM simulation is 0.0670 s. The relative error is 0.37%, suggesting that the simulation has a remarkable agreement with the theory. Therefore, this simulation method has been validated to be sufficiently accurate to study the periodic rotation of particle in this work.

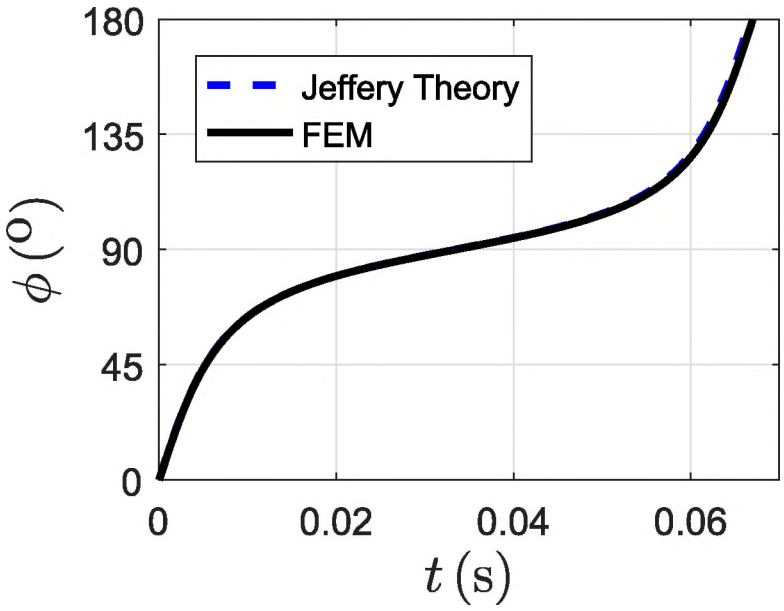

Figure 3. Comparison between the FEM simulation and Jeffery's theory on particle rotation.

3.2. PARTICLE MOTION WITHOUT A MAGNETIC FIELD

In this section, we investigate the effect of particle aspect ratio, AR, and its initial particle-wall separation distance, y_{p0}, on particle motion without a magnetic field. Figure 4 shows the trajectory of an elliptical particle with $AR = 4$ initially located at $y_{p0} = 12$ μm. As can be seen, the particle oscillate away from the wall in the first half period (from 0° to 90°) and towards the wall in the second half period (from 90° to 180°), but there is a negligible net lateral migration. We define the difference between the maximum and minimum values of the oscillatory motion in the y direction as the amplitude, A, as shown in Figure 4(a), and define the period as the time spent by the particle to rotate from 0° to 180°, T_0, as shown in Figure 4(b).

The orientation of the particle, ϕ, as a function of the dimensionless time, t/T_0, over a period is shown in Figure 4(c). As can be seen, the particle has a symmetry of rotation with respect to $\phi = 90°$. The rotational velocity due to the shear flow is symmetric about $\phi = 90°$

as shown in Figure 4(d), meaning that the particle spends the same amount of time in the first and second half periods. The presence of the wall induces particle-wall hydrodynamic interaction which causes the oscillatory motion of the elliptical particle. However, due to the equal time the particle spends in the first and second half rotational period, the lateral distance of the particle moving upwards and moving downwards are equal. Thus, there is no net lateral migration.

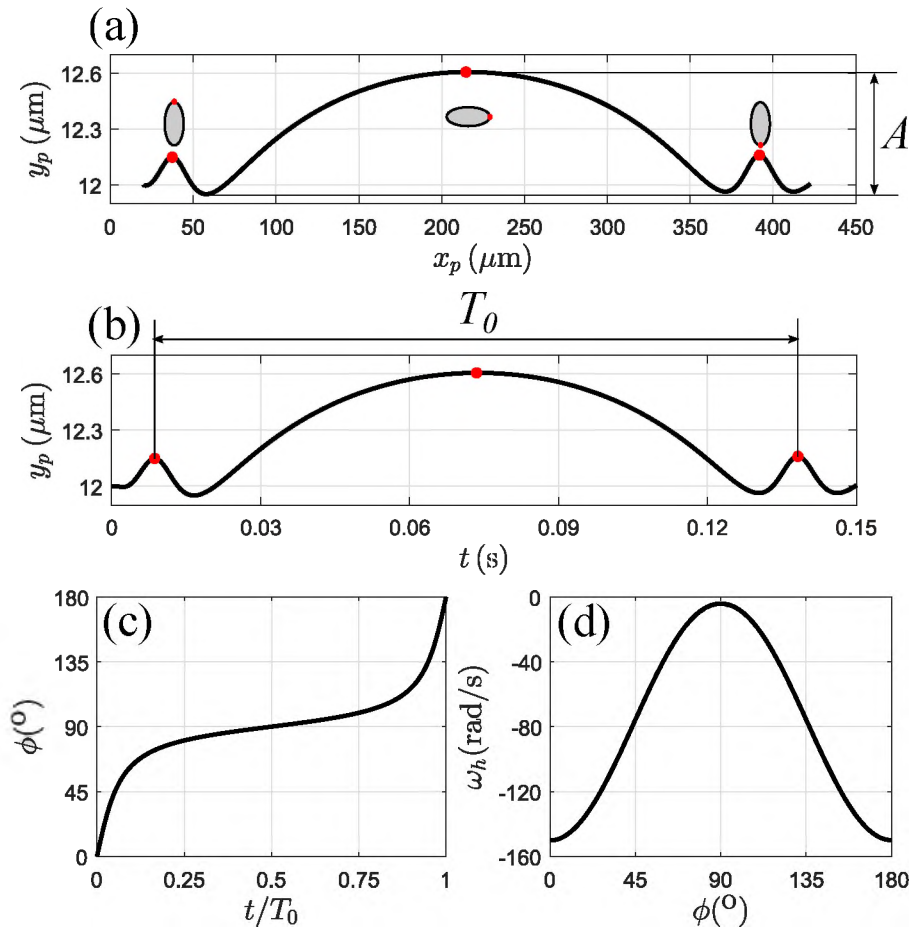

Figure 4. Translation and rotation of the particle without a magnetic field. The particle (AR = 4) is initially located at y_{p0}=12 μm. (a) Trajectory of the particle over a rotation of 180°, with A denoting the amplitude of oscillatory motion. (b) The particle-wall separation distance over one period T_0. (c) The evolution of orientation angle, ϕ with the dimensionless time t/T_0. (d) The rotational velocity ω_h versus ϕ.

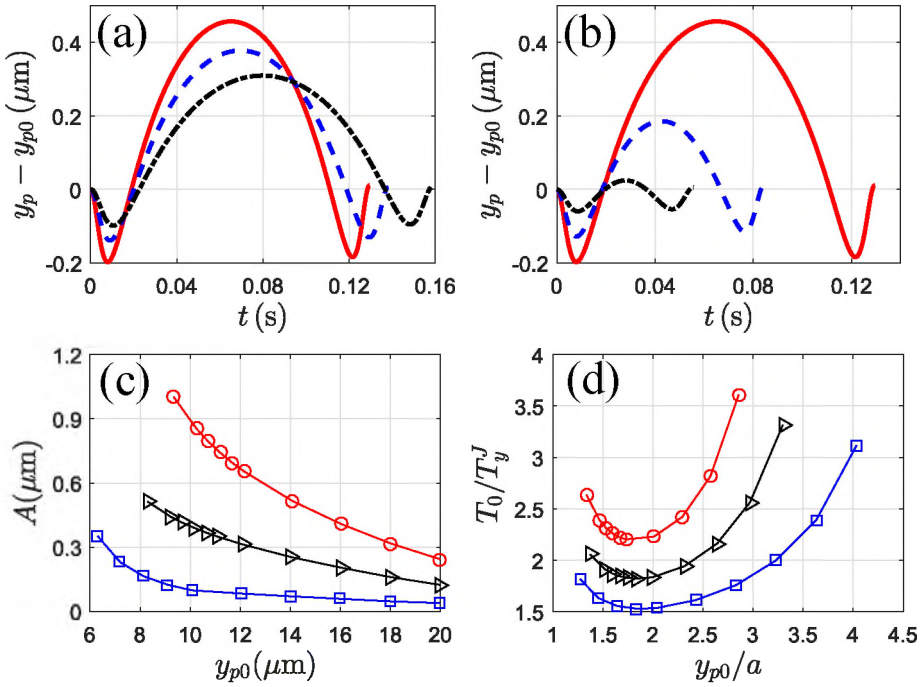

Figure 5. The effects of initial position y_{p0} and particle aspect ratio AR on transport of elliptical particles without a magnetic field. (a) The effect y_{p0} on the lateral particle-wall separation: y_{p0} = 12 μm (solid line), 14 μm (dash line) and 16 μm (dash-dot line). The particle has a particle aspect ratio AR = 4. (b) The effect of particle aspect ratio on the lateral particle-wall separation distance: AR = 4 (solid line), AR = 3 (dash line), and AR = 2 (dash-dot line). The particles are initially located at y_{p0} = 12 μm. (c) Dependence of amplitude of the oscillatory motion, A on y_{p0}. (d) The dimensionless period T_0/T_y^J varies with dimensionless distance y_{p0}/a, for AR = 4 (circle), 3 (triangle), and 2 (rectangle). $T_y^J$is the period of Jeffery's orbit calculated by using the shear rate at the position of the particle centroid.

The lateral migration of the elliptical particle for three initial particle-wall separation distances y_{p0}, and different aspect ratio AR, are shown in Figure 5(a)(b). In Figure 5(a), as y_{p0} is increased from 12 μm to 16 μm, the period of rotation becomes longer, and the amplitude A becomes smaller for a fixed AR. As AR is decreased from 4 to 2, the period of rotation becomes shorter, and the amplitude A becomes smaller for a fixed y_{p0} (Figure 5(b)). For example, at y_{p0} = 12 μm, the period of rotation T_0 = 0.1295 s and the amplitude A = 0.6547 μm for AR = 4; T_0 = 0.0844 s and A = 0.3137 μm for AR = 3; T_0 = 0.0556 s and A =

0.0841 μm for $AR = 2$. Further, the net lateral migration is almost zero, regardless of its initial particle-wall separation distance and aspect ratio. It is consistent with our previous experimental observation (Zhou *et al.*, 2017b).

The amplitude and period of the oscillatory motion for different y_{p0} and different AR are shown in Figure 5(c)(d). As can be seen, for a fixed AR, the curve becomes steeper when the particle approaches to the wall (i.e., y_{p0} is decreased). The slope of curve becomes larger when the particle shape becomes more non-spherical (AR is increased). Figure 5(d) shows the dimensionless period of rotation, T_0/T_y^J , varying with the dimensionless particle-wall separation distance, y_{p0}/a, T_y^J is the period of Jeffery's orbit calculated by using the shear rate at the position of the particle centroid and a is the semi-major axis of the particle, respectively. As can be seen in Figure 5(d), the dimensionless time, T_0/T_y^J , is larger than 1 for the all results. As y_{p0}/a is increased, T_0/T_y^J is decreased first and then is increased for a constant AR. Further, the decreasing rate in first part and the increasing rate in the second part of T_0/T_y^J become steeper as AR increases from 2 to 4.

The effect of y_{p0} and AR on A and T_0^J in Figure 5(c)(d) can be explained as follows. When the particle is transported in the channel flow, the wall induces particle-wall hydrodynamic interactions and increases resistance on the rotation of particle (Gavze and Shapiro, 1997; Hsu and Ganatos, 1994). The smaller the particle-wall separation (y_{p0} varying from 16 μm to 12 μm) is, the more prominent the particle-wall interaction is. The amplitude (A) thus increases with decreasing y_{p0} i.e., increased hydrodynamic interactions, as shown in Figure 5(c)). On the other hand, the particle aspect ratio represents the degree of deviation from the spherical particle. A larger particle aspect ratio induces more prominent particle-wall interaction than a spherical particle ($AR = 1$). The increasing resistance on the rotation of particle causes the particle spending longer time than that in the absence of the wall. Therefore, the particle-wall separation distance and particle aspect ratio are two important factors affecting the oscillatory motion of the particle in the microchannel.

3.3. PARTICLE MOTION IN A MAGNETIC FIELD

3.3.1. Magnetic Field at $\alpha = 0°$. In this section, we investigate the effect of magnetic fields with the direction $\alpha = 0°$ on the lateral migration of the particle. The particle with $AR = 4$ is initially placed at $y_{p0} = 12$ μm. The magnetic field of $H_0 = 3000$ A/m is imposed at the direction of $\alpha = 0°$. Figure 6(a)(b) shows the particle orientation angle and the lateral migration as a function of time. For convenience of discussion, we define a dimensionless parameter, τ, as the ratio of the time that the particle rotates from 0° to 90° to the entire period of the particle rotation as shown in Figure 6(a). Here, The period of particle rotation is defined the same as in Section 3.2. To distinguish the period of rotation from Section 3.2, we use T as the period of rotation when the magnetic field is applied. As can be seen in Figure 6(a), when $H_0 = 0$, $\tau = 0.5$ and the curve is anti-symmetric to $(0.5, 90°)$; when the magnetic field strength $H_0 = 3000$ A/m, $\tau > 0.5$ and the curve is no longer anti-symmetric to $(0.5, 90°)$. Thus, we can use the dimensionless parameter τ to characterize the symmetry and asymmetry property of the particle's rotation. Second, we define the net lateral migration of the particle, Δy_p, as the difference between the position of particle centroid at $\phi = 0°$ and at $\phi = 180°$ in the y direction as shown in Figure 6(b). As can be seen, when a magnetic field is applied at $\alpha = 0°$, $\Delta y_p > 0$, meaning that the particle moves away from the channel wall over a period.

The influence of the perpendicular magnetic field can be explained as follows. In the absence of a magnetic field, the hydrodynamic torque causes the rotational motion of the particle. The corresponding rotational velocity is shown as the dashed line in Figure 6(c). As we discussed before, there is a negligible net migration due to the symmetry of the particle rotational velocity. When a magnetic field is applied at $\alpha = 0°$, the total rotational velocity, $\omega_p = \omega_h + \omega_m$, is asymmetric with respect to $\phi = 90°$, shown as the solid line in Figure 6(c). The rotational velocity due to the magnetic field, ω_m, and the rotational velocity due to the hydrodynamic torque, ω_h have opposite directions when the particle orientation ϕ is between 0° to 90°; ω_m and ω_h have the same direction when $90° < \phi < 180°$. As a result,

the particle spends more time in the first half period than in the second half period, causing the asymmetry of the particle rotational velocity. The asymmetric particle rotation further leads to a broken symmetry of the particle's lateral oscillation motion, via hydrodynamic interactions (Gavze and Shapiro, 1997). Consequently, the particle spends more time moving upwards than moving downwards, and exhibits a net lateral migration away from the wall, as shown in Figure 6(b).

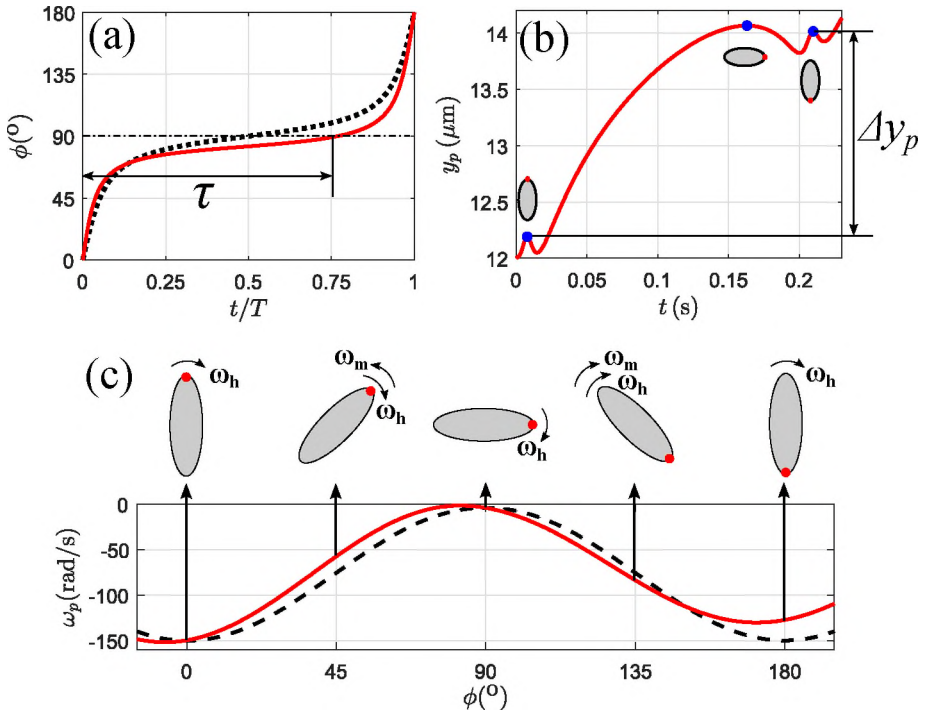

Figure 6. Transport of the particle when the magnetic field is applied perpendicular to the flow direction, i.e., $\alpha = 0°$. The particle ($AR = 4$) is initially located at $y_{p0} = 12$ μm. (a) The orientation angle, ϕ versus dimensionless time t/T. A dimensionless time parameter τ is defined as the ratio of the time for the particle rotating from 0° to 90° to the period of rotation, T. (b) The particle-wall separation distance, y_{p0} as a function of time ($H_0 = 3000$ A/m, $\alpha = 0°$). Δy_p denotes the net lateral migration of the particle over one period. (c) The rotational velocity ω_p versus ϕ: $H_0 = 0$ A/m (dash line), and 3000 A/m (solid line). The symmetry of particle rotational velocity ω_p about $\phi = 90°$ is broken, and $\tau > 0.5$.

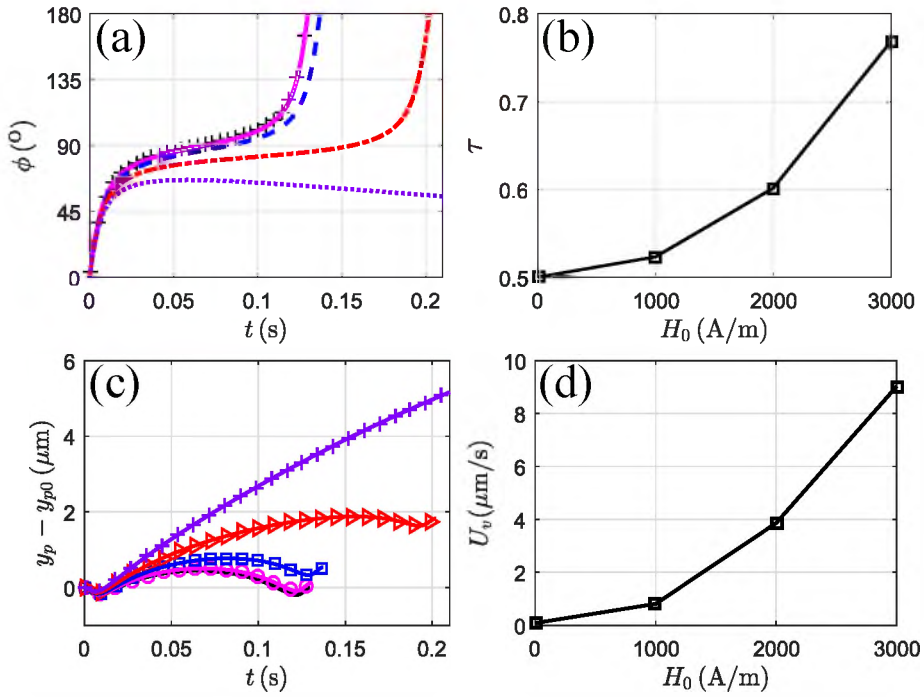

Figure 7. The effect of magnetic field strength on particle transport, with $AR = 4$, $y_{p0} = 12$ μm, and $\alpha = 0°$. (a) ϕ versus time t over a period: $H_0 = 0$ (plus symbol), 1000 A/m (solid line), 2000 A/m (dash line), 3000 A/m(dash-dot line) and 4000 A/m (dot line). (b) τ varies with the magnetic field strength H_0. (c) The net migration of particle $y_p - y_{p0}$ over a period: $H_0 = 0$ (solid symbol), 1000 A/m (circle symbol), 2000 A/m (square symbol), 3000 A/m (triangle symbol) and 4000 A/m (plus symbol). (d) The average vertical migration velocity U_v varies with the magnetic field strength H_0.

We investigate the effect of the magnetic field strength on the particle rotation and lateral migration. Figure 7(a) shows the orientation of the particle, ϕ, with time, t, in one period for different magnetic field strengths. As can be seen, when the magnetic field is applied, the period of rotation becomes longer as compared to that without a magnetic field ($H_0 = 0$). From Figure 7(a), we can see that the period of rotation, T, is increased as the magnetic field strength is increased from $H_0 = 1000$ A/m to 3000 A/m. In this case, there are two factors affecting the period of rotation. One is the magnetic field. In the simple shear flow, as the magnetic field strength is increased, the period of rotation is increased when $\alpha = 0°$ (Zhang and Wang, 2017). The other factor is the decreased shear rate as the particle moved toward the center. The magnetic field caused that the particle migrated

toward the center, where the shear rate is decreased. Thus, the magnetic field coupled with the nonlinear shear rate induced the increase of period of the rotation. Figure 7(b) shows the dependence of dimensionless parameter, τ, on the magnetic field strength. When the magnetic field strength is applied, $\tau > 0.5$, meaning that the symmetry of particle rotation is broken. As the magnetic field strength increases, τ increases, meaning that the asymmetry of the particle rotation becomes more pronounced. This asymmetry of particle rotation, combined with oscillatory motion, causes the net lateral migration. Figure 7(c) shows the net migration of particle, Δy_p, as a function of time, t, in one period for different magnetic field strengths. Because $\alpha = 0°$, the particle moves upwards, and the net lateral migration, Δy_p, increases with the increase of the magnetic field strength.

To characterize the net lateral migration, we define an average vertical migration velocity, $U_v = \Delta y_p / T$, which is the net lateral migration over the rotational period of the particle. The average vertical velocity, U_v, for different magnetic field strengths are shown in Figure 7(d). As can be seen, the vertical velocity increases when the magnetic field strength increases from 0 to 3000 A/m. This means that the particle moves upwards faster as the magnetic field increases. Further, as can be seen in Figure 7(a) and (d), when the magnetic field strength is 4000 A/m, the particle could not perform a complete rotation but continuously moved upwards. The reason for the impeded rotation is because of the dynamic balances between the hydrodynamic and magnetic torques. Due to the parabolic velocity profile of the Poiseuille flow, the shear rate becomes smaller closer to the channel center. As a result, the particle orientation continuously decreases as the particle moves towards the channel center.

3.3.2. Magnetic Field at $\alpha = 90°$. In this section, we investigate the effect of magnetic fields with the direction $\alpha = 90°$ on the lateral migration of the elliptical particle. The particle with $AR = 4$ is initially located at $y_{p0} = 12$ μm. The magnetic field with a strength of 3000 A/m is imposed at the direction of 90°. The orientation and the lateral migration varying with time are shown in Figure 8. When the magnetic field is applied at

$\alpha = 90°$, $\tau < 0.5$ and $\Delta y_p < 0$, as we can see in Figure 8(a) and (b). The reason can be similarly explained for the case of $\alpha = 0°$. Here, the magnetic rotational velocity, ω_m, and the hydrodynamic rotational velocity, ω_h, have the same direction in the first half period and opposite directions in the second half period of rotation. The total rotational velocity, ω_p, is asymmetric with respect to $\phi = 90°$, shown as the solid line in Figure 8(c). The particle spends less time to move upwards in the first half period than the second half period. Therefore, the symmetry of the particle rotation is broken and there is a net lateral migration over one period.

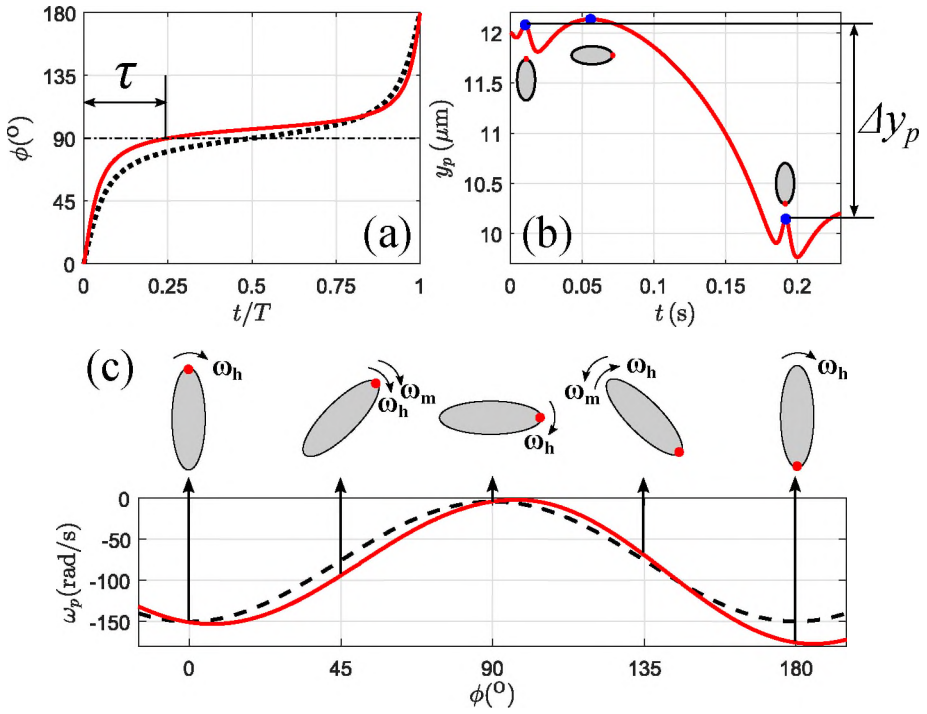

Figure 8. Transport of the particle when the magnetic field is applied parallel to the flow direction, i.e., $\alpha = 90°$. The particle ($AR = 4$) is initially located at $y_{p0} = 12$ μm. (a) ϕ varies with dimensionless time t/T. (b) variation of the particle-wall separation distance with time, and (c) the total rotational velocity ω_p varies with ϕ for $H_0 = 0$ A/m (dash line) and 3000 A/m (solid line).

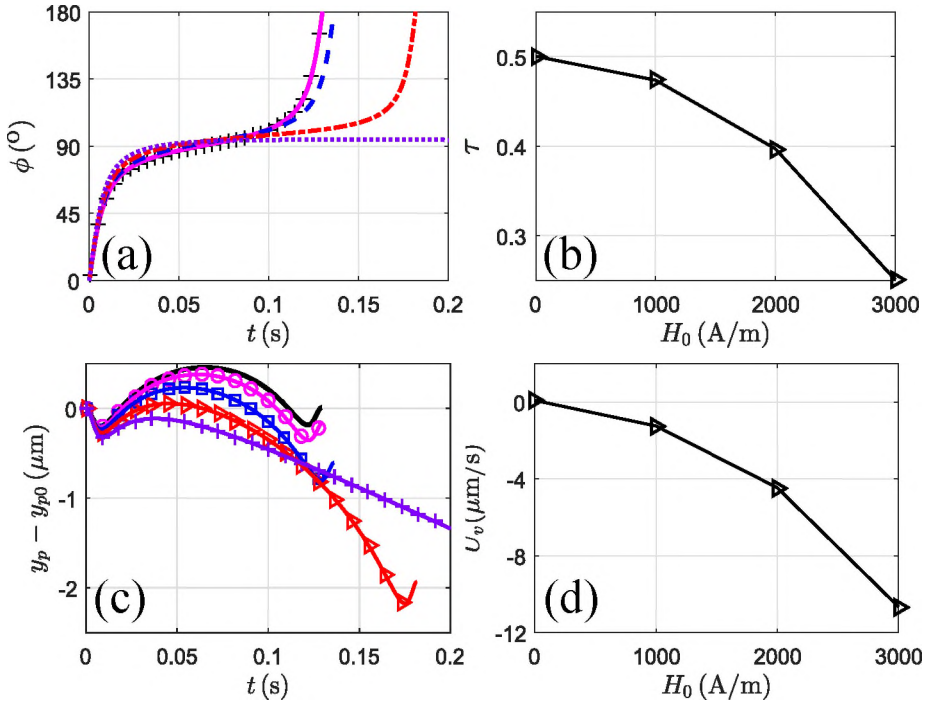

Figure 9. The effect of magnetic field strength on particle transport, with $AR = 4$, $y_{p0} = 12$ μm, and $\alpha = 90°$. (a) ϕ versus t over a period for $H_0 = 0$ (plus symbol), 1000 A/m (solid line), 2000 A/m (dash line), 3000 A/m (dash-dot) and 4000 A/m (dot); (b) τ versus H_0; (c) The lateral migration of particle $y_p - y_{p0}$ with time t over a period for $H_0 = 0$ (solid line), 1000 A/m (circle symbol), 2000 A/m (square symbol), 3000 A/m (triangle symbol) and 4000 A/m (plus symbol); (d) The vertical velocity U_v versus magnetic field strength H_0.

For different magnetic field strength, as the magnetic field strength increases, the period of rotation becomes longer as shown in Figure 9(a). It is the same as the case of $\alpha = 0°$. When the magnetic field strength is 4000 A/m, the particle could not perform a complete rotation as well. The difference between cases of $\alpha = 0°$ and $\alpha = 90°$ is the impeded orientation: the maximum orientation is larger than 90° when $\alpha = 90°$, whereas the maximum orientation is smaller than 90° when $\alpha = 0°$. Figure 9(b) shows the variation of τ with different magnetic field strengths. As we can see, $\tau < 0.5$ and becomes smaller with an increase of the magnetic field strength, meaning the asymmetry of rotation becomes more pronounced. The lateral migration for different magnetic field strength, and the average vertical velocity, U_v, are shown in Figure 9(c) and (d), respectively. As the magnetic

field strength is increased, the particle moves downwards quicker. Interestingly, when the magnetic field strength is 4000 A/m, the rate of the lateral migration becomes slower than H = 3000 A/m as shown in the line with plus symbol in Figure 9(c).

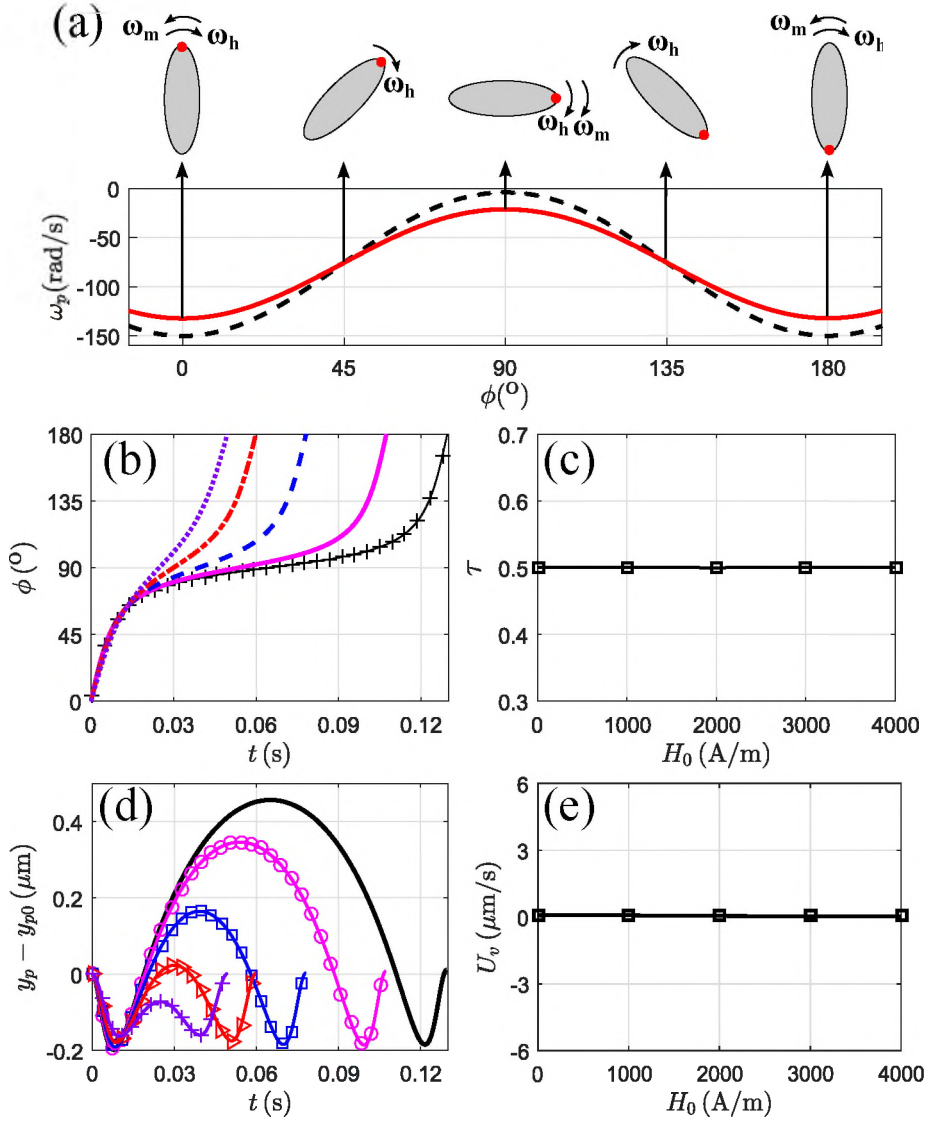

Figure 10. Effect of the magnetic field when it is applied at $\alpha = 135°$. The particle ($AR = 4$) is initially located at $y_{p0} = 12$ μm. (a) ω_p versus ϕ for $H_0 = 0$ (dash) and 3000 A/m (solid). (b) ϕ versus t over a period for $H_0 = 0$ (plus), 1000 A/m (solid), 2000 A/m (dash), 3000 A/m (dash-dot) and 4000 A/m (dot). (c) The dimensionless parameter τ as a function of H_0. (d) The migration of particle $y_p - y_{p0}$ with time t over a period for $H_0 = 0$ (solid), 1000 A/m (circle), 2000 A/m (rectangle), 3000 A/m (triangle) and 4000 A/m (plus). (e) Dependence of lateral migration velocity U_v on magnetic field strength H_0.

3.3.3. Magnetic Field at $\alpha = 135°$. In this section, we investigate the effect of magnetic fields with $\alpha = 135°$ on the lateral migration of the elliptical particle. When the magnetic field is imposed at $\alpha = 135°$, the total rotational velocity, ω_p, is symmetric to $\phi = 90°$ as shown in Figure 10(a). For four different magnetic field strengths, the orientation varying with time is shown in Figure 10(b). As the magnetic field strength is increased, the period of rotation becomes shorter, which is different from the results when the magnetic field is imposed at $\alpha = 0°$ and $90°$. But the particle preserves the symmetry of rotational velocity as can be seen in Figure 10(c): $\tau \approx 0.5$ for these four magnetic field strengths. The lateral migration for different magnetic field strengths is shown in Figure 10(d). The oscillatory amplitude is decreased with increasing the magnetic field strength, which is different from the results when the magnetic field is imposed at $\alpha = 0°$ and $90°$. Such a decrease of oscillation is due to the decrease of the rotational velocity, and translation-and-rotation coupling. There is no net migration as can be seen in Figure 10(e). $U_v \approx 0$ for these four magnetic field strengths that have been investigated.

3.3.4. Magnetic Field at $\alpha = 45°$. In this section, we investigate the effect of magnetic fields applied at $\alpha = 45°$ on the lateral migration of the elliptical particle. When the magnetic field is imposed at $\alpha = 45°$, the total rotational velocity, ω_p, is symmetric to $\phi = 90°$ as shown in Figure 11(a). When $H_0 = 1000$ A/m, $\tau \approx 0.5$ and $U_v \approx 0$, meaning that the particle's rotation velocity is symmetric about $\phi = 90°$ and there is no net lateral migration. However, when the magnetic field strength is equal or larger than 2000 A/m, the particle could not complete a full rotation, but continuously moves upwards as shown in Figure 11(b) and (c). The lateral motion is due to the particle being pinned at a steady angle (Matsunaga *et al.*, 2017a). As the magnetic field strength is increased, the maximum orientation becomes smaller and the lateral migration becomes faster.

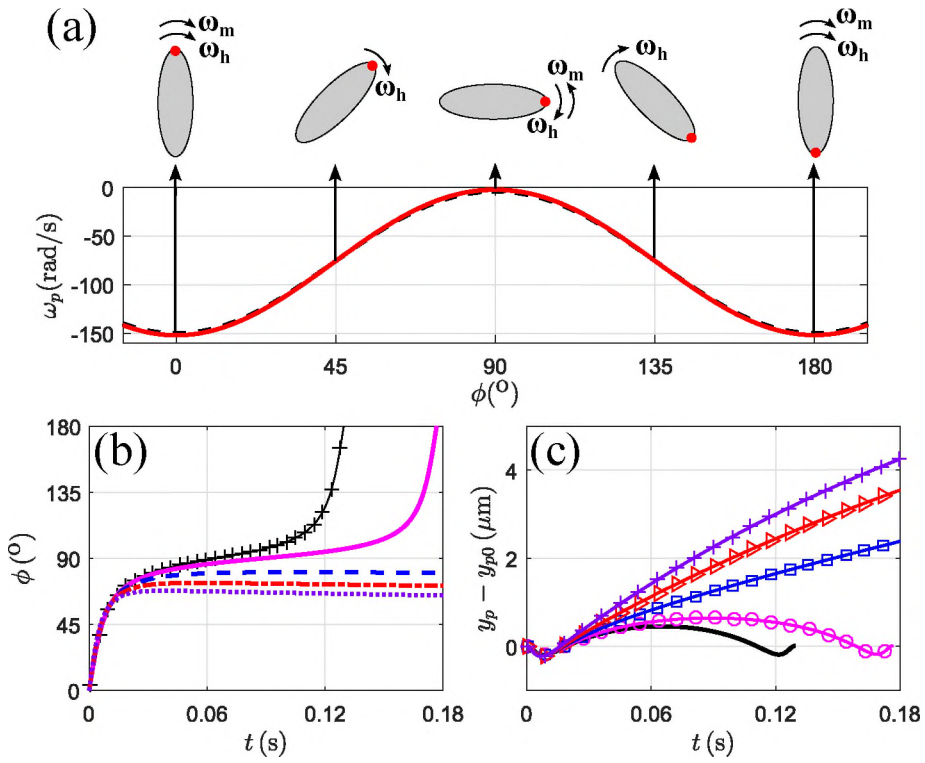

Figure 11. Effect of the magnetic field when it is applied at $\alpha = 45°$. The particle ($AR = 4$) is initially located at $y_{p0} = 12$ μm. (a) The total rotational velocity ω_p versus ϕ for $H_0 = 0$ (dash) and 3000 A/m (solid). (b) ϕ versus time t over a period for $H_0 = 0$ (plus), 1000 A/m (solid), 2000 A/m (dash), 3000 A/m (dash-dot) and 4000 A/m (dot). (c) The migration of particle $y_p - y_{p0}$ as a function of t for $H_0 = 0$ (solid), 1000 A/m (circle), 2000 A/m (rectangle), 3000 A/m (triangle) and 4000 A/m (plus).

3.3.5. Effects of Particle Shape and the Wall. As we discussed in Section 3.2, the particle-wall separation distance and particle aspect ratio are two important factors on the oscillatory motion of the particle. In this section, we investigate the effect of these two factors on particle lateral migration with a magnetic field. Here, the magnetic field strength $H_0 = 2000$ A/m is applied at $\alpha = 0°$. The dimensionless parameter, τ, and the average vertical velocity, U_v, for three different particle aspect ratios are shown in Figure 12(a1) and (a2). As the particle aspect ratio is increased, both τ and U_v increase. The particle aspect ratio represents the degree of deviation from the spherical particle. As the particle shape deviates more from the spherical particle, the asymmetry of particle rotation

becomes more pronounced, and the particle moves up faster. Therefore, particle aspect ratio is an essential factor on particle lateral migration when a magnetic field is applied. Figure 12(b1) and (b2) show the results when the particle is released at different initial particle-wall separation distances. τ is increased but U_v is decreased as y_{p0} is increased from 10 μm to 16 μm. As the particle is at a larger distance away from the wall, the asymmetry of particle rotation becomes more pronounced. However, the particle moves up slower, due to the small amplitude A.

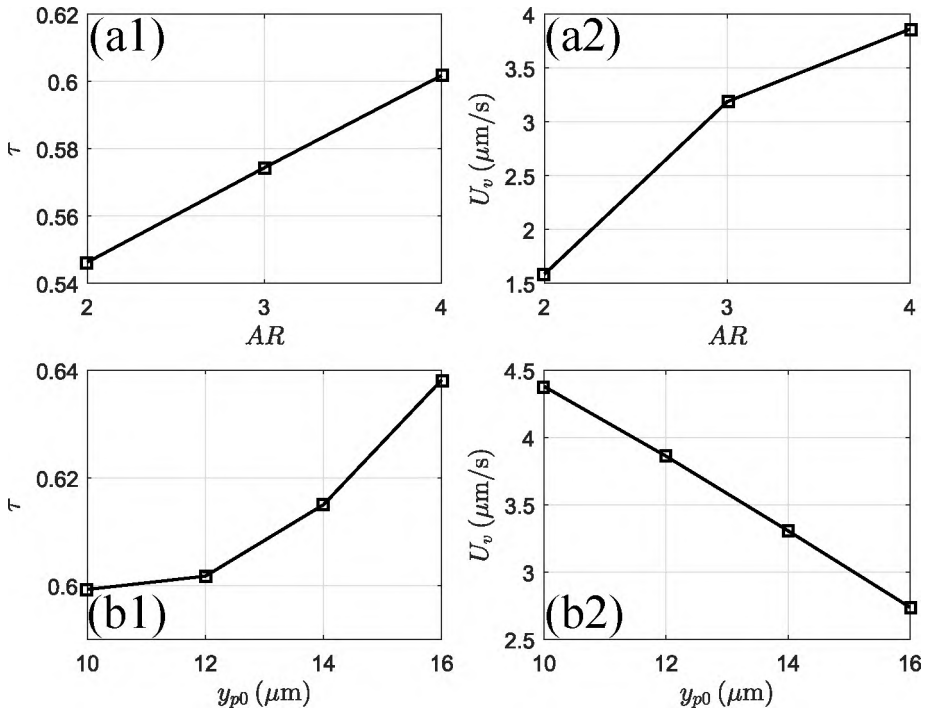

Figure 12. Dependence of (a1) τ and (a2) U_v on particle aspect ratio AR, with the particle is initially located at y_{p0} = 12 μm. Dependence of (b1) τ and (b2) U_v on initial particle-wall separation distances y_{p0} when the particle aspect ratio is AR = 4. The magnetic field strength H_0 = 2000 A/m is applied at α = 0°.

3.4. LATERAL MIGRATION MECHANISM

From previous analysis, we can see that the net lateral migration of the particle depends on the lateral oscillation and the asymmetric rotation. The particle lateral oscillation depends on the particle shape (aspect ratio AR) and the proximity to the wall (initial particle-wall separation distance y_{p0}). The larger deviation from the spherical shape and the closer to the wall are, the more pronounced particle-wall hydrodynamic interaction is (Gavze and Shapiro, 1997). The degree of particle-wall hydrodynamic interaction is characterized by the amplitude A for a fixed particle aspect ratio. The asymmetric rotation of the particle depends on the non-zero magnetic torque acting on the particle, which in turn depends on the field direction and magnitude. The direction of the magnetic field controls the nature of the asymmetry and thus the direction of the net lateral migration. When $\tau > 0.5$, the particle move upwards; when $\tau < 0.5$, the particle move downwards. The strength of the magnetic field controls the speed of the lateral migration. The more τ deviates from 0.5, the larger the migration speed is. In other words, the direction of the magnetic field determines whether $\tau - 0.5$ is positive or negative, and the strength of the magnetic field determines the absolute value of $\tau - 0.5$. Therefore, we use $(\tau - 0.5)$ to characterize the asymmetric rotation of the particle. Based on the above analysis, we propose a scaling relationship, $\Delta y_p \propto (\tau - 0.5)A$ for all particle aspect ratios investigated, AR = 2, 3, 4. As shown in Figure 13, the numerical results and the linear fitted curves are shown as symbols and lines respectively. The agreement between the fitted curves and numerical results confirms the scaling relationships. Our numerical results suggest that it is reasonably applicable when $|\tau - 0.5| < 0.2$ from Figure 13. However, due to the complex particle-wall hydrodynamic interactions, it is difficult to obtain a quantitative expression relating Δy_p to A and $(\tau - 0.5)$. In this work, the linear scaling is fitted very well when $|\tau - 0.5| < 0.2$, which can provide a useful guideline on the effective design for other researchers.

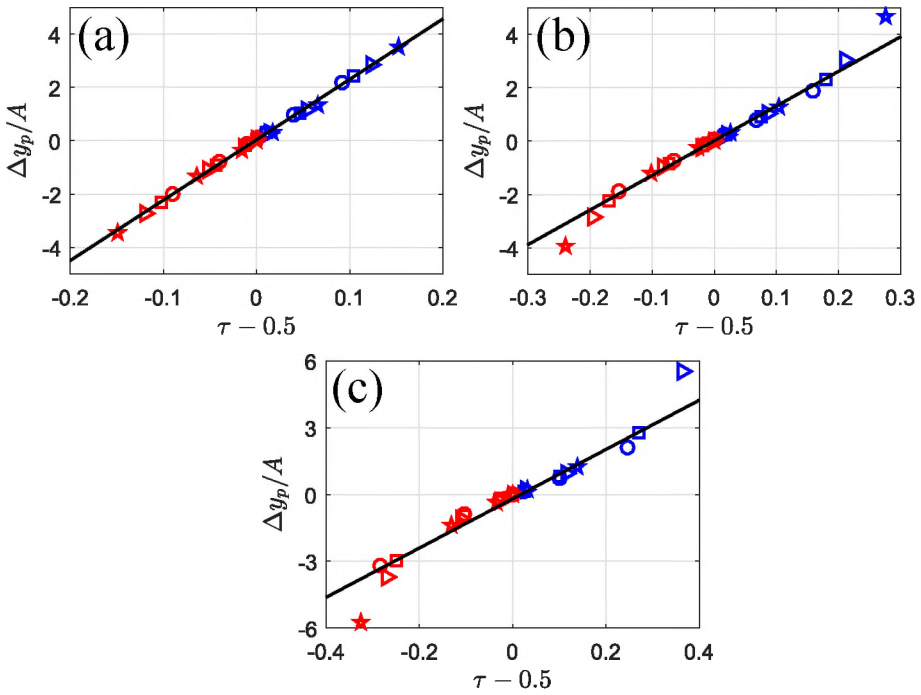

Figure 13. The scaling relationship between $\Delta y_p/A$ and $(\tau - 0.5)$ for AR = 2(a), 3(b) and 4(c). The circle, square, triangle and star stands for numerical results of y_{p0} = 10 μm, 12 μm, 14 μm and 16 μm, respectively. The solid lines are the fitting results.

4. CONCLUSIONS

In this paper, we developed a multi-physics numerical model based on direct numerical simulations to investigate the lateral migration of a paramagnetic elliptical particle in a plane Poiseuille flow under a uniform magnetic field. When the magnetic field is absent, there is a negligible net lateral migration of the particle. When the magnetic field is present, the particle migrates laterally. The direction of the magnetic field controls the asymmetric rotation of the particle and the direction of the net lateral migration. The strength of the magnetic field controls the speed of the net lateral migration. We also investigated the effects of particle aspect ratio and initial particle-wall separation distance, on the lateral migration behaviors of the particles. Based on these findings, we explained the lateral migration

mechanism and proposed a scaling relationship which can provide a guideline on effective design of microfluidic devices to manipulate non-spherical micro-particles and biological cells.

ACKNOWLEDGMENTS

The authors gratefully acknowledge the financial support from the Department of Mechanical and Aerospace Engineering at Missouri University of Science and Technology.

REFERENCES

Ai, Y., Beskok, A., Gauthier, D. T., Joo, S. W., and Qian, S., 'Dc electrokinetic transport of cylindrical cells in straight microchannels,' Biomicrofluidics, 2009a, **3**(4), p. 044110.

Ai, Y., Joo, S. W., Jiang, Y., Xuan, X., and Qian, S., 'Pressure-driven transport of particles through a converging-diverging microchannel,' Biomicrofluidics, 2009b, **3**(2), p. 022404.

Ai, Y. and Qian, S., 'Dc dielectrophoretic particle–particle interactions and their relative motions,' Journal of colloid and interface science, 2010, **346**(2), pp. 448–454.

Ai, Y., Zeng, Z., and Qian, S., 'Direct numerical simulation of ac dielectrophoretic particle–particle interactive motions,' Journal of colloid and interface science, 2014, **417**, pp. 72–79.

Arruebo, M., Fernández-Pacheco, R., Ibarra, M. R., and Santamaría, J., 'Magnetic nanoparticles for drug delivery,' Nano today, 2007, **2**(3), pp. 22–32.

Cao, Q., Li, Z., Wang, Z., and Han, X., 'Rotational motion and lateral migration of an elliptical magnetic particle in a microchannel under a uniform magnetic field,' Microfluidics and Nanofluidics, 2018, **22**(1), p. 3.

Chen, Q., Li, D., Zielinski, J., Kozubowski, L., Lin, J., Wang, M., and Xuan, X., 'Yeast cell fractionation by morphology in dilute ferrofluids,' Biomicrofluidics, 2017, **11**(6), p. 064102.

Chen, S.-D., Pan, T.-W., and Chang, C.-C., 'The motion of a single and multiple neutrally buoyant elliptical cylinders in plane poiseuille flow,' Physics of Fluids, 2012, **24**(10), p. 103302.

Feng, J., Hu, H. H., and Joseph, D. D., 'Direct simulation of initial value problems for the motion of solid bodies in a newtonian fluid. part 2. couette and poiseuille flows,' Journal of fluid mechanics, 1994, **277**, pp. 271–301.

Gavze, E. and Shapiro, M., 'Particles in a shear flow near a solid wall: effect of nonsphericity on forces and velocities,' International Journal of Multiphase Flow, 1997, **23**(1), pp. 155–182.

Gijs, M. A., Lacharme, F., and Lehmann, U., 'Microfluidic applications of magnetic particles for biological analysis and catalysis,' Chemical reviews, 2009, **110**(3), pp. 1518–1563.

Goldsmith, H. and Mason, S., 'Axial migration of particles in poiseuille flow,' Nature, 1961, **190**(4781), pp. 1095–1096.

Hejazian, M., Li, W., and Nguyen, N.-T., 'Lab on a chip for continuous-flow magnetic cell separation,' Lab on a Chip, 2015, **15**(4), pp. 959–970.

Hsu, R. and Ganatos, P., 'Gravitational and zero-drag motion of a spheroid adjacent to an inclined plane at low reynolds number,' Journal of Fluid Mechanics, 1994, **268**, pp. 267–292.

Hu, H. H., Patankar, N. A., and Zhu, M., 'Direct numerical simulations of fluid–solid systems using the arbitrary lagrangian–eulerian technique,' Journal of Computational Physics, 2001, **169**(2), pp. 427–462.

Huang, S.-L., Chen, S.-D., Pan, T.-W., Chang, C.-C., and Chu, C.-C., 'The motion of a neutrally buoyant particle of an elliptic shape in two dimensional shear flow: A numerical study,' Physics of Fluids, 2015, **27**(8), p. 083303.

Jeffery, G. B., 'The motion of ellipsoidal particles immersed in a viscous fluid,' Proceedings of the Royal Society of London A: Mathematical, Physical and Engineering Sciences, 1922, **102**(715), pp. 161–179.

Lee, S.-Y., Ferrari, M., and Decuzzi, P., 'Design of bio-mimetic particles with enhanced vascular interaction,' Journal of biomechanics, 2009a, **42**(12), pp. 1885–1890.

Lee, S.-Y., Ferrari, M., and Decuzzi, P., 'Shaping nano-/micro-particles for enhanced vascular interaction in laminar flows,' Nanotechnology, 2009b, **20**(49), p. 495101.

Martinez, R., Roshchenko, A., Minev, P., and Finlay, W., 'Simulation of enhanced deposition due to magnetic field alignment of ellipsoidal particles in a lung bifurcation,' Journal of aerosol medicine and pulmonary drug delivery, 2013, **26**(1), pp. 31–40.

Matsunaga, D., Meng, F., Zöttl, A., Golestanian, R., and Yeomans, J. M., 'Focusing and sorting of ellipsoidal magnetic particles in microchannels,' Phys. Rev. Lett., 2017a, **119**, p. 198002, doi:10.1103/PhysRevLett.119.198002.

Matsunaga, D., Zöttl, A., Meng, F., Golestanian, R., and Yeomans, J. M., 'Far-field theory for trajectories of magnetic ellipsoids in rectangular and circular channels,' arXiv preprint arXiv:1711.00376, 2017b.

Pamme, N., 'Magnetism and microfluidics,' Lab on a Chip, 2006, **6**(1), pp. 24–38.

Pan, T.-W. and Glowinski, R., 'Direct simulation of the motion of neutrally buoyant circular cylinders in plane poiseuille flow,' Journal of Computational Physics, 2002, **181**(1), pp. 260–279.

Pan, T.-W., Huang, S.-L., Chen, S.-D., Chu, C.-C., and Chang, C.-C., 'A numerical study of the motion of a neutrally buoyant cylinder in two dimensional shear flow,' Computers & Fluids, 2013, **87**, pp. 57–66.

Sinha, A., Ganguly, R., De, A. K., and Puri, I. K., 'Single magnetic particle dynamics in a microchannel,' Physics of Fluids, 2007, **19**(11), p. 117102.

Smistrup, K., Hansen, O., Bruus, H., and Hansen, M. F., 'Magnetic separation in microfluidic systems using microfabricated electromagnets—experiments and simulations,' Journal of Magnetism and Magnetic Materials, 2005, **293**(1), pp. 597–604.

Stratton, J. A., *Electromagnetic theory*, John Wiley & Sons, 2007.

Trevelyan, B. and Mason, S., 'Particle motions in sheared suspensions. i. rotations,' Journal of Colloid Science, 1951, **6**(4), pp. 354–367.

Yang, B. H., Wang, J., Joseph, D. D., Hu, H. H., Pan, T.-W., and Glowinski, R., 'Migration of a sphere in tube flow,' Journal of Fluid Mechanics, 2005, **540**, pp. 109–131.

Yavuz, C. T., Prakash, A., Mayo, J., and Colvin, V. L., 'Magnetic separations: from steel plants to biotechnology,' Chemical Engineering Science, 2009, **64**(10), pp. 2510–2521.

Zhang, J. and Wang, C., 'Study of rotation of ellipsoidal particles in combined simple shear flow and magnetic fields,' COMSOL Conference 2017 Boston, 2017.

Zhou, R., Bai, F., and Wang, C., 'Magnetic separation of microparticles by shape,' Lab on a Chip, 2017a, **17**(3), pp. 401–406.

Zhou, R., Sobecki, C. A., Zhang, J., Zhang, Y., and Wang, C., 'Magnetic control of lateral migration of ellipsoidal microparticles in microscale flows,' Physical Review Applied, 2017b, **8**(2), p. 024019.

Zhou, Y. and Xuan, X., 'Diamagnetic particle separation by shape in ferrofluids,' Applied Physics Letters, 2016, **109**(10), p. 102405.

III. NUMERICAL INVESTIGATION OF ROTATIONAL DYNAMICS OF ELLIPTICAL MAGNETIC MICROPARTICLES IN SHEAR FLOWS

Jie Zhang, Christopher A. Sobeck, Yanzhi Zhang, Cheng Wang

Department of Mechanical & Aerospace Engineering

Department of Mathematics & Statistics

Missouri University of Science and Technology

Rolla, Missouri 65409

Tel: 573–341–4636, Fax: 573–341–4607

Email: wancheng@mst.edu

ABSTRACT

We study the rotational dynamics of magnetic prolate elliptical particles in a simple shear flow subjected to a uniform magnetic field, by using direct numerical simulations based on the finite element method (FEM). Focusing on paramagnetic and ferromagnetic particles, we investigate the effects of the magnetic field strength and direction on their rotational dynamics. In the weak field regime (below a critical field strength), the particles are able to perform complete rotations, and the symmetry property of particle rotational speed are influenced by the direction and strength of the magnetic field. In the strong field regime (above a critical strength), the particles are pinned at steady angles. The steady angle depends on both the direction and strength of the magnetic field. Our results show that paramagnetic and ferromagnetic particles exhibit markedly different rotational dynamics in a uniform magnetic field. The numerical findings are in good agreement with theoretical prediction. Our numerical investigation further reveals drastically different lateral migration behaviors of paramagnetic and ferromagnetic particles in a wall bounded simple shear flow under a uniform magnetic field. These two kinds of particles can thus be separated by

combining a shear flow and a uniform magnetic field. We also study the lateral migration of paramagnetic and ferromagnetic particles in a pressure-driven flow (a more practical flow configuration in microfluidics), and observe similar lateral migration behaviors. These findings demonstrate a simple but useful way to manipulate non-spherical microparticles in microfluidic devices.

Keywords: microfluidics; particle separation; magnetic particles; rotational dynamics; lateral migration

1. INTRODUCTION

Magnetic particles have been used in a vast number of applications including biomedicine (Pankhurst *et al.*, 2003), biological analysis, and chemical catalysis (Gijs *et al.*, 2009; Pamme, 2012). The separation of magnetic microparticles and nanoparticles in microscale fluid environments is one of the most important processes in the systems and platforms based on microfluidic technology (Pamme, 2006, 2012). A magnetic field is a powerful tool to separate magnetic particles or magnetically labelled cells, antigens, and enzymes (Gijs, 2004; Pamme, 2006; Suwa and Watarai, 2011). Most magnetic separation methods are based on magnetophoresis, which manipulates magnetic particles in a viscous fluid by using magnetic forces. To generate the magnetic force, it requires both magnetic particles and a spatially non-uniform field (magnetic field gradient) (Pamme, 2006). There are two different types of magnetophoresis: one is called negative magnetophoresis – manipulating diamagnetic particles in a magnetic fluid such as ferrofluids (Bucak *et al.*, 2011; Winkleman *et al.*, 2007; Zhou *et al.*, 2016; Zhou and Xuan, 2016); the other one is called positive magnetophoresis – separating paramagnetic or ferromagnetic particles in a non-magnetic fluid such as water (Chen *et al.*, 2015; Zborowski *et al.*, 1999).

In contrast to conventional magnetophoresis, several recent experimental, numerical, and theoretical studies (Cao *et al.*, 2018; Matsunaga *et al.*, 2017a,b; Zhang and Wang, 2018; Zhou *et al.*, 2017a,b) have demonstrated a different way to manipulate magnetic non-spherical

particles by a uniform magnetic field in the microchannel. The uniform magnetic field does not generate a magnetic force, but instead generates non-zero magnetic torques due to the non-spherical particle shape. When coupled with particle-wall hydrodynamic interaction (Gavze and Shapiro, 1997; Leal, 1980), the uniform magnetic field alters the rotational dynamics of non-spherical particles, and consequently controls the lateral migration of particles. Experiments preformed by Zhou et al. (Zhou *et al.*, 2017a,b) have demonstrated that a weak uniform magnetic field can separate *paramagnetic* particles in a microchannel pressure-driven flow. The magnetic torque broke the symmetry of the particle rotation. Due to the particle-wall hydrodynamic interaction, the particles migrated laterally towards or away from the wall depending on the direction of magnetic field. By using the finite element method (FEM), Cao et al. (Cao *et al.*, 2018) and Zhang et al. (Zhang and Wang, 2018) investigated the effect of several parameters, such as the strength and direction of the magnetic field, particle aspect ratio, and flow rate, on the lateral migration of the *paramagnetic* particles in microchannels. In another study, Matsunaga et al. (Matsunaga *et al.*, 2017a,b) proposed a far-field theory and used the boundary element method to demonstrate that a strong uniform magnetic field can separate the *ferromagnetic* particles in both simple shear flow near the wall and Poiseuille flow between two walls. In this method, ferromagnetic particles are pinned at steady angles and the lateral migration results from particle-wall hydrodynamic interactions as well.

Previous investigations have either studied the lateral migration of *paramagnetic* particles under a weak magnetic field (Cao *et al.*, 2018; Zhang and Wang, 2018; Zhou *et al.*, 2017a,b) or *ferromagnetic* particles under a strong magnetic field (Matsunaga *et al.*, 2017a,b). A comprehensive understanding on the difference of the lateral migration mechanism between the paramagnetic and ferromagnetic particles under both the weak and strong magnetic fields is absent. In our previous theoretical work (Sobecki *et al.*, 2018), we theoretically analyzed the difference of particle rotational dynamics between the paramagnetic and ferromagnetic particles in a simple shear flow under a magnetic field. However, due to the inherent

complexity of particle dynamics in bounded flows, systematic theoretical analysis is difficult. In this work, we systematically investigate the rotational dynamics of both paramagnetic and ferromagnetic elliptical particles under a uniform magnetic field in simple shear and bounded flows by using direct numerical simulations. Our results suggest that the difference in magnetic properties leads to markedly different rotational dynamics as well as lateral migration. Based on these insights, we demonstrate feasible ways to separate these two kinds of magnetic particles in a pressure-driven flow configuration, which are commonly used in practical applications such as microfluidic devices.

This paper is organized as follows. Section 2 presents the numerical method including mathematical modeling, material parameters used in the simulation, and validation of the numerical method. Section 3 presents a brief theoretical analysis for comparing the numerical and theoretical results in following sections. Section 4 and 5 numerically investigate the rotational dynamics of paramagnetic and ferromagnetic particles in a simple shear flow under weak and strong magnetic fields, and compare the numerical and theoretical results. Based on the discussion in Section 4 and 5, Section 6 studies the lateral migration of paramagnetic and ferromagnetic particles in a simple shear flow near the wall. Finally, in Section 7, the simulation for the lateral migration of paramagnetic and ferromagnetic particles in a microchannel pressure-driven flow under both a weak and strong magnetic fields is preformed to demonstrate particle separation in more practical flows.

2. NUMERICAL METHOD

2.1. MATHEMATICAL MODEL

We consider a rigid prolate elliptical particle suspended in a simple shear flow as shown in Figure 1. The computational domain, Ω, is bounded by the boundary, ABCD, and particle surface, Γ. The width and length of the computational domain are W and L, respectively. The center of the particle is set to be the center of the computational domain.

The particle aspect ratio is $r_p = a/b$, where a and b are the major and minor semi-axis lengths of particles, respectively. The orientation angle of the particle, ϕ, is the angle between the major axis of the particle and the positive y axis. The background flow is a simple shear flow, where the velocity $\mathbf{u}_\infty = \dot{\gamma} y \mathbf{e}_x$ is imposed, with $\dot{\gamma}$ being the shear rate. A uniform magnetic field, $\mathbf{H}_0$, is applied at an arbitrary direction, denoted by α. The fluid is assumed

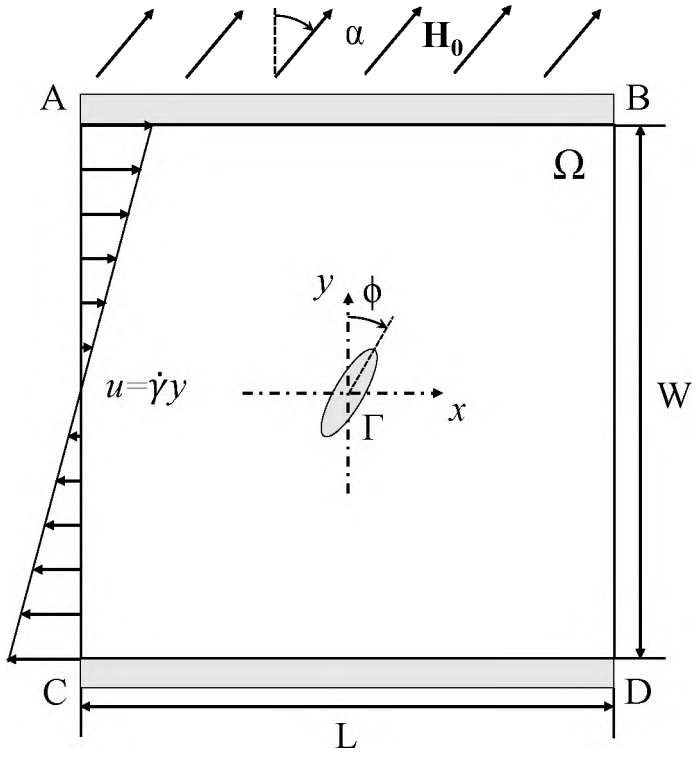

Figure 1. Schematic of the numerical model of an elliptical particle suspended in a simple shear flow under a uniform magnetic field $\mathbf{H}_0$. The fluid domain and particle surface are Ω and Γ, respectively. The orientation angle of the particle is denoted by ϕ.

to be incompressible, Newtonian, and non-magnetic. The transient flow field is governed by the continuity equation and Navier-Stokes equation:

$$\nabla \cdot \mathbf{u} = 0, \tag{1}$$

$$\rho_f \left[\frac{\partial \mathbf{u}}{\partial t} + (\mathbf{u} \cdot \nabla)\, \mathbf{u} \right] = -\nabla p + \nabla \cdot \eta_f \left(\nabla \mathbf{u} + (\nabla \mathbf{u})^T \right), \tag{2}$$

where $\mathbf{u}$ is the velocity vector, ρ_f and η_f are the density and dynamic viscosity of the fluid, respectively, p is the pressure, and t is the time.

To impose simple shear, the velocities at the top (AB) and bottom (CD) walls are set to be $\pm\frac{1}{2}\dot{\gamma} W \mathbf{e}_x$ respectively. The boundaries AC and BD are set to periodic flow conditions. With the no-slip condition applied on the particle surface, the fluid velocities on the particle surface Γ are expressed as:

$$\mathbf{u} = \mathbf{U}_p + \boldsymbol{\omega}_p \times (\mathbf{x}_s - \mathbf{x}_p), \tag{3}$$

where $\mathbf{U}_p$ and $\boldsymbol{\omega}_p$ are the translational and rotational velocities of particle, respectively, $\mathbf{x}_s$ and $\mathbf{x}_p$ are the position vectors of the surface and the center of the particle. The hydrodynamic force and torque acting on the particle are:

$$\mathbf{F}_h = \int (\boldsymbol{\tau}_h \cdot \mathbf{n}) d\Gamma, \tag{4}$$

$$\mathbf{L}_h = \int (\boldsymbol{\tau}_h \times (\mathbf{x}_s - \mathbf{x}_p) \cdot \mathbf{n}) d\Gamma, \tag{5}$$

where $\boldsymbol{\tau}_h = \eta_f \left(\nabla \mathbf{u} + (\nabla \mathbf{u})^T \right)$ is the hydrodynamic stress tensor on the particle surface Γ.

The magnetic field is governed by the static Maxwell equations:

$$\nabla \times \mathbf{H} = 0, \tag{6}$$

$$\nabla \cdot \mathbf{B} = 0, \tag{7}$$

where $\mathbf{H}$ and $\mathbf{B}$ are the magnetic field and the magnetic flux density, respectively. To impose a uniform magnetic field, a magnetic scalar potential difference is set across boundaries AB and CD, with a zero magnetic potential $V_m = 0$ on AB and a magnetic potential $V_m = V_{m0}$ on CD. Magnetic insulation condition is applied on boundaries AC and BD.

Assuming that the particle is homogeneous and isotropic in magnetic properties, the magnetic force acting on the particle, due to a uniform magnetic field, is zero (Stratton, 2007). The magnetic torque acting on a magnetic particle is expressed as (Stratton, 2007):

$$\mathbf{L}_m = \mu_0(\mathbf{m} \times \mathbf{H}_0), \tag{8}$$

where $\mathbf{m}$ is the magnetic moment of the particle, and μ_0 is the magnetic permeability of the vacuum.

For two-dimensional elliptical particles, the rotational motion is in the x–y plane, thus $\omega_p = \omega_p \mathbf{e}_z$, $\mathbf{L}_h = L_h \mathbf{e}_z$, and $\mathbf{L}_m = L_m \mathbf{e}_z$. The translation and rotation of particles are governed by Newton's second law and Euler's equation:

$$m_p \frac{d\mathbf{U}_p}{dt} = \mathbf{F}_h, \tag{9}$$

$$I_p \frac{d\omega_p}{dt} = L_h + L_m, \tag{10}$$

where m_p and I_p are the mass and the moment of inertia of the particle, respectively.

The position of the particle center $\mathbf{x}_p(t) = (x_p, y_p)$ and the orientation ϕ of the particle are expressed as:

$$\mathbf{x}_p(t) = \mathbf{x}_p(0) + \int_0^t \mathbf{U}_p(t')dt', \tag{11}$$

$$\phi(t) = \phi(0) + \int_0^t \omega_p(t')dt', \tag{12}$$

where $\mathbf{x}_p(0)$ and $\phi(0)$ are the initial position and orientation of the particle.

The dynamic motions of the particle, the flow field, and the magnetic field are coupled via Equations (3)-(5) and (8)-(10). We use direct numerical simulation (DNS) based on FEM and arbitrary Lagrangian-Eulerian(ALE) method to simultaneously calculate the flow field and particle motion. Similar methodologies have been successfully used by Hu et al. (Hu *et al.*, 2001) and Ai et al. (Ai *et al.*, 2009a,b; Ai and Qian, 2010; Ai *et al.*, 2014).

The numerical model is implemented and solved with a commercial FEM solver (COMSOL Multiphysics). First, we use a stationary solver to calculate the magnetic field inside and outside of the particle and compute the magnetic torque acting on the particle. Then, the two-way coupling of fluid-particle interaction model is solved by using a time-dependent solver and by importing the previously determined magnetic torque. The deformation of the computational domain is solved with the Moving Mesh interface based on the ALE algorithm. The meshes of fluid domain are free to deform, while the particle domain are determined by its trajectory and orientation. As the mesh deforms, the mesh quality is decreased. When the quality value is decreased to 0.2, the re-meshing process initiates. Similar modeling strategy has been successfully carried out in our previous work (Zhang and Wang, 2018) and other work e.g., Cao et al (Cao *et al.*, 2018). Quadratic triangular elements are employed in this simulation. A fine mesh around the particle and a finer mesh around the tip of the particle are created to accurately calculate the hydrodynamic force and torque acting on the particle. The total number of elements was about 7,000 in the fluid domain Ω, and about 130 elements were used to discretize the particle surface Γ.

2.2. MATERIAL PROPERTIES

In this numerical study, water is used as the nonmagnetic fluid ($\chi_f = 0$), which has a density $\rho_f = 1000$ kg/m^3 and a dynamic viscosity $\eta_f = 1 \times 10^{-3}$ Pa·s. The shear rate of the flow is kept constant, such that $\dot{\gamma} = 200$ s^{-1}. The particle is assumed to be polystyrene particles containing magnetic nanoparticles, similar to those used in earlier experiments (Zhou *et al.*, 2017a,b), which could be either paramagnetic or ferromagnetic particles. The density of the particle is $\rho_p = 1100$ kg/m^3. Here, the particle motion is in the x-y plane and the inertia effect is negligible, thus the density difference between the particle and fluid has negligible effect on the particle dynamics. The equivalent diameter of the particle used in this simulation is $d = 7\ \mu$m and the particle aspect ratio $r_p = 4$, thus the major and minor

semi-axis lengths of particles are $a = 7$ μm and $b = 1.75$ μm. We consider two kinds of magnetic particles: paramagnetic particles with $\chi_p = 0.26$ and ferromagnetic particle with permanent magnetization $\boldsymbol{M}_0 = 2000$A/m.

2.3. VALIDATION OF NUMERICAL METHOD

In this section, we present validation of the numerical method by comparing the results with Jeffery's theory, which describes the periodic rotation of an axisymmetric ellipsoidal particle in a simple shear unbounded flow (Jeffery, 1922). Without a magnetic field, the ferromagnetic and paramagnetic particles behave the same way. Here, the width and length of the computational domain are $W = L = 150$ μm, which will also be used in the simulations in Section 4 and 5. The confinement effects the walls are negligible due to the large computational domain relative to the particle size. The period of the particle rotation, T^J, is defined as the time taken by the particle to rotate from $\phi = 0°$ to $\phi = 360°$, and $T^J = 2\pi/\dot{\gamma}(r_p + 1/r_p)$ (Jeffery, 1922). Due to the fore-aft symmetry of the particle, we define T_0^J as the time taken for rotation from 0° to 180°, i.e., $T_0^J = T^J/2$. Note that for ease of visualizing results, we use both 'degree' and 'radian' as units for angles in the remaining sections of this paper.

Figure 2 compares the time evolution of particle orientation angle predicted by Jeffery's theory and our simulation for a particle with $r_p = 4$ in a simple shear flow ($\dot{\gamma} = 200$ s^{-1}). The theoretical value of T_0^J from Jeffery's theory is 0.0668 s, while the period obtained in our FEM simulation is 0.0670 s. The relative error is 0.3%, suggesting that the simulation has excellent agreement with the theory. Therefore, this simulation method has been validated to be sufficiently accurate to study the dynamics of the particle in a simple shear flow.

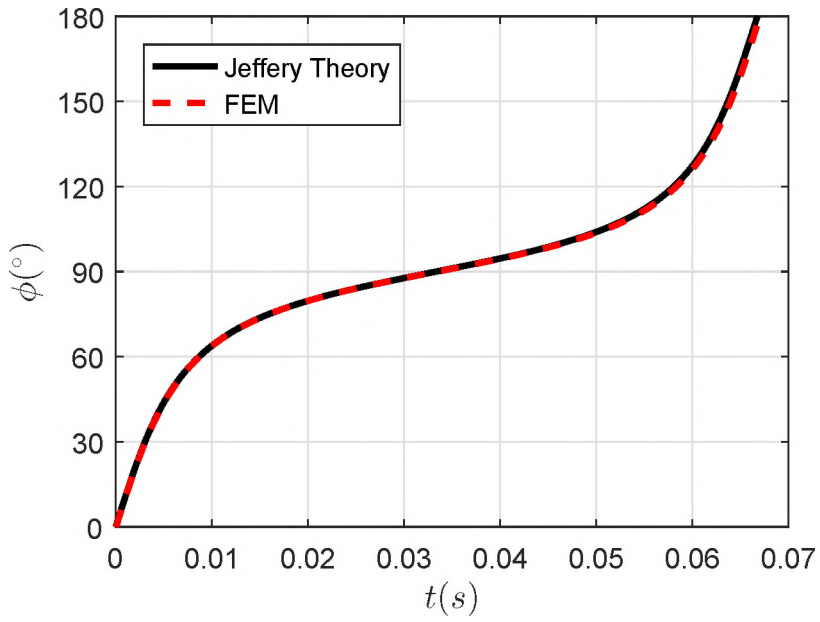

Figure 2. Comparison between the FEM simulation and Jeffery's theory for particle aspect ratio $r_p = 4$ and the shear rate $\dot{\gamma} = 200s^{-1}$.

Table 1. Four meshes for grid independence analysis

	Domain elements	Boundary elements on particle surface
Mesh 1	3734	48
Mesh 2	4812	76
Mesh 3	6952	124
Mesh 4	7548	148

2.4. GRID INDEPENDENCE ANALYSIS

We perform grid independence analysis to determine the appropriate meshes for cost-effective numerical simulations without comprising accuracy. The results for four different meshes in a simple shear flow in the absence of the magnetic field are shown in Table 1 and Figure 3. As can be seen, the convergence of numerical results is considered sufficient when the domain element number is larger than 6,952 and the boundary element

number on the particle surface is larger than 124. In this work, we use about 7500 elements in the computational domain Ω in Figure 1, and about 150 elements on the particle surface Γ, which give reasonably accurate results.

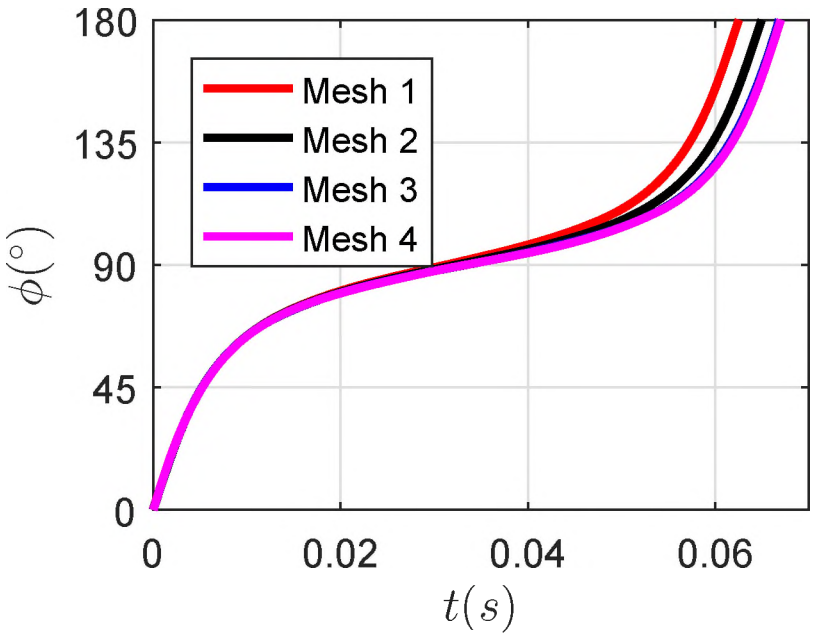

Figure 3. Grid independence analysis: particle orientation ϕ as a function of time t for particle aspect ratio $r_p = 4$ and the shear rate $\dot{\gamma} = 200s^{-1}$.

3. THEORETICAL ANALYSIS

In this section, we briefly present the theoretical analysis pertaining to the rotational dynamics of paramagnetic and ferromagnetic particles. We also define relevant dimensionless parameters as well as physical quantities to characterize the rotational behaviors.

Assuming a small particle Reynolds number, (i.e., $\mathrm{Re}_p = \rho_p d^2\dot{\gamma}/\eta_f \ll 1$, justified by typical microfluidic experimental conditions), the particle inertia is negligible and the particle motion is quasi-steady, similar to the previous studies (Allan and Mason, 1962;

Chaffey and Mason, 1964; Okagawa *et al.*, 1974). Equation (10) is then reduced to:

$$L_h + L_m = 0. \tag{13}$$

Under the assumption of Stokes flow, the hydrodynamic torque in the xy plane acting on an ellipsoidal particle in a simple shear flow with a shear rate $\dot{\gamma}$ is (Jeffery, 1922; Okagawa *et al.*, 1974):

$$L_h = \frac{8\pi\eta_f a^3(r_p^2+1)}{3r_p^2(D_{xx}+D_{yy})}\left(\frac{r_p^2-1}{r_p^2+1}\frac{\cos(2\phi)}{2}\dot{\gamma} + \frac{\dot{\gamma}}{2} - \omega_p\right), \tag{14}$$

where $\omega_p = d\phi/dt$ is the particle rotational speed, $D_{xx} = 1 - A$ and $D_{yy} = A/2$ are the ellipsoidal demagnetizing factors, and $A = \frac{r_p^2}{r_p^2-1} - \frac{r_p \cos^{-1}(r_p)}{(r_p^2-1)^{3/2}}$ for a prolate ellipsoid (Okagawa *et al.*, 1974). When the magnetic field is absent, we obtain the rotational speed due to the hydrodynamic torque only:

$$\omega_h = \frac{r_p^2\cos(\phi)^2 + \sin^2(\phi)}{r_p^2+1}\dot{\gamma}, \tag{15}$$

which is the Jeffery equation.

When subjected to an external magnetic field, a magnetic moment is induced in a *paramagnetic* particle, thus resulting a magnetic torque. According to previous works (Shine and Armstrong, 1987; Zhou *et al.*, 2017a,b), the torque experienced by the paramagnetic particle is

$$L_{mp} = -V_p\frac{\mu_0\chi_p^2 H_0^2(D_{yy}-D_{xx})\sin(2(\phi-\alpha))}{2(\chi_p D_{xx}+1)(\chi_p D_{yy}+1)}, \tag{16}$$

where V_p is the volume of the particle. Substituting Equations (14) and (16) into Equation (13), the total particle rotational speed is obtained:

$$\omega_p = \frac{d\phi}{dt} = \frac{r_p^2\cos(\phi)^2 + \sin^2(\phi) - S_p\sin(2(\phi-\alpha))}{r_p^2+1}\dot{\gamma}, \tag{17}$$

where

$$S_p = \frac{\mu_0 \chi_p^2 H_0^2 (r_p^2 D_{xx} + D_{yy})(D_{yy} - D_{xx})}{4\dot{\gamma}\eta_f (1 + \chi_p D_{xx})(1 + \chi_p D_{yy})}. \tag{18}$$

The dimensionless parameter S_p measures the relative strength between the magnetic and hydrodynamic effects on a paramagnetic particle (Zhou *et al.*, 2017a,b).

For a *ferromagnetic* particle, it is assumed that the magnetization of the particle, $\mathbf{M_0}$ (its magnitude denoted by M_0) is parallel to the particle's major axis. The magnetic moment of the particle $\mathbf{m} = V_p \mathbf{M_0} = V_p M_0 (\sin(\phi), \cos(\phi), 0)$. Thus, Equation (8) can be written as $\mathbf{L}_{mf} = \mu_0 V_p (\mathbf{M}_0 \times \mathbf{H}_0) = L_{mf} \mathbf{e}_z$, with the magnitude of the torque (Shine and Armstrong, 1987),

$$L_{mf} = -\mu_0 V_p M_0 H_0 \sin(\phi - \alpha). \tag{19}$$

We obtain the total rotational speed of a ferromagnetic particle in a simple shear flow (Sobecki *et al.*, 2018):

$$\omega_p = \frac{d\phi}{dt} = \frac{r_p^2 \cos(\phi)^2 + \sin^2(\phi) - S_f \sin(\phi - \alpha)}{r_p^2 + 1} \dot{\gamma}, \tag{20}$$

where

$$S_f = \frac{\mu_0 M_0 H_0 (r_p^2 D_{xx} + D_{yy})}{2\eta_f \dot{\gamma}} \tag{21}$$

is a dimensionless parameter that measures the relative strength between the magnetic and hydrodynamic effects on a ferromagnetic particle.

As can be seen in equations (17) and (20), the particle rotational behaviour depends on the direction of magnetic field α and the parameters S_p or S_f. When S_p or S_f is increased to a large enough value, the particle rotation is impeded. In our previous work (Zhou *et al.*, 2017b), we defined S_{cr} as the critical value of S for the existence of real solutions to $\omega_p = 0$. When $S \geq S_{cr}$, the particle is impeded at a certain steady angle ϕ_s, and we define this field as the strong magnetic field. When $S < S_{cr}$, the particle is able to perform full rotations, so

we define this field as the weak magnetic field. For simplicity of notation, in the following sections, we use S to represent either S_p for paramagnetic particles or S_f for ferromagnetic particles.

The critical relative strength, S_{cr}, can be calculated from the Equation (17) for paramagnetic particles and the Equation (20) for ferromagnetic particles. The values of S_{cr} for $r_p = 4$ is shown in Table 2 for various magnetic field directions (α) (Sobecki *et al.*, 2018).

In the weak field regime, to better compare the difference between paramagnetic and ferromagnetic particles, we define the period of rotation as the time taken by the particle to rotate from 0 to 2π (or 360°) as $T = T_1 + T_2$ with:

$$T = \int_0^{2\pi} \frac{d\phi}{\omega_p}, \qquad T_1 = \int_0^{\pi} \frac{d\phi}{\omega_p}, \qquad T_2 = \int_{\pi}^{2\pi} \frac{d\phi}{\omega_p}. \tag{22}$$

In our previous work (Zhou *et al.*, 2017b), due to $\pi(180°)$ period of the paramagnetic particle, we defined a ratio parameter,

$$\tau_1 = \int_0^{\pi/2} \frac{d\phi}{\omega_p} \Big/ \int_0^{\pi} \frac{d\phi}{\omega_p}, \tag{23}$$

to characterize the symmetry property of the paramagnetic particle rotation. However, the ferromagnetic particle rotates periodically with a period of 2π (or 360°), thus we define an additional ratio parameter:

$$\tau_2 = \int_{\pi}^{3\pi/2} \frac{d\phi}{\omega_p} \Big/ \int_{\pi}^{2\pi} \frac{d\phi}{\omega_p}. \tag{24}$$

We use the average of τ_1 and τ_2 as τ to characterize the overall symmetry property of the particle rotation, that is,

$$\tau = \frac{\tau_1 + \tau_2}{2}. \tag{25}$$

As can be seen, for the paramagnetic particle, $\tau_1 = \tau_2 = \tau$.

Table 2. The critical strength, S_{cr}, calculated for paramagnetic and ferromagnentic particles with $r_p = 4$, and different α (Sobecki *et al.*, 2018).

$\alpha(^\circ)$	0	45	90	135	180	225	270	315
Paramagnetic	4	1	4	16	4	1	4	16
Ferromagnetic	1	1.38	7.75	1.38	1	1.38	7.75	1.38

In the following sections, we will investigate the difference of rotational dynamics between paramagnetic and ferromagnetic particles by using systematic numerical simulations under both weak and strong magnetic fields. Specifically, we will study the effect of magnetic field on the period of rotation, symmetry properties of the particle rotation, and impeded angles. In addition, the numerical and theoretical results are compared and discussed.

4. WEAK MAGNETIC FIELD

We will focus on the rotational dynamics of paramagnetic and ferromagnetic particles in the presence of a weak magnetic field ($S < S_{cr}$). In this regime, both particles are able to perform complete rotations. However, the magnetic field will affect their rotation differently because the the magnetic torques have different dependence on the parameter $(\phi - \alpha)$ as in Equations (16) and (19).

4.1. PARAMAGNETIC PARTICLES

First, we discuss the rotational dynamics of paramagnetic particle in a weak magnetic field. The rotational motion of the paramagnetic magnetic particle with $r_p = 4$ when the magnetic field is applied perpendicular to the flow direction ($\alpha = 0^\circ$) is shown in Figure 4. Figure 4(a) shows the time evolution of orientation angle of the particle, ϕ, with time t when the relative strength S is increased from 0 to 5.04. As can be seen, the period of rotation increases with an increasing S. With $S \approx 5.04$, the particle is impeded at a steady angle $\phi_s = 61.56^\circ$. The numerical results are in quantitative agreement with the prediction

(S_{cr} = 4) from our previous theory (Zhou *et al.*, 2017b). We study the dimensionless parameters τ_1 and τ_2 in Figure 4(b) and (c). The numerical results show that $\tau_1 = \tau_2 = \tau$ for the paramagnetic particle, independent of the magnetic strength $S < S_{cr}$, which is consistent with the theoretical results in Section 3. Thus, we only discuss τ in the remaining of this section.

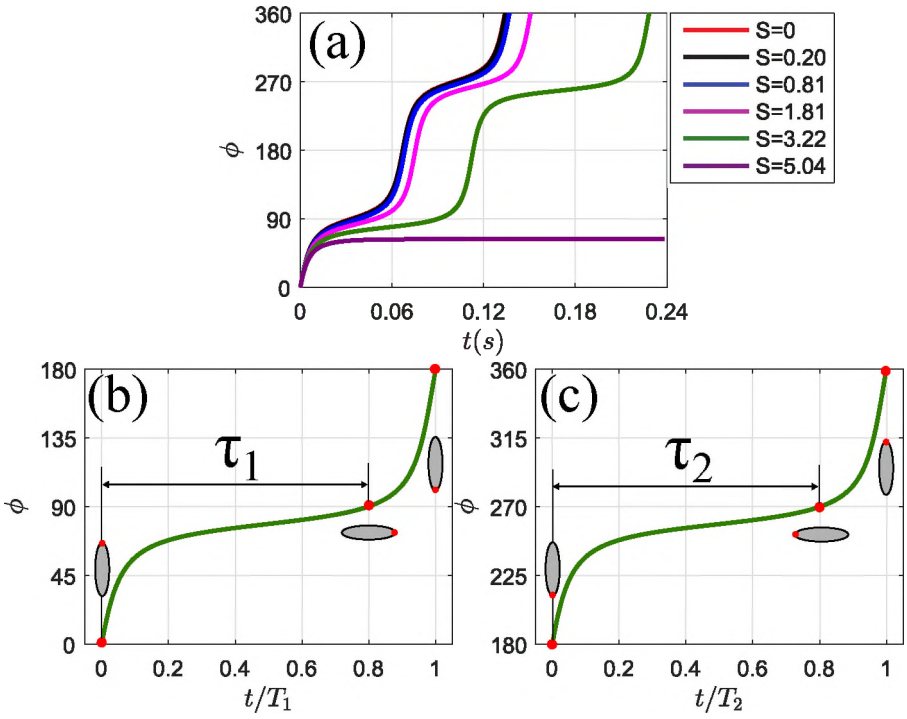

Figure 4. Rotation of the paramagnetic magnetic particle (r_p = 4) when the magnetic field is applied perpendicular to the flow direction ($\alpha = 0°$). (a) The times evolution of orientation angle, ϕ; (b) The evolution of orientation angle, ϕ, with the dimensionless time, t/T_1; (c) The evolution of orientation angle, ϕ, with the dimensionless time, t/T_2. T_1 and T_2 denote times taken by the particle to rotate from 0° to 180° and from 180° to 360°, respectively.

The effect of the magnetic field on the period of rotation is shown in Figure 5. To better illustrate this effect, the dimensionless period is defined by normalizing T with the Jeffery period T^J. We investigate four different directions of the magnetic field. At each direction, the dimensionless period changing with magnetic field strength S is studied. The

symbols represent the numerical results and the solid lines are the theoretical predictions from Equation (22). We observe that the dimensionless period, T/T^J, increases monotonically with an increase of S when the magnetic field is applied at $\alpha = 0°$(a), $\alpha = 45°$(b), and $\alpha = 90°$(c). When the magnetic field is applied at $\alpha = 135°$(d), the dimensionless period, T/T^J, decreases first, and then increases. Furthermore, these numerical results are in quantitative agreement with those when the paramagnetic particle is transported in a pressure-driven flow (Zhang and Wang, 2018). Additionally, the numerical results are in a very good agreement with the theoretical prediction.

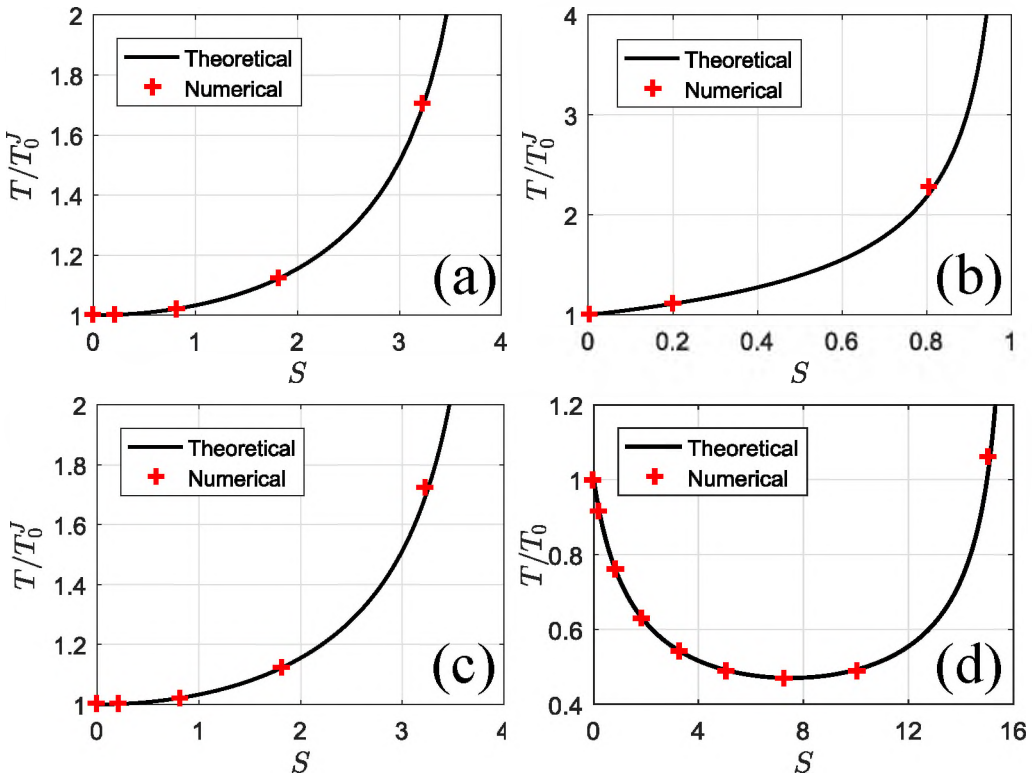

Figure 5. The dimensionless period, T/T^J, varies with the dimensionless magnetic field strength, S when the magnetic field is applied at $\alpha = 0°$(a), $\alpha = 45°$(b), $\alpha = 90°$(c) and $\alpha = 135°$(d) for the paramagnetic particle.

Figure 6 shows the dimensionless parameter, τ, as a function of S when the magnetic field is applied at $\alpha = 0°$, $\alpha = 45°$, $\alpha = 90°$ and $\alpha = 135°$. When the field is applied at $\alpha = 0°$ and $90°$, as can be seen in Figure 6 (a) and (c), τ deviates further from 0.5 as S is increased, meaning the asymmetry of the particle rotation becomes more pronounced. Interestingly, when the magnetic field is applied at $\alpha = 45°$ and $135°$ as can be seen in Figure 6 (b) and (d), τ is always equal to 0.5, independent of the strength S, meaning the particle rotation is always symmetric with respect to $\phi = 90°$ and $270°$. The numerical simulation results have a remarkable agreement with the theoretical results.

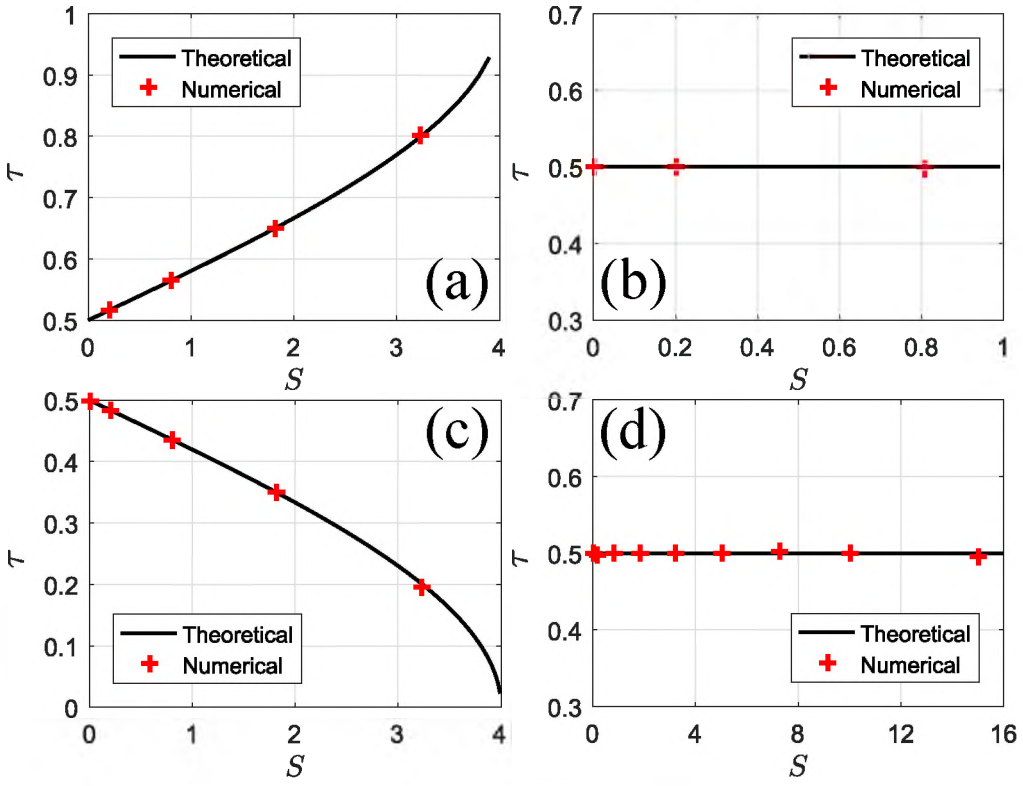

Figure 6. The dimensionless parameter, τ, varies with the dimensionless magnetic field strength, S when the magnetic field is applied at $\alpha = 0°$(a), $\alpha = 45°$(b), $\alpha = 90°$(c) and $\alpha = 135°$(d) for the paramagnetic particle.

4.2. FERROMAGNETIC PARTICLES

We now look at the rotational dynamics of a ferromagnetic particle under the weak magnetic field regime. Because the rotation of ferromagnetic particle has a period of 2π (or 360°) in ϕ, we perform simulations with the magnetic field applied at $\alpha = 0°$, 45°, 90°, 135°, 180°, 225°, 270° and 315°. Figure 7 shows the dimensionless period, T/T^J, changing with the dimensionless magnetic field strength, S, when the magnetic field is applied at these eight angles. As we can see, the dimensionless period of rotation, T/T^J, increases monotonically with an increase of S at all directions of the magnetic field, which is different from the phenomena observed in Figure 6 for paramagnetic particles. When the magnetic field is applied at 135°, T/T^J is decreased first and then increased monnotonically with increasing S for a paramagnetic particle, but for a ferromagnetic particle, T/T^J is increased with increasing S. The numerical simulation results show remarkable agreement with the theoretical results.

The dimensionless parameter, τ, depends on the direction of the magnetic field, α, and field strength, S, as shown shown in Figure 8. As can be seen from Figure 8(a) and (e), when the magnetic field is applied at $\alpha = 0°$ and 180° , $\tau_1 = \tau_2 = \tau = 0.5$ as S is increased, which is different from the paramagnetic particle in Section 4.1 where $\tau_1 = \tau_2 = \tau > 0.5$ and increases with increasing S. Note that paramagnetic particles behave the same when the magnetic field is applied at $\alpha = 180°$ and $\alpha = 0°$. When the magnetic field is applied at $\alpha = 90°$ as shown in Figure 8(c), $\tau_1 < 0.5$, $\tau_2 > 0.5$, and both deviate more from 0.5 with increasing S, but τ remains 0.5. Similar results are observed when the magnetic field is applied at $\alpha = 270°$ as shown in Figure 8(g). In this case, $\tau_1 > 0.5$, $\tau_2 < 0.5$, and $\tau = 0.5$ for all values of S. These results are different from the paramagnetic particle in Section 4.1 where $\tau_1 = \tau_2 = \tau < 0.5$ and are decreased with increasing S.

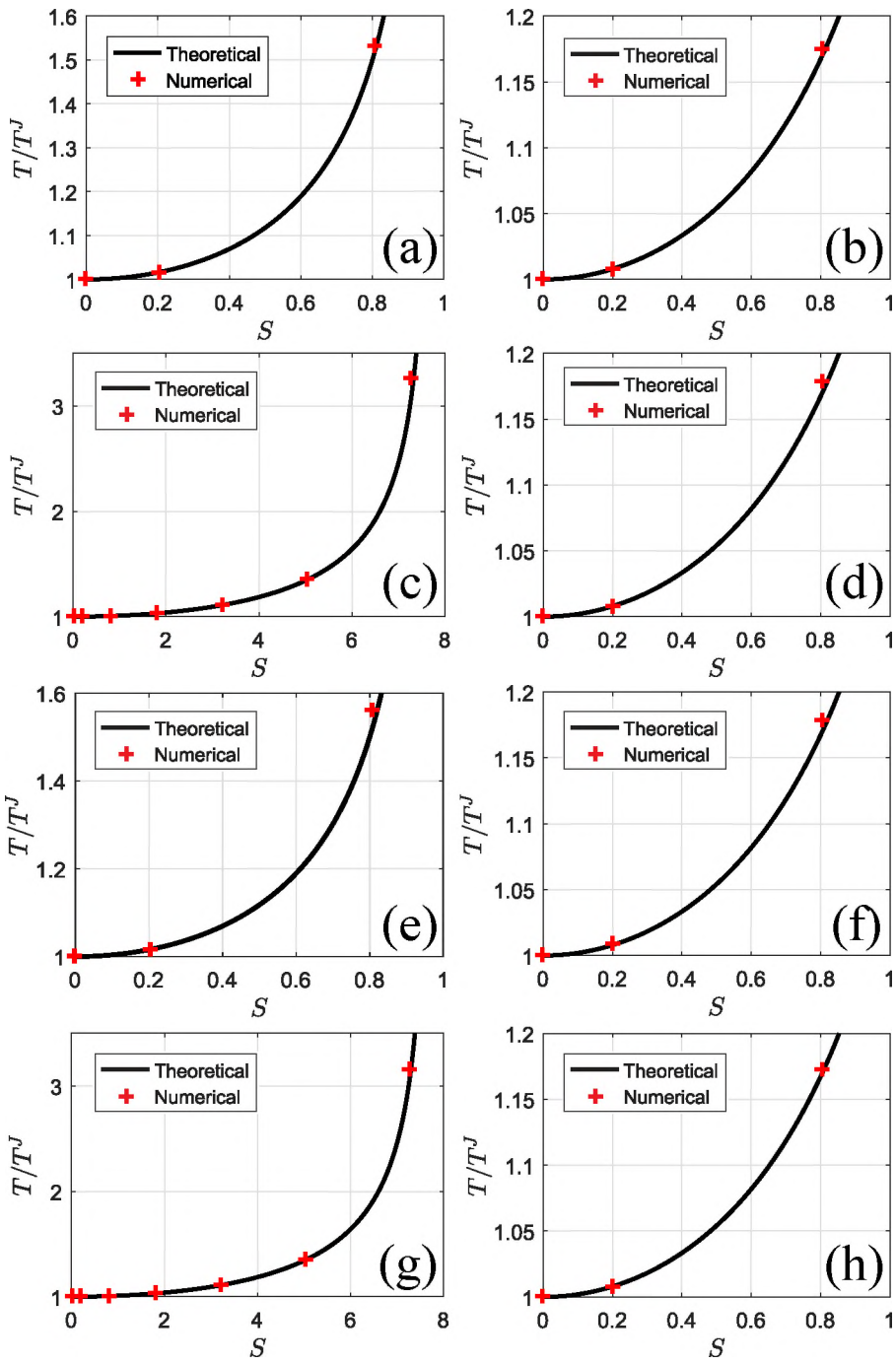

Figure 7. The dimensionless period, T/T^J, varies with the dimensionless magnetic field strength, S, when the magnetic field is applied at $\alpha = 0°$(a), $\alpha = 45°$(b), $\alpha = 90°$(c), $\alpha = 135°$(d), $\alpha = 180°$(e), $\alpha = 225°$(f), $\alpha = 270°$(g) and $\alpha = 315°$(h) for the ferromagnetic particle.

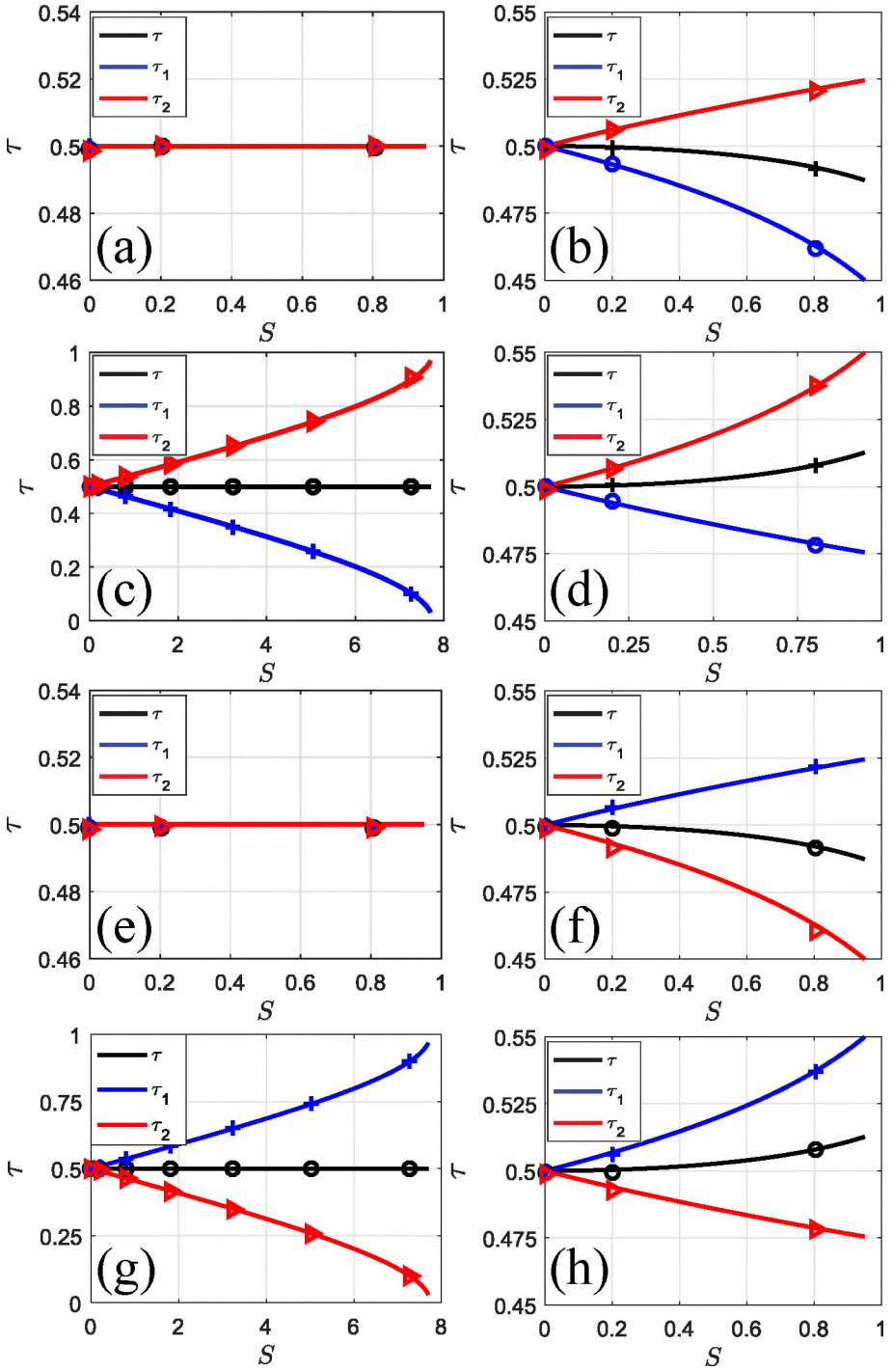

Figure 8. The dimensionless parameter, τ, varies with the dimensionless magnetic field strength,S, when the magnetic field is applied at $\alpha = 0°$(a), $\alpha = 45°$(b), $\alpha = 90°$(c), $\alpha = 135°$(d), $\alpha = 180°$(e), $\alpha = 225°$(f), $\alpha = 270°$(g) and $\alpha = 315°$(h) for ferromagnetic particle.

When the magnetic field is applied at $\alpha = 45°$, $\tau_1 < 0.5$, $\tau_2 > 0.5$, and $\tau < 0.5$; When the magnetic field is applied at $\alpha = 135°$, $\tau_1 < 0.5$, $\tau_2 > 0.5$, but $\tau > 0.5$; When the magnetic field is applied at $\alpha = 225°$, $\tau_1 > 0.5$, $\tau_2 < 0.5$, and $\tau < 0.5$; When the magnetic field is applied at $\alpha = 315°$, $\tau_1 > 0.5$, $\tau_2 < 0.5$, but $\tau > 0.5$. These three parameters deviate further away from 0.5 with increasing S when the magnetic field is applied at $\alpha = 45°$, 135°, 225° and 315°, which are different from the paramagnetic particle in Section 4.1, where $\tau_1 = \tau_2 = \tau = 0.5$ in the weak field regime.

5. STRONG MAGNETIC FIELD

As we explained earlier, the particle could not have a full rotation when the magnetic field strength is increased to a certain value. So, in this section, we will focus on the impeded steady angles of paramagnetic and ferromagnetic particles in the presence of a strong magnetic field.

5.1. PARAMAGNETIC PARTICLES

We first examine the rotational dynamics of a paramagnetic particle under a strong magnetic field. Figure 9 shows the evolution of particle orientation angle, ϕ with time, t, and the corresponding impeded angles for different magnetic field strengths and directions. As can be seen, for a fixed magnetic field direction, when the relative strength S is increased, the impeded angle, ϕ_s, is decreased; for a fixed relative strength, when the magnetic field direction is increased, the impeded angle is increased as can be seen in Figure 9(a2), (b2), (c2) and (d2). For example, when $S = 30$, $\phi_s = 14.95°$ for $\alpha = 0°$; $\phi_s = 51.43°$ for $\alpha = 45°$; $\phi_s = 90.93°$ for $\alpha = 90°$; $\phi_s = 146.09°$ for $\alpha = 135°$. Recall that S is a parameter to characterize the relative strength between the magnetic and hydrodynamic effects on a magnetic particle. A larger S means the magnetic effect is more pronounced than hydrodynamic effect, and the major axis of the particle becomes more aligned to the

magnetic field direction. The theoretical impeded angle, determined from equation (17) for S range from 10 to 40 (20 to 40 for $\alpha = 135°$ due to $S_{cr} = 16$), are shown as solid lines in Figure 9(a2), (b2), (c2) and (d2). The numerical results of the impeded angles are in close agreement with the theoretical prediction.

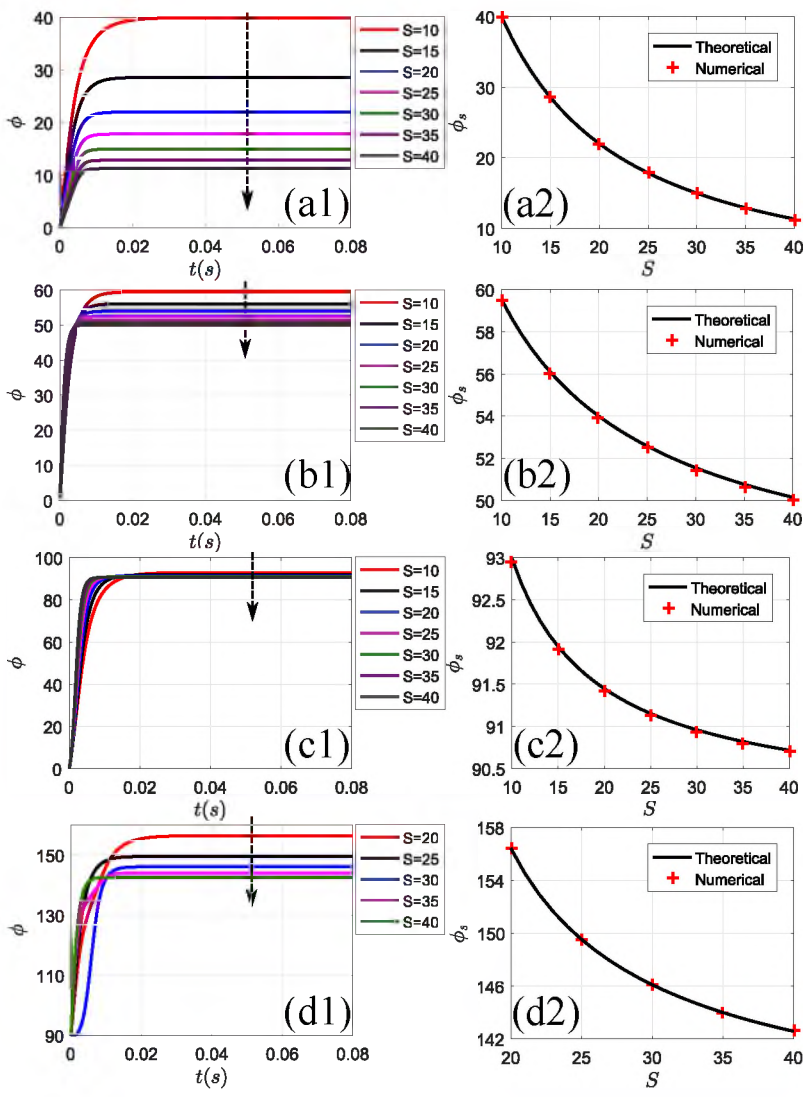

Figure 9. The time evolution of orientation angle, ϕ, and the stable orientation angle, ϕ_s as a function of S, when the magnetic field is applied at $\alpha = 0°$(a), $\alpha = 45°$(b), $\alpha = 90°$(c) and $\alpha = 135°$(d) for the paramagnetic particle.

5.2. FERROMAGNETIC PARTICLES

Here, we will discuss the rotational dynamics of a ferromagnetic particle ($r_p = 4$) under the strong magnetic field. Figure 10 shows the time evolution of orientation angle, ϕ, and the corresponding impeded angles for different relative strengths and different magnetic field directions. The dependence of ϕ_s on S and α is similar to that of paramagnetic particles. For a fixed magnetic field direction, when the relative strength S is increased, the impeded angle, ϕ_s, is decreased; for a fixed relative strength, when the magnetic field direction is increased, the impeded angle is increased. For example, when $S = 30$, $\phi_s = 25.76°$ for $\alpha = 0°$; $\phi_s = 55.85°$ for $\alpha = 45°$; $\phi_s = 91.82°$ for $\alpha = 90°$; $\phi_s = 163.70°$ for $\alpha = 135°$. The impeded angle, computed from the equation (17) for S range from 10 to 40, are shown as solid lines in Figure 10 (a2), (b2), (c2) and (d2), suggesting good agreement between the numerical results and theoretical prediction.

However, compared with the results of paramagnetic particle shown in Figure 9, the impeded angles of ferromagnetic particles is always larger than those of paramagnetic particles when they are subjected to the same relative strengths(S) and magnetic field direction (α). For example, when $S = 20$ and $\alpha = 0°$, $\phi_s = 22.00°$ for the paramagnetic particle, while $\phi_s = 34.15°$ for the ferromagnetic particle.

6. PARTICLE LATERAL MIGRATION IN A SIMPLE SHEAR FLOW NEAR THE WALL

The results presented in the previous sections have illustrated many differences of rotational dynamics between paramagnetic and ferromagnetic particles when they are subjected a uniform magnetic field, where the wall effects can be neglected. Prior investigations have shown lateral migration in wall-bounded shear flows for either paramagnetic particles in a weak magnetic field (Cao *et al.*, 2018; Zhang and Wang, 2018; Zhou *et al.*, 2017a,b), or ferromagnetic particles in a strong magnetic field (Matsunaga *et al.*, 2017a,b). However,

systemic studies on the lateral migration of paramagnetic and ferromagnetic particles under the weak and strong magnetic field are absent. Therefore, in this section, we will use numerical simulations to study the lateral migration of the two different particles in a simple shear flow near the wall.

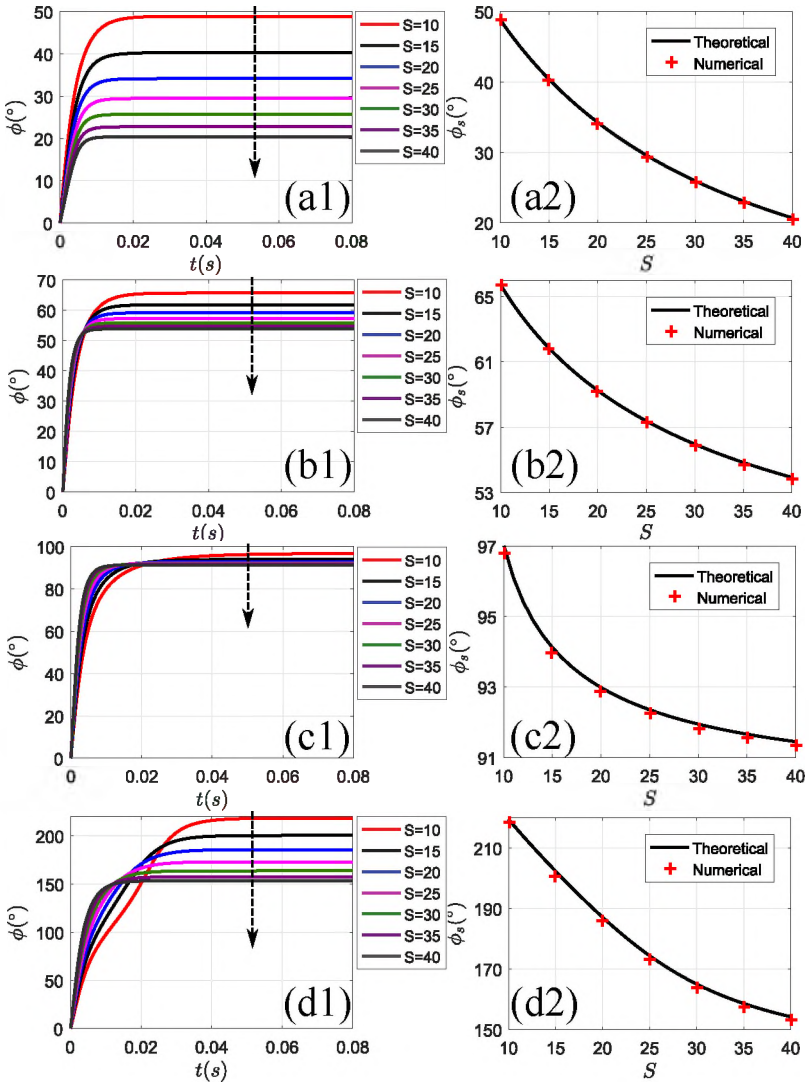

Figure 10. The time evolution of orientation angle, ϕ, and the stable orientation angle, ϕ_s, as a function of S, when the magnetic field is applied at $\alpha = 0°$(a), $\alpha = 45°$(b), $\alpha = 90°$(c) and $\alpha = 135°$(d) for the ferromagnetic particle.

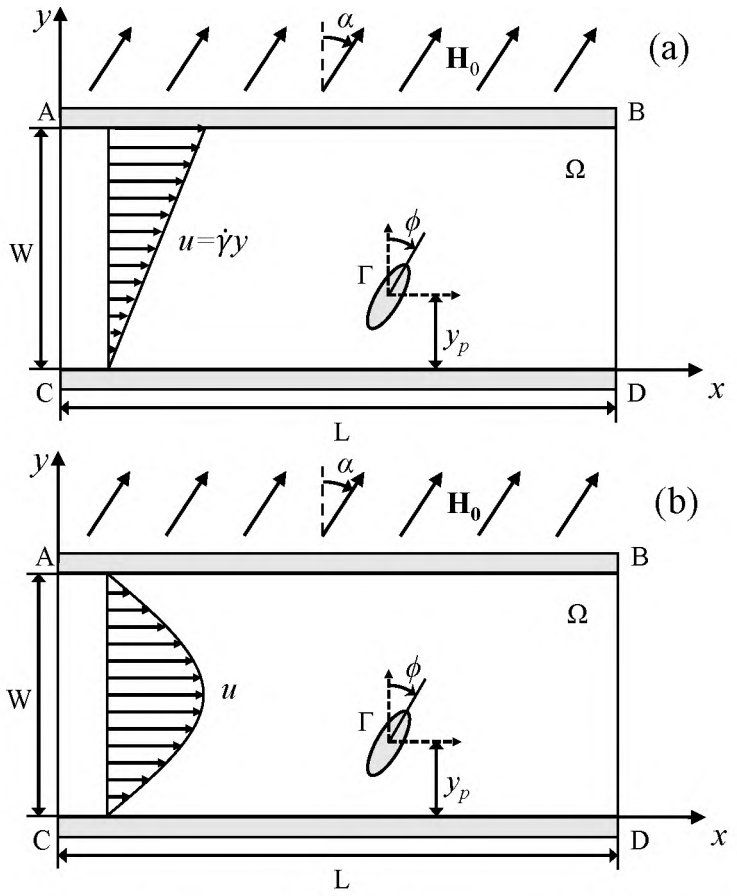

Figure 11. Schematic illustration of the numerical model of an elliptical particle suspended in a simple shear flow near the wall and in a plane Poiseuille flow in a microchannel under the influence of a uniform magnetic field $\mathbf{H}_0$. The fluid and particle domains are Ω and Γ, respectively. The orientation angle of the particle is denoted by ϕ. The particle-wall separation distance is denoted by y_p.

The numerical model of an elliptical particle suspended in a simple shear flow near the wall is shown in Figure 11(a). In this model, the velocity of the bottom wall is kept at zero, while the velocity of the top wall is at a constant velocity $\dot{\gamma}W\mathbf{e}_x$. The length of the channel $L = 900\ \mu m$. The width of the channel W is set to $100\ \mu m$. To investigate the effect of the wall, the particle is initially placed at a particle-wall separation distance $y_{p0} = 10\,\mu$m. The effect of the other wall is negligible due to the large separation distance. Our previous numerical study (Zhang and Wang, 2018) indicated that the inertia effect (Re = 0.125) can cause a small net lateral migration in the absence of magnetic field. Thus, to avoid the

inertia effect, the viscosity of the fluid is set to 0.1 Pa·s and the shear rate is set to $\dot{\gamma} = 80\ s^{-1}$, resulting in a small Reynolds number ($Re = 0.008 \ll 1$). This way, the effect of magnetic field is isolated in order to study its influence on particle migration. The other parameters are the same as before.

6.1. WEAK MAGNETIC FIELD

As we have discussed in Section 4, the symmetry property (characterized by τ) of particle's rotational velocity depends on the magnetic properties of the particle, and the direction of the magnetic field. Specifically, for paramagnetic particles, $\tau > 0.5$ when the magnetic field is applied at 0°, and $\tau < 0.5$ for paramagnetic particles when the magnetic field is applied at 90°, while for ferromagnetic particles, $\tau = 0.5$ when the magnetic field is applied at 0°, 90°, 180° and 270°. Second, for paramagnetic particles, $\tau = 0.5$ when the magnetic field is applied at 45° and 135°, while for ferromagnetic particles, $\tau < 0.5$ when the magnetic field is applied at 45° and 225°, and $\tau > 0.5$ when the magnetic field is applied at 135° and 315°. We will discuss those two cases separately to understand their lateral migration.

First, let us discuss about the lateral migration of paramagnetic and ferromagnetic particles when the magnetic field is applied at 0°, 90°, 180° and 270°. Due to a periodicity of $\pi(180°)$ in ϕ for paramagnetic particles, the results for $\alpha = 0°$ and 180°, $\alpha = 90°$ and 270° are the same, so we only need to perform simulations for $\alpha = 0°$ and $\alpha = 90°$. Figure 12 shows that the lateral migration with time over a 2π (or 360°) period for paramagnetic and ferromagnetic particles when the magnetic field of $S = 0.67$ is applied at 0°, 90°, 180° and 270°. As can be seen in Figure 12(a) for the paramagnetic particle, the net lateral migration is away from the wall when $\alpha = 0°$, and towards the wall when $\alpha = 90°$. However, for the ferromagnetic particle as shown in Figure 12(b), there are negligible net lateral migrations

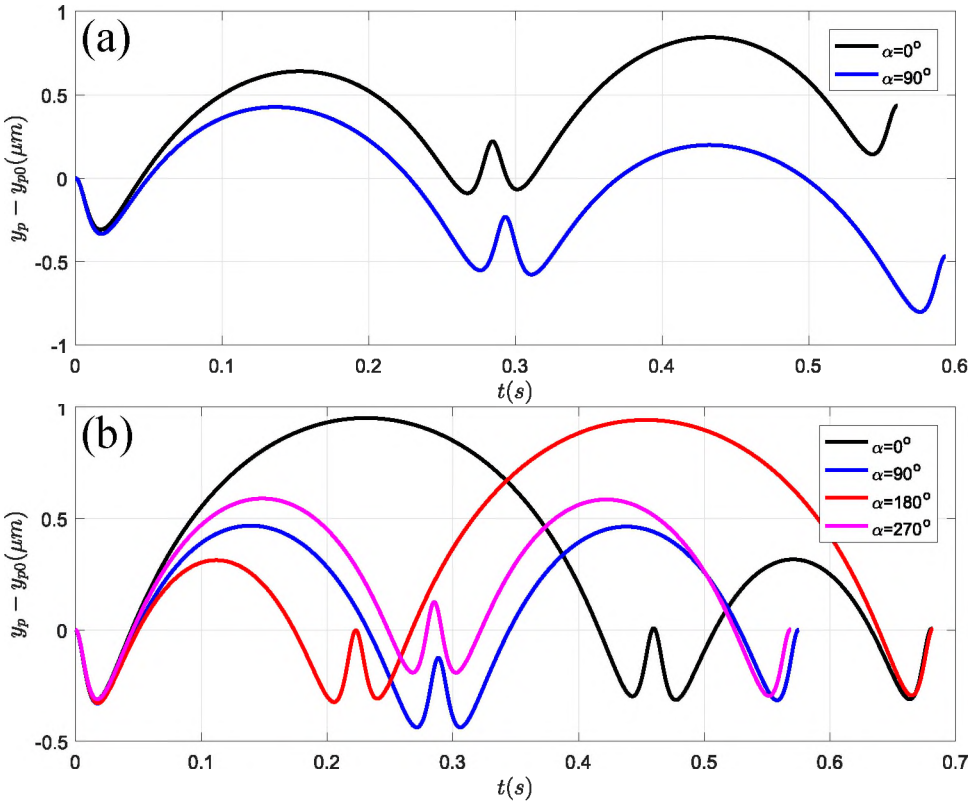

Figure 12. Transport of the magnetic particles ($r_p = 4$) near the wall under a weak magnetic field. (a) The lateral position of the paramagnetic particle, $(y_p - y_{p0})$, over a period; (b) The lateral position of the ferromagnetic particle, $(y_p - y_{p0})$, over a period.

when the magnetic field is applied at $\alpha = 0°$, $90°$, $180°$ and $270°$. Therefore, we can separate paramagnetic and ferromagnetic particles by using a simple shear flow near the wall when a weak magnetic field is applied at $0°$, $90°$, $180°$ and $270°$.

Next, we examine lateral migration of paramagnetic and ferromagnetic particles when $\alpha = 45°$, $135°$, $225°$ and $315°$. We only carry out simulations when $\alpha = 45°$ and $135°$ for paramagnetic particles. Figure 13 shows that the lateral migration changes with time over a 2π (or $360°$) period for paramagnetic and ferromagnetic particles when a magnetic field of strength $S = 0.67$ is applied at $\alpha = 45°$, $135°$, $225°$ and $315°$. As can be seen in

Figure 13(a), for the paramagnetic particle, there are no net lateral migrations when $\alpha = 45°$, or 135°. However, for the ferromagnetic particle as shown in Figure 13(b), there is a positive net lateral migration when $\alpha = 135°$ or 225°, and a negative net lateral migration when the magnetic field is applied at $\alpha = 45°$ and 315°. Therefore, we can separate the paramagnetic and ferromagnetic particles in a simple shear flow near the wall when the weak magnetic field is applied at 45°, 135°, 225° and 315°. But the net lateral migration over a period is smaller than the first case.

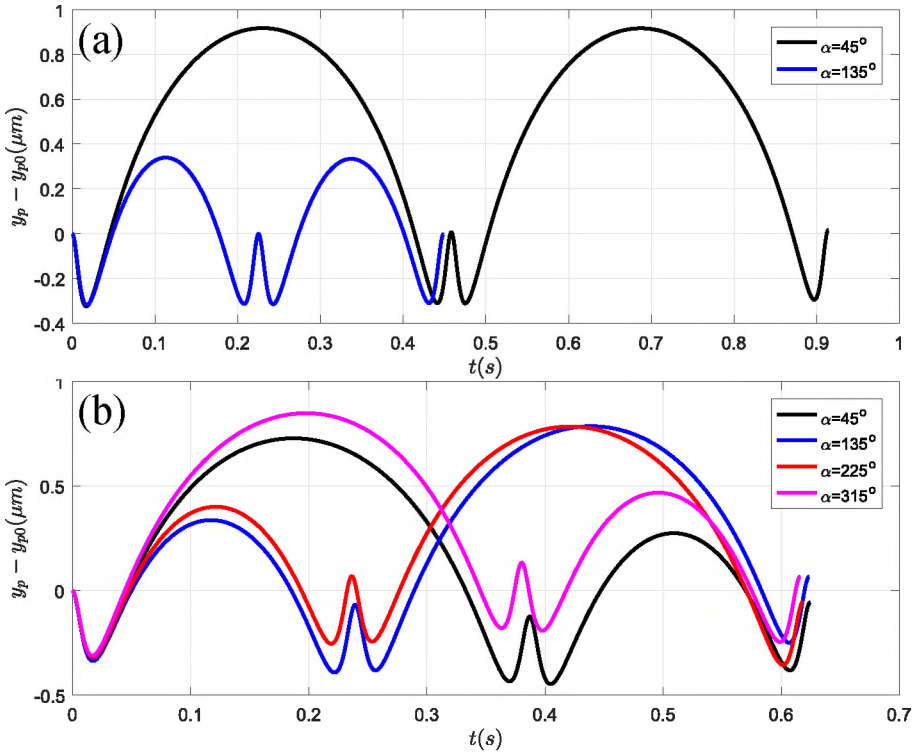

Figure 13. Transport of the magnetic particles ($r_p = 4$) near the wall under a weak magnetic field. (a) The lateral position of the paramagnetic particle, $(y_p - y_{p0})$, over a period; (b) The lateral position of the ferromagnetic particle, $(y_p - y_{p0})$, over a period.

For the paramagnetic particle in a weak magnetic field, our numerical results are consistent with findings of several previous studies (Cao *et al.*, 2018; Zhang and Wang, 2018; Zhou *et al.*, 2017b): the particle moves away from the wall when $\tau > 0.5$; the particle moves

downwards when $\tau < 0.5$; no net lateral migration when $\tau = 0.5$. This numerical study further confirms same results for the ferromagnetic particle in a weak magnetic field: the particle will move upwards when $\tau > 0.5$; the particle will move downwards when $\tau < 0.5$; no net lateral migration when $\tau = 0.5$.

6.2. STRONG MAGNETIC FIELD

As we have discussed in Section 5, the impeded angles of the paramagnetic and ferromagnetic particles are different for the same S and α. Thus, we carry out simulations for the paramagnetic and ferromagnetic particles to understand the effect of a strong magnetic field on lateral migration, as shown in Figure 14. When a strong magnetic field is applied at $\alpha = 0°$, the time evolution of orientation angle ϕ and the lateral migration, $(y_p - y_{p0})$, of paramagnetic (red line) and ferromagnetic (black line) particles are shown in Figure 14(a) and (b). For both particles, a moderate strength $S = 10$ (solid line) and a large strength $S = 40$ (dash line), the impeded angles and lateral migration are different. But the difference of the impeded angles for $S = 40$ is more significant than those for $S = 10$. The net lateral migration between paramagnetic and ferromagnetic particles also shows marked difference for $S = 40$. This comparison suggests that it would be advantageous to use stronger field strength to separate the paramagnetic and ferromagnetic particles when the magnetic field is applied at $\alpha = 0°$.

Figure 14(c) and (d) shows the evolution of orientation angle ϕ and the lateral migration, $(y_p - y_{p0})$, of paramagnetic (red line) and ferromagnetic (black line) particles when a strong magnetic field is applied at $\alpha = 90°$. In this case, there is a larger difference of both impeded angle and lateral migration for $S = 10$ (solid line) than for $S = 40$ (dash line). This finding suggests that a moderate field strength ($S = 10$) can result in better separation between the paramagnetic and ferromagnetic particles than a stronger field ($S = 40$) if the magnetic field is perpendicular to the flow, i.e., $\alpha = 90°$.

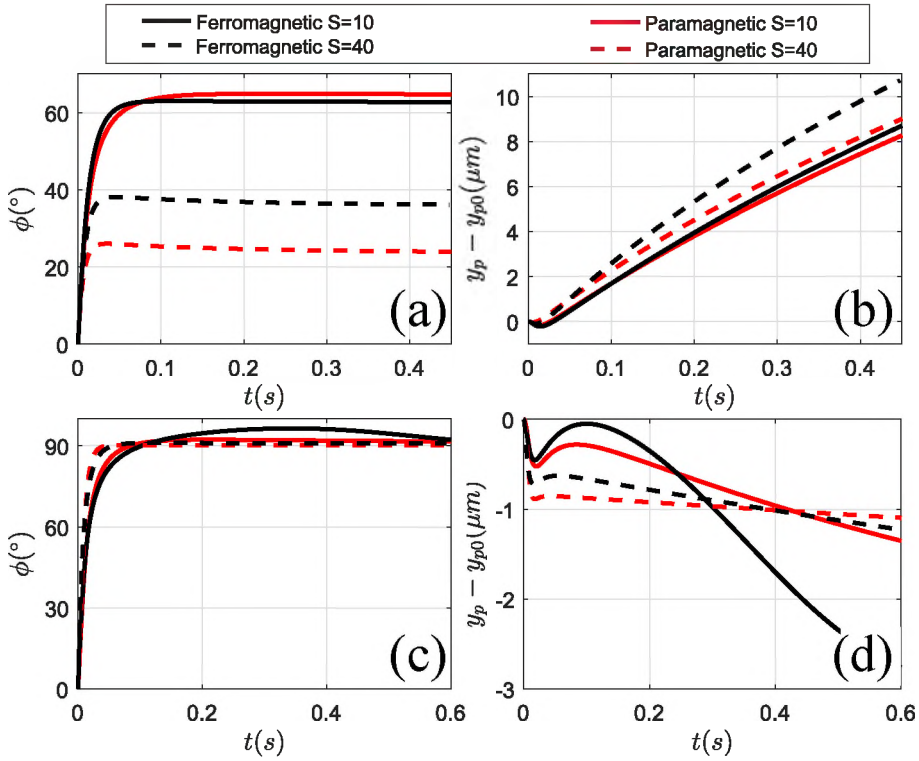

Figure 14. Transport of the magnetic particle (r_p = 4) near the wall under a strong magnetic field.(a) The evolution of orientation angle ϕ and (b) the lateral position of the paramagnetic (red) and ferromagnetic (black) particles ($y_p - y_{p0}$) vary with the time t when the magnetic field is applied at 0°; (c) The evolution of orientation angle ϕ and (d) the lateral migration, ($y_p - y_{p0}$), of paramagnetic(red) and ferromagnetic(black) particles vary with the time t when the magnetic field is applied at 90°.

7. PARTICLE LATERAL MIGRATION IN A PLANE POISEUILLE FLOW IN A MICROCHANNEL

While the previous findings are obtained for particles suspended in simple shear flows (constant shear rate), we expect that they are qualitatively valid for Poiseulle flows, which are the predominant form of flow in practical applications. In this section, we study particle lateral migration in a plane Poiseuille flow in a microchannel. The numerical model is shown in Figure 11(b). The width and length of the channel are W = 50 μm and L = 1200 μ m, respectively. The initial particle-wall separation distance is y_{p0} = 12 μm. Water is the

most commonly used fluid medium, thus we use water as the fluid in this simulation. The average inlet flow velocity is 2.5 mm/s, resulting Reynolds number Re = 0.125. As we have

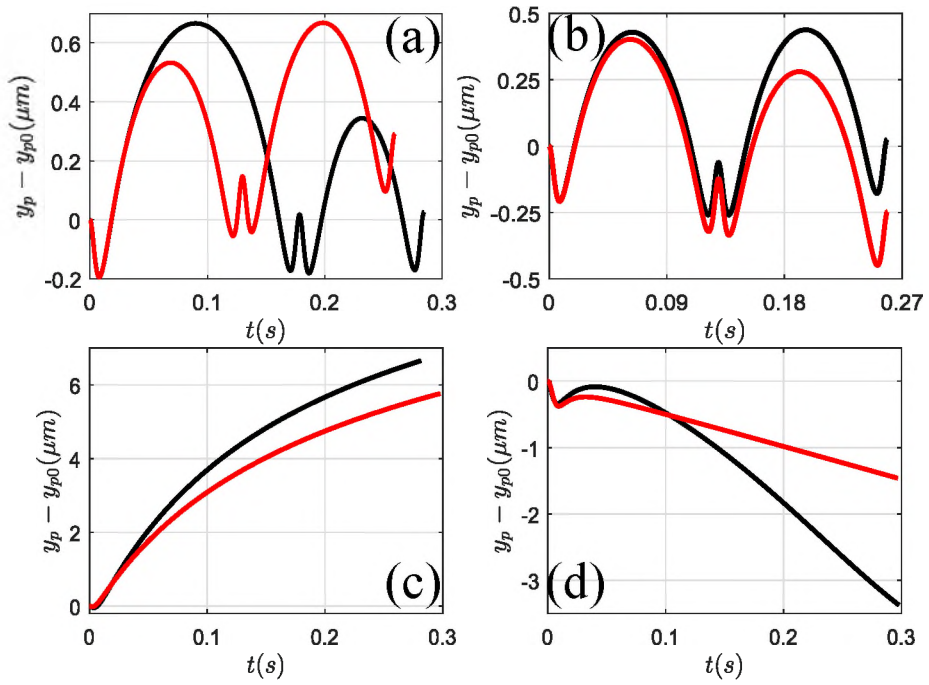

Figure 15. Transport of the magnetic particle ($r_p = 4$) in a plane Poiseuille flow in a microchannel when the magnetic field is applied at 0°$(a)(c)$ and 90°$(b)(d)$. $S = 0.48$ for (a) and (b); $S = 40$ for (c); $S = 12$ for (d). The red line represents for the paramagnetic particle and the black line for the ferromagnetic particle.

discussed in Section 6, the separation is possible when the magnetic field is applied at 0° and 90°. Here, we perform simulations when the magnetic field is applied at $\alpha = 0°$ and 90°. With a weak magnetic field applied, the particle lateral migration in the plane Poiseuille flow in the microchannel are shown in Figure 15(a) and (b). As can be seen, the trajectories of paramagnetic particle (red line in Figure 15) and ferromagnetic particle (black line in Figure 15) are qualitatively similar to those in a simple shear flow near a wall (Figure 11(b)).

When a strong field is used, previous discussions have indicated better separation performance when the magnetic field is applied at $\alpha = 0°$; while for a moderate relative strength (still must be larger than S_{cr}), the field applied at $\alpha = 90°$ leads to a better separation. This finding is confirmed by numerical simulations for $S = 40$ with $\alpha = 0°$ and $S = 12$ with $\alpha = 90°$, as shown in Figure 15(c). Note that the parabolic velocity profile does affect the critical strength, and $S = 12$ is used to impede particle rotation. Nevertheless, the conclusions from simple shear flows apply qualitatively to pressure driven flows in a channel.

8. CONCLUSION

In this work, we developed a multi-physics numerical model to investigate the rotational dynamics of paramagnetic and ferromagnetic particles that have elliptical shape, in a simple shear flow and under a uniform magnetic field. We investigated the effects of strength and direction of the magnetic field on rotational dynamics of paramagnetic and ferromagnetic particles. The results show that the symmetry of rotational velocity is modified by the magnetic field. When the magnetic field strength increases to a large enough value (the critical magnetic field strength), the particle rotation is impeded. In a weak field regime (below the critical magnetic field), the particle complete a full rotation, and the symmetrical property of particle rotations depend on the direction of the magnetic field. For the same strength and direction of the magnetic field, paramagnetic and ferromagnetic particles exhibit different asymmetric rotational behaviors. In the strong field (above the critical strength), the particles are pinned at their respected steady angles, which depend on the direction of magnetic field. The steady angles of paramagnetic and ferromagnetic particles are different for the same magnetic field strength and direction. The numerical results have very good agreement with that of theoretical analysis.

Based on the findings of the particle rotational dynamics, the lateral migration of paramagnetic and ferromagnetic elliptical particles in a simple shear flow near the wall is investigated. The results show that the paramagnetic and ferromagnetic particles have

different lateral migration motions for the same flow and magnetic conditions. Thus, we can separate these two kinds of particles in a simple shear flow under the magnetic field. Finally, the lateral migration of paramagnetic and ferromagnetic particles in a pressure-driven channel flow is investigated. Paramagnetic and ferromagnetic particles in pressure-drive flows behave qualitatively similar to those in simple shear flows, suggesting a useful strategy to manipulate non-spherical micro-particles in the microfluidic devices.

REFERENCES

Ai, Y., Beskok, A., Gauthier, D. T., Joo, S. W., and Qian, S., 'Dc electrokinetic transport of cylindrical cells in straight microchannels,' Biomicrofluidics, 2009a, **3**(4), p. 044110.

Ai, Y., Joo, S. W., Jiang, Y., Xuan, X., and Qian, S., 'Pressure-driven transport of particles through a converging-diverging microchannel,' Biomicrofluidics, 2009b, **3**(2), p. 022404.

Ai, Y. and Qian, S., 'Dc dielectrophoretic particle–particle interactions and their relative motions,' Journal of colloid and interface science, 2010, **346**(2), pp. 448–454.

Ai, Y., Zeng, Z., and Qian, S., 'Direct numerical simulation of ac dielectrophoretic particle–particle interactive motions,' Journal of colloid and interface science, 2014, **417**, pp. 72–79.

Allan, R. and Mason, S., 'Particle behaviour in shear and electric fields. ii. rigid rods and spherical doublets,' Proceedings of the Royal Society of London A: Mathematical, Physical and Engineering Sciences, 1962, **267**(1328), pp. 62–76.

Bucak, S., Sharpe, S., Kuhn, S., and Hatton, T. A., 'Cell clarification and size separation using continuous countercurrent magnetophoresis,' Biotechnology progress, 2011, **27**(3), pp. 744–750.

Cao, Q., Li, Z., Wang, Z., and Han, X., 'Rotational motion and lateral migration of an elliptical magnetic particle in a microchannel under a uniform magnetic field,' Microfluidics and Nanofluidics, 2018, **22**(1), p. 3.

Chaffey, C. and Mason, S., 'Particle behavior in shear and electric fields. III. rigid spheroids and discs,' Journal of Colloid Science, 1964, **19**(6), pp. 525–548.

Chen, P., Huang, Y.-Y., Hoshino, K., and Zhang, J. X., 'Microscale magnetic field modulation for enhanced capture and distribution of rare circulating tumor cells,' Scientific reports, 2015, **5**, p. 8745.

Gavze, E. and Shapiro, M., 'Particles in a shear flow near a solid wall: effect of nonsphericity on forces and velocities,' International Journal of Multiphase Flow, 1997, **23**(1), pp. 155–182.

Gijs, M. A., 'Magnetic bead handling on-chip: new opportunities for analytical applications,' Microfluidics and Nanofluidics, 2004, **1**(1), pp. 22–40.

Gijs, M. A., Lacharme, F., and Lehmann, U., 'Microfluidic applications of magnetic particles for biological analysis and catalysis,' Chemical reviews, 2009, **110**(3), pp. 1518–1563.

Hu, H. H., Patankar, N. A., and Zhu, M., 'Direct numerical simulations of fluid–solid systems using the arbitrary lagrangian–eulerian technique,' Journal of Computational Physics, 2001, **169**(2), pp. 427–462.

Jeffery, G. B., 'The motion of ellipsoidal particles immersed in a viscous fluid,' Proceedings of the Royal Society of London A: Mathematical, Physical and Engineering Sciences, 1922, **102**(715), pp. 161–179.

Leal, L., 'Particle motions in a viscous fluid,' Annual Review of Fluid Mechanics, 1980, **12**(1), pp. 435–476.

Matsunaga, D., Meng, F., Zöttl, A., Golestanian, R., and Yeomans, J. M., 'Focusing and sorting of ellipsoidal magnetic particles in microchannels,' Phys. Rev. Lett., 2017a, **119**, p. 198002, doi:10.1103/PhysRevLett.119.198002.

Matsunaga, D., Zöttl, A., Meng, F., Golestanian, R., and Yeomans, J. M., 'Far-field theory for trajectories of magnetic ellipsoids in rectangular and circular channels,' arXiv preprint arXiv:1711.00376, 2017b.

Okagawa, A., Cox, R., and Mason, S., 'Particle behavior in shear and electric fields. VI. the microrheology of rigid spheroids,' Journal of Colloid and Interface Science, 1974, **47**(2), pp. 536–567.

Pamme, N., 'Magnetism and microfluidics,' Lab on a Chip, 2006, **6**(1), pp. 24–38.

Pamme, N., 'On-chip bioanalysis with magnetic particles,' Current opinion in chemical biology, 2012, **16**(3-4), pp. 436–443.

Pankhurst, Q. A., Connolly, J., Jones, S., and Dobson, J., 'Applications of magnetic nanoparticles in biomedicine,' Journal of physics D: Applied physics, 2003, **36**(13), p. R167.

Shine, A. and Armstrong, R., 'The rotation of a suspended axisymmetric ellipsoid in a magnetic field,' Rheologica Acta, 1987, **26**(2), pp. 152–161.

Sobecki, C. A., Zhang, J., Zhang, Y., and Wang, C., 'Dynamics of paramagnetic and ferromagnetic ellipsoidal particles in shear flow under a uniform magnetic field,' Physical Review Fluids, 2018, **3**(8), p. 084201.

Stratton, J. A., *Electromagnetic theory*, John Wiley & Sons, 2007.

Suwa, M. and Watarai, H., 'Magnetoanalysis of micro/nanoparticles: A review,' Analytica chimica acta, 2011, **690**(2), pp. 137–147.

Winkleman, A., Perez-Castillejos, R., Gudiksen, K. L., Phillips, S. T., Prentiss, M., and Whitesides, G. M., 'Density-based diamagnetic separation: devices for detecting binding events and for collecting unlabeled diamagnetic particles in paramagnetic solutions,' Analytical chemistry, 2007, **79**(17), pp. 6542–6550.

Zborowski, M., Sun, L., Moore, L. R., Williams, P. S., and Chalmers, J. J., 'Continuous cell separation using novel magnetic quadrupole flow sorter,' Journal of Magnetism and Magnetic Materials, 1999, **194**(1-3), pp. 224–230.

Zhang, J. and Wang, C., 'Numerical study of lateral migration of elliptical magnetic microparticles in microchannels in uniform magnetic fields,' Magnetochemistry, 2018, **4**(1), p. 16.

Zhou, R., Bai, F., and Wang, C., 'Magnetic separation of microparticles by shape,' Lab on a Chip, 2017a, **17**(3), pp. 401–406.

Zhou, R., Sobecki, C. A., Zhang, J., Zhang, Y., and Wang, C., 'Magnetic control of lateral migration of ellipsoidal microparticles in microscale flows,' Physical Review Applied, 2017b, **8**(2), p. 024019.

Zhou, Y., Song, L., Yu, L., and Xuan, X., 'Continuous-flow sheathless diamagnetic particle separation in ferrofluids,' Journal of Magnetism and Magnetic Materials, 2016, **412**, pp. 114–122.

Zhou, Y. and Xuan, X., 'Diamagnetic particle separation by shape in ferrofluids,' Applied Physics Letters, 2016, **109**(10), p. 102405.

IV. DYNAMICS OF A PAIR OF ELLIPSOIDAL MICROPARTICLES UNDER UNIFORM MAGNETIC FIELDS

Jie Zhang, Ran Zhou, Cheng Wang

Department of Mechanical & Aerospace Engineering

Missouri University of Science and Technology

Rolla, Missouri 65409

Department of Mechanical and Civil Engineering

Purdue University Northwest

Hammond, Indiana, 46323

Tel: 573–341–4636, Fax: 573–341–4607

Email: wancheng@mst.edu

ABSTRACT

Under a uniform magnetic field, magnetic particles tend to form chains, clusters or columns due to particle-particle interactions between the particles. The magnetic particles with non-spherical shape dispersed in liquid medium show different rheological properties. However, there is a lack of fundamental mechanism of the particle-particle interactions of non-spherical particles under the uniform magnetic field. In this work, we numerically investigate the particle-particle interactions and relative motions of a pair of paramagnetic elliptical particles by using direct numerical simulations to create two-dimensional models that resolve the magnetic and flow fields around the finite sized particles. The modeling is based on the finite element method and arbitrary Lagrangian-Eulerian approach with a full consideration of particle-fluid-magnetic field interaction. The effects of initial position and aspect ratio of the particles are investigated. The results show that the particles spend much more time for the global reorientation than for the local magneto-orientation. Larger initial

relative angles and distances, and larger aspect ratios tend to require more time to form a stable chain. The particle-particle interactions and relative motion of a pair of elliptical particles in this study provide insights on the particle alignment and chaining processes under uniform magnetic fields, which are closely related to the response of magneto-rheological fluids to magnetic fields.

Keywords: microfluidics, magnetic field, particle interactions, elliptical particles, direction numerical simulation

1. INTRODUCTION

Due to their significant advantages, magnetic particles have been using in various applications, which includes chemical, biomedical, biological and industrial fields (Gijs, 2004; Gijs *et al.*, 2009; Jamshaid *et al.*, 2016). Under an external magnetic field, magnetic microparticles or nanoparticles immersed in non-magnetic fluid tend to form chains, clusters or columns due to the particle-particle interaction between the particles. The suspension consisting of high density magnetic microparticles or nanoparticles is called as magnetorheological fluids (MRFs) (De Vicente *et al.*, 2011). The MRFs are smart materials which show various rheological properties, such as yield stress and apparent viscosity. The values of these rheological properties are increased to several orders of magnitude under the appropriately applied magnetic field. Due to their remarkable properties and the quick response to the magnetic field, MRFs are the good candidates for a vast number of industrial and medical applications, such as magnetorheological rotor damper, brakes, clutches, valves and cancer therapeutic (Bica *et al.*, 2013; Rabinow, 1948; Sheng *et al.*, 1999). In addition, magnetic particles have been also used in a wide number of microfluidic applications since it is easy and wireless manipulated by the external magnetic field. Cell separation is one of most important areas benefiting from those applications (Hejazian *et al.*, 2015). The cells digested with magnetic nanoparticles or attaching magnetic microparticles to the cell surface could easily be manipulated by the magnetic field (Gijs *et al.*, 2009).

A pair of magnetic particles suspended in a quiescent fluid is a basic model to investigate the particle-particle interactions in particle suspensions. There are many numerical investigations on the motion of magnetic spherical particles under the magnetic field. The particle-based numerical method are the most popular one, which is based on point-dipole approximation and stokes drag law (Melle and Martin, 2003; Petousis *et al.*, 2007; Stuart *et al.*, 2011). The particle is modeled as a dipole point and the dipole-dipole model is applied to study the particle-particle interactions between the particles. However, the particle-particle interactions due to the hydrodynamic and magnetic effects are neglected in this method, which may result in the quantitatively inaccurate or even erroneous results. More precise models are introduced to investigate the field-induced coupling and hydrodynamic interactions between the particles. Keaveny and Maxey (Keaveny and Maxey, 2008) reported a dipole model including the locally higher-order multipoles to resolve the near-field magnetic interactions between two paramagnetic particles. To consider both hydrodynamic and magnetic interactions between the particles, Gao et al. (Gao *et al.*, 2012) reported a particle-based numerical scheme by using magnetic dipole moments and extended forms of the Oseen-Burgers tensor to study the dynamics of magnetic particle chains in a viscous fluid under the rotating magnetic field. Their numerical results are qualitatively and quantitatively in agreement with the results obtained from video-microscopy experiments. Kang et al. (Kang *et al.*, 2013, 2008) presented a direct numerical simulation model based on finite element method(FEM) and fictitious domain method to solve both two-and three-dimensional flow problems with paramagnetic particles in a non-magnetic fluid under both uniform and rotating magnetic field. The magnetic force acting on the particles are computed through the divergence of Maxwell stress tensor, and works as a body force applied to the momentum equation. Suh and Kang (Kang and Suh, 2011; Suh and Kang, 2011) introduced a direct numerical simulation model based on immersed-boundary finite volume method to solve two-dimensional motion of paramagnetic particles in a viscous fluid under

the uniform magnetic field. They have the similar particle trajectories of two magnetic particles under the uniform magnetic field as two-dimensional simulations in Kang's paper (Kang *et al.*, 2008).

In regard to the practical application, the complex shapes are also one of the most important properties of the magnetic particles. Recently, the experimental (Anupama *et al.*, 2018; Bell *et al.*, 2008, 2007; Bombard *et al.*, 2014; de Vicente *et al.*, 2010; Dong *et al.*, 2015; Jiang *et al.*, 2011; López-López *et al.*, 2009, 2007; Morillas *et al.*, 2015; Ngatu *et al.*, 2008; Sedlacik *et al.*, 2013) and theoretical (Bossis *et al.*, 2015; De Vicente *et al.*, 2009; Kuzhir *et al.*, 2009) investigations reported that the MRFs with non-spherical particles have stronger magnetorheological properties and better sedimentation stability compared to those with spherical particles. Thus, it is urgent need of an better understanding of the particle-particle interactions and motion behaviors of non-spherical particles under the magnetic field. Even though previous numerical methods have been successfully applied to magnetic spherical particles, there has been limited simulations on two non-spherical particles. Recently, Abbas and Bossis (Abbas and Bossis, 2017) numerically and theoretically investigated the dynamics of two ellipsoidal ferromagnetic particles under the externally alternating magnetic field. They reported that two ellipsoidal ferromagnetic particles repelled with each other due to hydrodynamic interactions under the alternating magnetic field. Despite lots of experimental studies on non-spherical particles, there has little work been done to study the basic particle-particle interactions of magnetic non-spherical particles under a uniform magnetic field.

In this study, we developed a transient multi-physics numerical model to investigate the particle-particle interactions and relative motions of a pair of paramagnetic elliptical particles under an uniform magnetic field. Numerical simulations will be performed by direct numerical simulation(DNS) based on finite element method and arbitrary Lagrangian-Eulerian(ALE) approach. The fluid field, magnetic field and particle motion are coupled and solved by using moving mesh based on ALE approach. For computational efficiency,

we have chosen to use two-dimensional(2D) simulations in order to study a wide range of parameters (i.e., magnetic field direction, initial particle-particle distance, and particle aspect ratio). Prior studies have shown that 2D numerical simulations are able to qualitatively capture the characteristics of the motion of a pair of spherical particles (Ai and Qian, 2010; Ai *et al.*, 2014; Kang and Suh, 2011; Kang *et al.*, 2013, 2008; Suh and Kang, 2011). Here, we have also validated the numerical model with previous studies in Section 3.1 (motion of a pair of circular particles) and 3.2 (motion of a single elliptical particle).

2. NUMERICAL METHOD

2.1. MATHEMATICAL MODEL

We consider a pair of identical rigid prolate elliptical particles immersed in a quiescent fluid in a square with a length of L as shown in Figure 1. Ω represents the entire computational domain, which includes fluid and two particle domains. Γ_1 and Γ_2 are the particle surfaces of those two particles. The center of the square is set as the origin of the Cartesian coordinate system. Two particles are set as axis-symmetric to the center of the square with the center-to-center distance of d and the relative angle of θ with respect to the positive x-axis. The major and minor semi-axis lengths of the particles are a and b, so the particle aspect ratio is defined as $r_p = a/b$. The orientation angle of the particle, α, is defined as the angle between the major axis of the particle and the positive x-axis. A uniform magnetic field, $\mathbf{H}_0$, is applied at the positive x direction.

The fluid is considered as an incompressible, Newtonian, and non-magnetic with the constant density of ρ_f, dynamic viscosity of η_f and magnetic susceptibility of χ_f. The particles are paramagnetic with magnetic susceptibility of χ_p. The transient flow field, $\mathbf{u}$, in the fluid domain is governed by the continuity equation and Navier-Stokes equation:

$$\nabla \cdot \mathbf{u} = 0, \tag{1}$$

$$\rho_f \left[\frac{\partial \mathbf{u}}{\partial t} + (\mathbf{u} \cdot \nabla)\,\mathbf{u} \right] = -\nabla p + \nabla \cdot \eta_f \left(\nabla \mathbf{u} + (\nabla \mathbf{u})^T \right), \tag{2}$$

where p and t are the pressure and the time, respectively. The open boundary conditions are set on boundaries ABCD, so that the fluid can both enter and leave the computational domain though boundaries. Here, the normal stress is zero on boundaries ABCD.

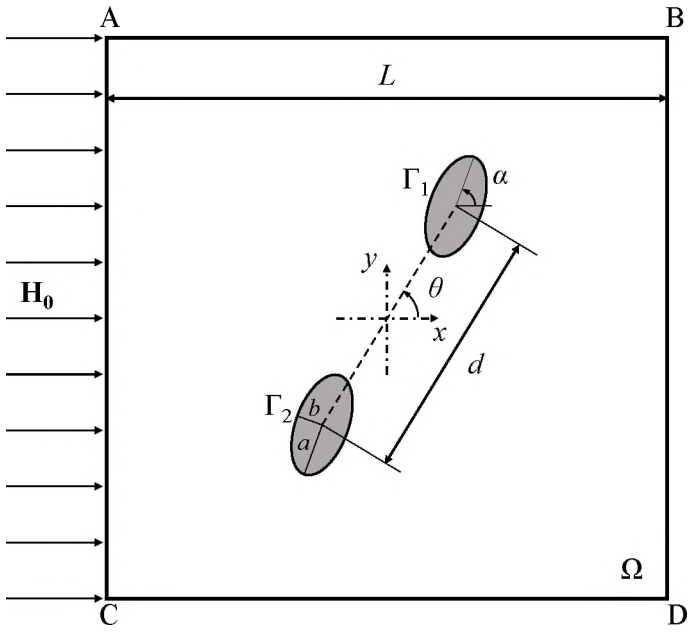

Figure 1. Schematic of Numerical Model of two elliptical particles suspended in a quiescent flow under the influence of a uniform magnetic field.

The particle surface is assumed as the no-slip condition, so the fluid velocities on the particle surface Γ_1 and Γ_2 are expressed as:

$$\mathbf{u}_i = \mathbf{U}_{pi} + \boldsymbol{\omega}_{pi} \times (\mathbf{x}_{si} - \mathbf{x}_{pi}), \tag{3}$$

where $i = 1$ and 2 representing the first and second particle. $\mathbf{U}_{pi}$ and $\boldsymbol{\omega}_{pi}$ are the transnational and rotational velocities of the ith particle , respectively. $\mathbf{x}_{si}$ and $\mathbf{x}_{pi}$ are the position vectors of the surface and the center of the ith particle, respectively.

The hydrodynamic stress tensor on the particle surface Γ_i are:

$$\boldsymbol{\tau}_{hi} = \eta_f \left(\nabla \mathbf{u}_i + (\nabla \mathbf{u}_i)^T \right). \tag{4}$$

Thus, the hydrodynamic force and torque acting on the particle are expressed as:

$$\mathbf{F}_{hi} = \int (\boldsymbol{\tau}_{hi} \cdot \mathbf{n}) d\Gamma_i, \tag{5}$$

$$\mathbf{L}_{hi} = \int (\boldsymbol{\tau}_{hi} \times (\mathbf{x}_{si} - \mathbf{x}_{pi}) \cdot \mathbf{n}) d\Gamma_i, \tag{6}$$

The magnetic field in the entire domain Ω is governed by the static Maxwell equations:

$$\nabla \times \mathbf{H} = 0, \tag{7}$$

$$\nabla \cdot \mathbf{B} = 0, \tag{8}$$

where $\mathbf{H}$ and $\mathbf{B}$ are the magnetic field and the magnetic flux density, respectively. The constitutive equation describing the relationship between magnetic field and magnetic flux density is $\mathbf{B} = \mu \mathbf{H}$, where μ is the magnetic permeability of a linear isotropic material. The relationship between magnetic permeability and magnetic susceptibility is $\mu = \mu_0(1 + \chi)$, where $\mu_0 = 4\pi \times 10^{-7}$ H/m is the magnetic permeability in vacuum.

The uniform magnetic field is applied by setting a magnetic scalar potential difference between boundaries AC and BD. A magnetic potential $V_m = V_{m0}$ and a zero magnetic potential $V_m = 0$ are set on boundaries AC and BD, respectively. The magnetic potential and magnetic field are related by $\mathbf{H} = -\nabla V_m$. The boundaries AB and CD are set as magnetic insulation condition.

The magnetic force and torque acting on the particles are expressed as (Stratton, 2007):

$$\mathbf{F}_{mi} = \int (\boldsymbol{\tau}_{mi} \cdot \mathbf{n}) d\Gamma_i, \tag{9}$$

$$\mathbf{L}_{mi} = \int (\boldsymbol{\tau}_{mi} \times (\mathbf{x}_{si} - \mathbf{x}_{pi}) \cdot \mathbf{n}) d\Gamma_i, \tag{10}$$

where $\boldsymbol{\tau}_{mi} = \mu(\mathbf{HH} - \frac{1}{2}H^2\mathbf{I})$ is the Maxwell stress tensor on the ith particle surface Γ_i, $H^2 = \mathbf{H} \cdot \mathbf{H}$, $\mathbf{I}$ is the identity tensor.

The x–y plane is the plane of the rotational motion for the two-dimensional elliptical particles, thus $\boldsymbol{\omega}_{pi} = \omega_{pi}\mathbf{e}_z$, $\mathbf{L}_{hi} = L_{hi}\mathbf{e}_z$, and $\mathbf{L}_{mi} = L_{mi}\mathbf{e}_z$. The Newton's second law and Euler's equation are used to describe the translation and rotation of the particles, which are governed by:

$$m_{pi}\frac{d\mathbf{U}_{pi}}{dt} = \mathbf{F}_{hi} + \mathbf{F}_{mi}, \tag{11}$$

$$I_{pi}\frac{d\omega_p}{dt} = L_{hi} + L_{mi}, \tag{12}$$

where m_{pi} and I_{pi} are the mass and the moment of inertia of the ith particle, respectively.

The particle trajectories of the ith particle are calculated by:

$$\mathbf{x}_{pi}(t) = \mathbf{x}_{pi}(0) + \int_0^t \mathbf{U}_{pi}(t')dt', \tag{13}$$

$$\alpha_i(t) = \alpha_i(0) + \int_0^t \omega_{pi}(t')dt', \tag{14}$$

where $\mathbf{x}_{pi}(t) = (x_{pi}, y_{pi})$ is the position of the ith particle center; $\alpha_i(t)$ is the orientation angle of the ith particle. Due to the axis-symmetric property, α_1 and α_2 have the same values. Thus, in the following discussion, α is used to represent both orientation angles.

The coupling of the particle motions, the flow field, and the magnetic field is through Equations (3)- (6) and (9)-(12). The direct numerical simulation (DNS) based on finite element method(FEM) and arbitrary Lagrangian-Eulerian(ALE) approach is used to calculate the magnetic field, flow field and particle motion at the same time. In the previous researches, Hu et al. (Hu *et al.*, 2001), Ai et al. (Ai *et al.*, 2009a,b; Ai and Qian, 2010; Ai *et al.*, 2014) and previous simulations (Zhang *et al.*, 2018; Zhang and Wang, 2018) employed the similar methodologies successfully applying to fluid-solid systems. The commercial

FEM solver – COMSOL Multiphysics is used to implement and solve the numerical model. The two-way coupling of particle-fluid-magnetic interaction model is solved by using a time-dependent solver through the ALE method, which solves the magnetic field in the entire domain, the fluid field in a Eulerian(deformed) frame, and tracks the particle motion in a Lagrangian(undeformed) frame at the same time. The moving meshing interface is used to track the deformation of the fluid domain where the meshes are free to deform. The meshes of particle domain are fixed which is determined by their trajectories and orientations. As the mesh deforms, the mesh distortion is increased. When the distortion value is increased to 0.3, the re-meshing process initiates. In this simulation, we used quadratic triangular elements in the entire domain. To accurately calculate the hydrodynamic force and torque, as well as magnetic force and torque acting on the particle, fine meshes are applied around the particle surfaces and finer meshes are applied around the tips of the particles. The total number of elements was about 16,000 in the entire domain and about 120 elements on each particle surface to obtain stable and mesh-independent results.

2.2. MATERIAL PROPERTIES

In this numerical study, water is used as the nonmagnetic fluid ($\chi_f = 0$). The density and dynamic viscosity of the water are $\rho_f = 1000$ kg/m^3 and $\eta_f = 1 \times 10^{-3}$ Pa·s in the room temperature, respectively. The particle is assumed to be polystyrene paramagnetic particles containing magnetic nanoparticles, similar to those used in previous experiments (Zhou *et al.*, 2017a,b). The density and magnetic susceptibility of the particle are $\rho_p = 1100$ kg/m^3 and $\chi_p = 0.26$, respectively. The equivalent radius of the particle used in this simulation is $R_0 = 3.5$ μm and the side length of the square domain is $L = 50R_0$, which is large enough for this work according to Ref (Ai *et al.*, 2014). The magnetic field strength is $H_0 = 10{,}000$ A/m.

3. RESULTS AND DISCUSSION

3.1. PARTICLE INTERACTION OF A PAIR OF CIRCULAR PARTICLES

In this section, as a validation of the numerical model, we compare the simulation results from our numerical model to the results from references for particle interaction of a pair of circular particles. When two circular particles suspended in the quiescent flow under a uniform magnetic field, the net forces acting on the particles have the equal magnitude but opposite directions. The directions of those two forces generated by magnetic interactions are changed with time except for the cases where the center-to-center line of the particles is perpendicular or parallel to the magnetic field. In these cases, the magnetic interaction between those two particles under the uniform magnetic field could be either attractive or repulsive, which depends on the center-to-center angle θ. According to the simulation results from Ref. (Kang *et al.*, 2008), the critical angle θ_c is approximately 45°, i.e. the magnetic force is attractive when $\theta < 45°$, while it is repulsive when $\theta > 45°$.

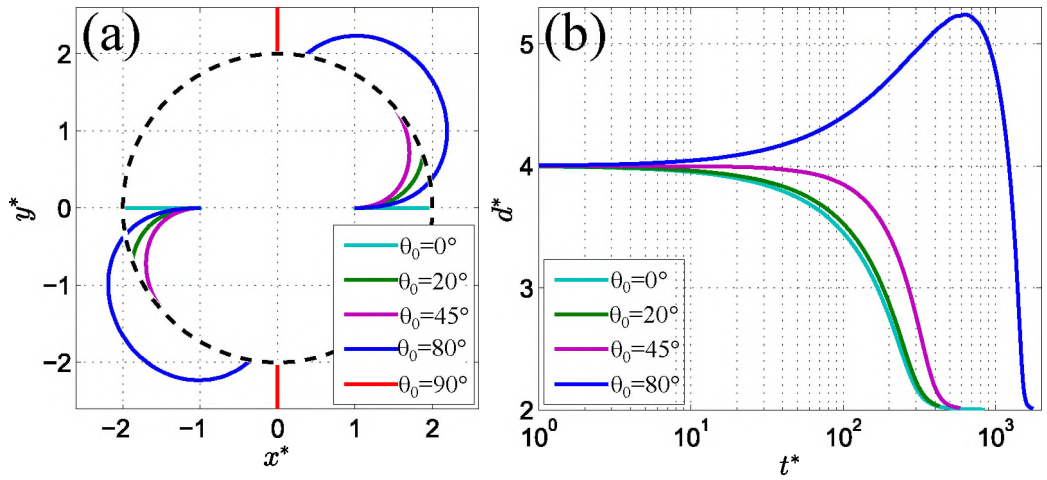

Figure 2. (a) Trajectories of the centers of the two circular particles under the uniform magnetic field at the five initial relative angles $\theta_0 = 0°$, $\theta_0 = 20°$, $\theta_0 = 45°$, $\theta_0 = 80°$ and $\theta_0 = 90°$; (b) The dimensionless center-to-center distance, d^*, varies with dimensionless time, t^*. The dash line is a circle of radius 4 where initial positions of the particles are located.

To compare our simulation results with results in Ref. (Kang *et al.*, 2008), we investigate the same initial positions, i.e. the constant initial center-to-center distance $d_0 = 4R_0$ for the initial relative angle $\theta_0 = 0°$, 20°, 45°, 80° and 90°. Here, particle position and center-to-center distance is dimensionless by the particle equivalent radius, R_0, i.e. $x^* = x/R_0$, $y^* = y/R_0$ and $d^* = d/R_0$. The dimensionless time is defined as $t^* = t/\tau_m$. For a linear magnetization of the particle we considered in this work, $\tau_m = \eta_f/(\mu_0 \chi_f^2 H_0^2)$ is referred to as the magnetoviscous time constant (Shine and Armstrong, 1987), which represents a characteristic time to measure the relative effect between viscous and magnetic stresses. Figure 2 shows the dimensionless particle trajectories and center-to-center distance of a pair of circular particles under the uniform magnetic field for different initial relative angles when dimensionless initial center-to-center distance $d_0^* = 4$. As we can see, the trajectories of the particles for $\theta_0 = 0°$, 20°, 45°, 80° and 90° in Figure 2a are the similar as in Ref. (Kang *et al.*, 2008). The two particles are aligned with the magnetic field regardless of the initial relative angle, θ_0, except for the case of $\theta_0 = 90°$. When $\theta_0 = 90°$, the two particle move away from each other. However, these positions are highly unstable. If there was a small disturbance acting on the particles, the two particles will also be aligned to the direction of magnetic field for the initial relative angle of 90°. From Figure 2b, we can see that the dimensionless distance, d^*, decreases monotonously with dimensionless time, t^*, when $\theta_0 = 0°$. It means that the two particles attract with each other and move towards with each other. As θ_0 increases, the decreasing rate becomes slower, meaning that the attractive force between two particles becomes weaker. When $\theta_0 = 80°$, d^* increases first and then decreases with dimensionless time, t^*, meaning that two particles first repulse with each other and then attract with each other. When $\theta_0 = 45°$, d^* increases monotonously with t^*, meaning that there are just attractive forces between the particles. These findings are also the same as in Ref. (Kang *et al.*, 2008). Therefore, this simulation method has been validated to be sufficiently accurate to study the dynamics of a pair of paramagnetic particles under the uniform magnetic field.

3.2. MAGNETO-ORIENTATION OF A SINGLE PROLATE ELLIPTICAL PARTICLE

In this section, we investigate the local magneto-orientation of a single prolate elliptical paramagnetic particle under a uniform magnetic field. Uniform magnetic fields are frequently used to align paramagnetic or ferromagnetic materials in the liquid medium. Assuming the magnetic susceptibility of the particle is homogeneous, the particle can also undergo magnetic orientation if its shape is anisotropic (Yamaguchi *et al.*, 2006). The induced magnetic moment of the particle depends on both magnetic susceptibility and particle shape. When a magnetic particle is place in a uniform magnetic field, the demagnetizing field is induced. As a result, the particle with isotropic magnetic susceptibility tends to be aligned to its major axis parallel to the magnetic field where the magnetic energy is minimum(Figure 3a). When its major axis is perpendicular to the magnetic field, the particle is in an equilibrium state, but is unstable. Once there is a small disturbance, the particle tends to reorient itself to the direction where its major axis parallel to the magnetic field. s

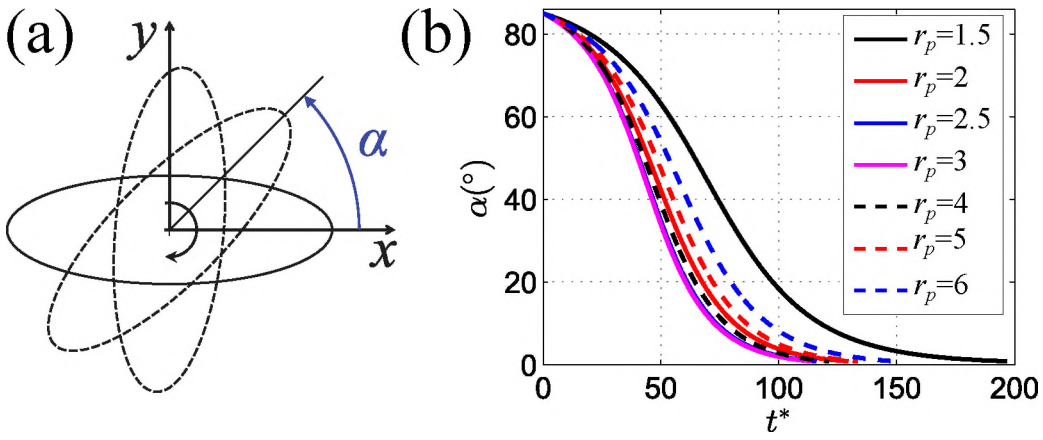

Figure 3. (a) A diagram of the magneto-orientation process for $r_p = 3$ when the magnetic field is directed left to right; (b) The self-orientation angle of a single prolate elliptical particle, α as a function of dimensionless time, t^*, for different aspect ratios.

Figure 3b shows the simulation result of the orientation angle of the particle, α, of a single elliptical particle varying with the dimensionless time, t^* for different aspect ratio, where the initial angle between the major axis of the particle and the magnetic field $\alpha_0 = 85°$. To compare the effect of aspect ratio on the particle rotation, the relaxation time is defined as the time required for the particle rotating from initial angle to the orientation angle α falling below 1% of its initial angle. From the figure 3b, we can see the effect of aspect ratio, r_p, on the dimensionless relaxation time, t^*. For a circular particle, there is no net magnetic torque acting on the particle under a uniform magnetic field, so the relaxation time is considered as infinite. For a nearly circular particle, we can except it has a larger relaxation time due to a smaller torque acting on the particle. From the figure 3b, we can see that the relaxation time of the particle with aspect ratio $r_p = 1.5$ is the longest among these seven cases. The relaxation time is reduced when r_p increases from 1.5 to 3 as shown in the solid line in Figure 3b. We also can see that the minimum relaxation time is achieved when $r_p = 3$ among those seven cases. As the aspect ratio continues to increase, the relaxation time is increased as shown in the dash line in Figure 3b. Those results have quantitative agreement with the theory from Ref. (Shine and Armstrong, 1987), where the relaxation time is first decreased and then increased as the aspect ratio is increased.

3.3. TWO PARTICLES: COMBINED MAGNETO-ORIENTATION AND GLOBAL REORIENTATION

In this section, we investigate the interaction of two particles for different orientation angle, α. Initially, two particles with $r_p = 2$ are place at $(x^*, y^*) = [\pm 2.2cos(80°), \pm 2.2sin(80°)]$ under an external magnetic field $H_0 = 10{,}000$ A/m along the x axis, i.e. $d_0^* = 2.2$ and $\theta_0 = 80°$. Figure 4 shows particle trajectories and orientation angle as a function of dimensionless time for three different initial orientation angle. To see the combination effect of the local

magneto-orientation and global reorientation and how it influences the particle interactions, we compare the relaxation time spending for the magneto-orientation to the relaxation time for the global reorientation.

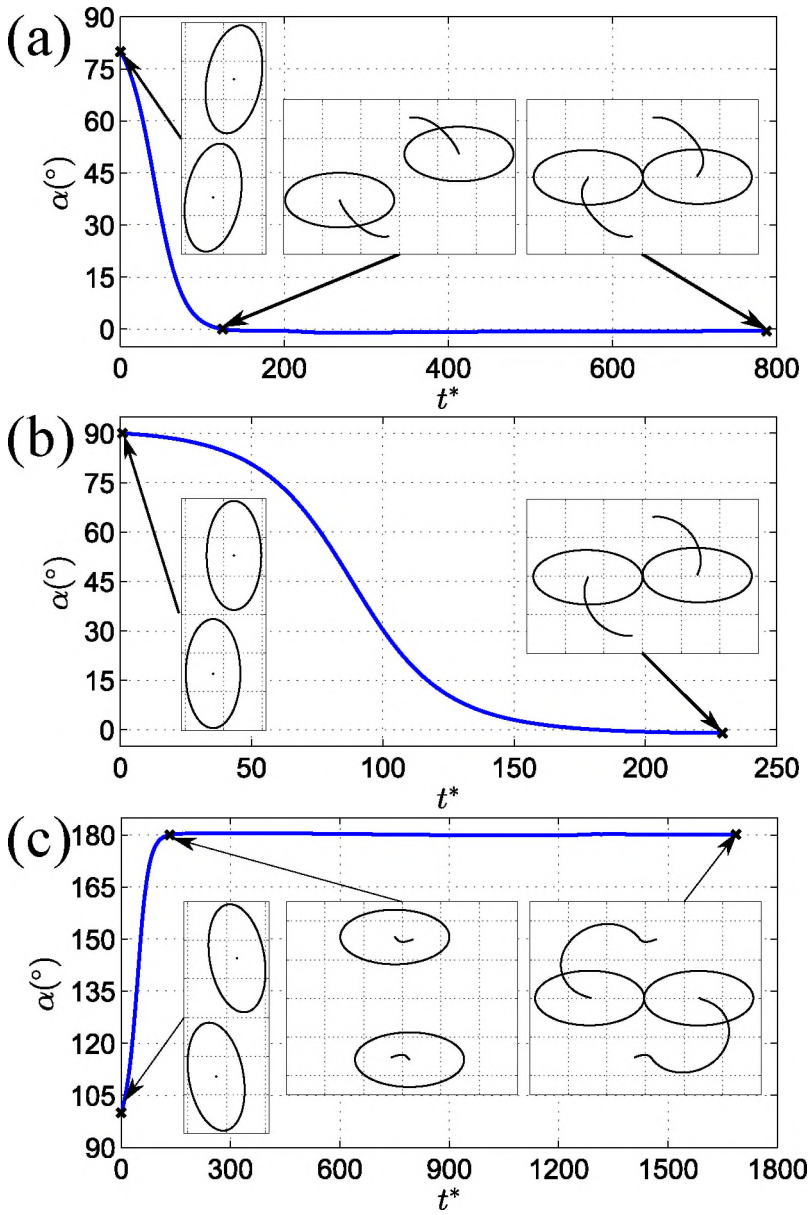

Figure 4. The orientation angle of the particle, α, and particle trajectory as a function of dimensionless time, t^*, for three initial orientation angle $\alpha_0 = 80°$(a), 90°(b) and 110°(c). The initial position of the particles are $d_0^* = 2.2$ and $\theta_0 = 80°$.

As can be seen, for initial orientation angle $\theta_0 = 80°$, the particles first have a clockwise local magneto-orientation from 80° to 0°, and then spend most of time for the global reorientation. Specifically, in this case, the local magneto-orientation is completed by $t^* = 125$, while the global reorientation requires about $t^* = 642$. There is a similar results for $\theta_0 = 100°$, but the particles have an anticlockwise local orientation and spend longer time in global reorientation than $\theta_0 = 80°$. The particles require $t^* = 133$ to complete the local magneto-orientation, while require $t^* = 1553$ to complete the global reorientation. In a special case when $\theta_0 = 90°$, there is just local magneto-orientation as shown in Figure 4(b). Thus, we can see that those two particles will spend much less time in the local magneto-orientation than global reorientation with the arbitrary initial orientation angle except for $\theta_0 = 90°$ where there is just local magneto-orientation. Since the global reorientation of the particles is what we are most interested in, it is reasonable to assume the particles have already completed the local magneto-orientation process and just simulate the global reorientation process for particles of different conditions.

3.4. TWO PARTICLES: PARALLEL($\theta_0 = 0°$) OR PERPENDICULAR($\theta_0 = 90°$) TO MAGNETIC FIELD

First, we consider the cases when the center-to-center line of two particles is parallel($\theta_0 = 0°$) or perpendicular($\theta_0 = 90°$) to the magnetic field when the initial orientation angle $\alpha_0 = 0°$. Figure 5 shows the magnetic field around the two particles when the magnetic field is applied at x direction. We can see that the magnetic field around those two particles is symmetric to each other. This symmetric field leads to the magnetic force that is attractive ($\theta_0 = 0°$) or repulsive ($\theta_0 = 90°$) while no magnetic torque is acting on the particles, so there is no global reorientation for those two particles. When $\theta_0 = 0°$, the region between the particles has a strong magnetic field, resulting in the total mutual magnetic force which drives the particles toward each other along the center-to-center line. When $\theta_0 = 90°$, the region between the particles has a weak magnetic field, resulting in the total mutual

magnetic force which drives the particles away from each other along the center-to-center line. These findings are similar to the circular particles in Section 3.1. However, It's worth mentioning that the particles are even more unstable for elliptical particles than circular particles when $\theta_0 = 90°$. Even a small disturbance could lead to the particles deviating from the perpendicular position.

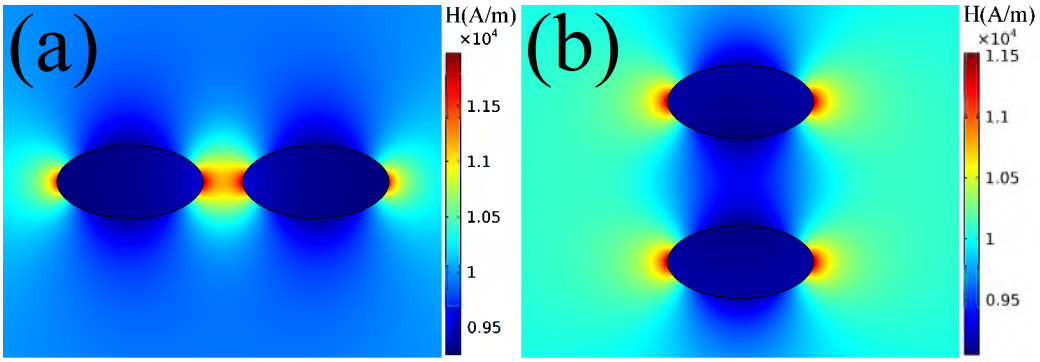

Figure 5. Magnetic field around two particles when the initial relative angle is 0°(a) and 90°(b).

3.5. TWO PARTICLES: GLOBAL REORIENTATION AT ARBITRARY INITIAL POSITION ($0° < \theta_0 < 90°$)

Generally, the initial orientation of two particles is a arbitrary angle other than two critical angles we mentioned before. Thus, it is more practical to understand the particle-particle interaction and relative motion of two arbitrarily oriented particles.

The global reorientation of two elliptical particle with aspect ratio $r_p = 2$ when $\alpha_0 = 0°$ are shown in Figure 6. Initially, the particles are placed at $(x^*, y^*) = [\pm 2.4cos(80°), \pm 2.4sin(80°)]$, i.e. $d_0^* = 2.4$ and $\theta_0 = 80°$. At the starting position (i.e. $t^* = 0$), the magnetic field around the particles is asymmetric to either x axis or y axis, but axisymmetric to the midpoint of center-to-center line. Specifically, it generates a weaker magnetic field between the particles than outside of the particles, resulting in net repulsive magnetic forces and net

torques acting on the particles. However, the magnetic field is axisymmetric to the midpoint of center-to-center line of the particles, so those forces and torques have the equal magnitude but opposite direction, which causes the particles moving away from each other in both vertical and horizontal direction. As the particles move, the vertical force become weaker. When the particles move to the position at $t^* = 242$, the vertical magnetic force becomes zero, just remain horizontal force, where the center-to-center distance in y direction reaches the maximum. As the particles continue to move, the asymmetry magnetic field between the particles causes the vertical magnetic forces to attractive, while the horizontal forces stay repulsive, where the vertically attractive forces become weaker and the horizontally repulsive forces become stronger. When the particles move to the position at $t^* = 762$, the horizontal forces become zero, just remain vertical forces, where the center-to-center distance in x direction reach the maximum. As the particles continue moving, the horizontal and vertical forces are both attractive, resulting in the particles moving towards each other. Finally, at $t^* = 1160$, the particles touch with each other to form a stable chain with a small final global orientation angle $\theta_f = 0.20°$. The corresponding velocity field demonstrated our analysis as shown in Figure(a3-d3).

To systematically investigate the global reorientation of two particles, the effect of some important factors on the particle-particle interaction will be studied in the following subsections.

3.5.1. The Effect of Initial Relative Angle Between Two Particles. First, we investigate the effect of initial relative angle between two particles, θ_0, on the particle-particle interaction. Initially, the particles with aspect ratio $r_p = 2$ are placed at $(x^*, y^*) = [\pm 2.4cos(\theta_0), \pm 2.4sin(\theta_0)]$ for different initial center-to-center distance, θ_0, as shown as cross dots in Figure 7(a). As can be seen Figure 7(a) and (b), the particles spend more time for the whole process, and particle trajectory becomes longer as θ_0 increases from 20° to 80°.

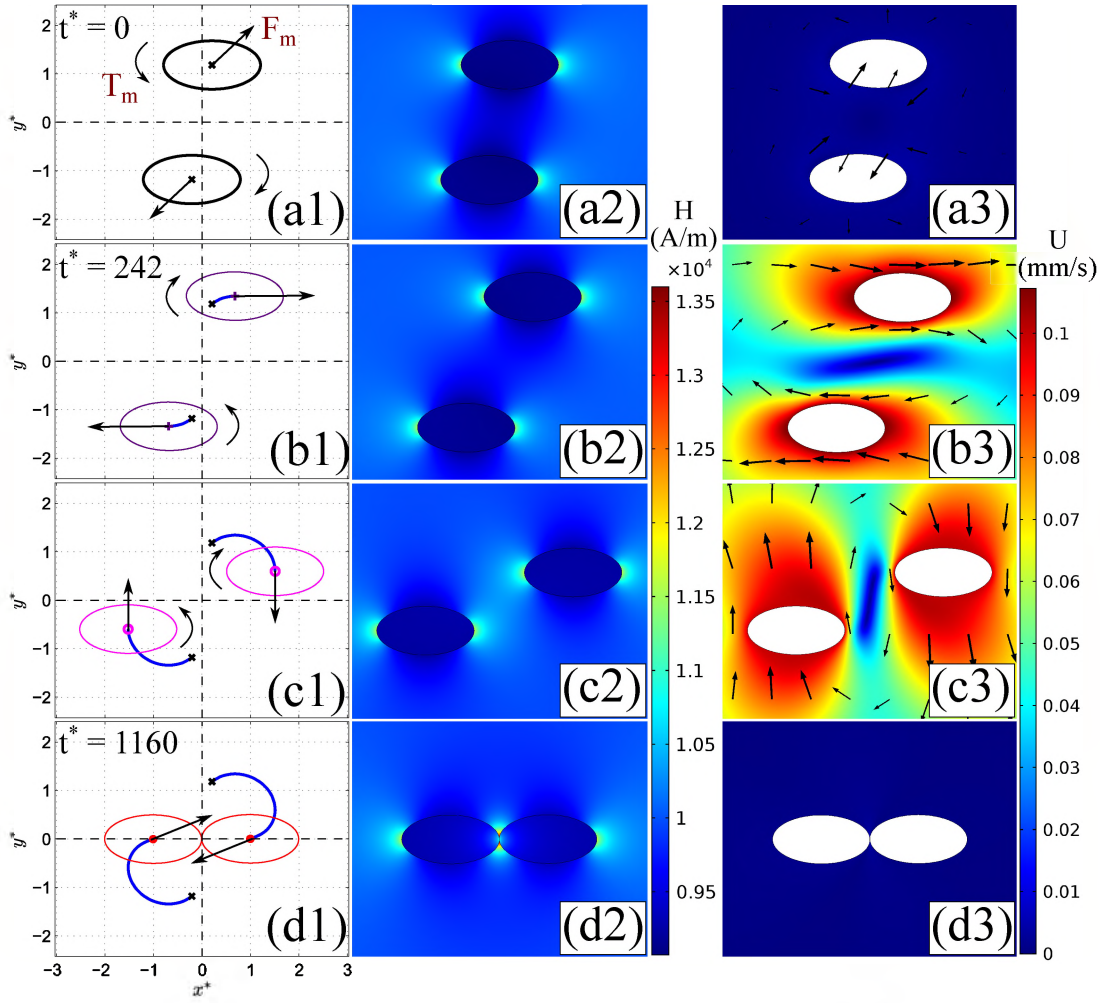

Figure 6. Global reorientation of two elliptical particles with $r_p = 2$, $d_0^* = 2.4$ and $\theta_0 = 80°$ for different time(a1-d1), where the magnetic field is applied left to right. The straight and curve vectors represents magnetic force $\mathbf{F_m}$ and torque $\mathbf{T_m}$, respectively. The corresponding magnetic and velocity fields around the particles are shown as (a2-d2) and (a3-d3) on the right side.

We can see from Figure 7(b) that, when the initial orientation angle $\theta_0 = 80°$ and 60°, the dimensionless center-to-center distance , d^*, first increases and then decreases with dimensionless time, t^*; when $\theta_0 = 20°$, d^* decreases with t^*. These findings are similar to circular particles discussed in Section 3.1. However, When $\theta_0 = 40°$, the dimensionless distance varying with dimensionless time has the similar result as $\theta_0 = 80°$ and 60°: d^* first increases and then decreases with t^*. It means that the critical angle, θ_c, of the elliptical

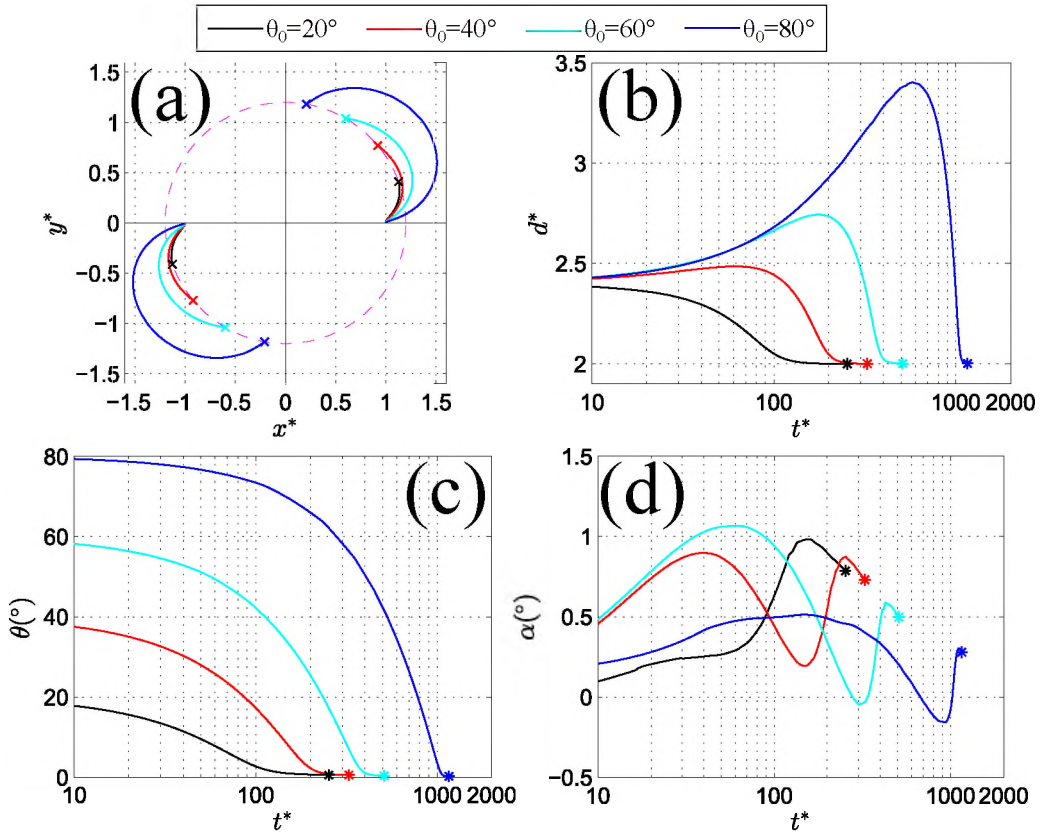

Figure 7. The effect of initial relative orientation angle between the particles on the particle-particle interaction. (a) Trajectories of particle centers, (b) center-to-center distance varying with dimensionless time, (c) the relative angle between the particles varying with dimensionless time, (d) the orientation angle of the particles varying with dimensionless time when $r_p = 2$ and $d_0^* = 2.4$. The cross and star dots represent the starting point and the ending point, respectively.

particles with $r_p = 2$ is smaller than 40°, which is different from the critical angle of circular particles. In addition, as θ_0 increases, the increasing and decreasing rates become steeper and the maximum d^* become larger. For a fixed relative orientation angle θ, it decreases monotonously with time shown in Figure 7(c). The final global orientation angle when the particles touch are $\theta_f = 0.54°$, 0.51°, 0.35° and 0.20° for $\theta_0 = 20°$, 40°, 60° and 80°, respectively. So we can see it becomes smaller as the initial orientation angle becomes larger. There is a similar results for the final particle orientation angle: it becomes smaller as θ_0 becomes larger. From Figure 7(d), we can see that the particle orientation angle

changes drastically. As time elapses, it increases first and then decreases. When it reaches a minimum, it increases and then decreases again until the particles touch. There are two increasing-and-decreasing circles, which are due to the change of direction of magnetic torque.

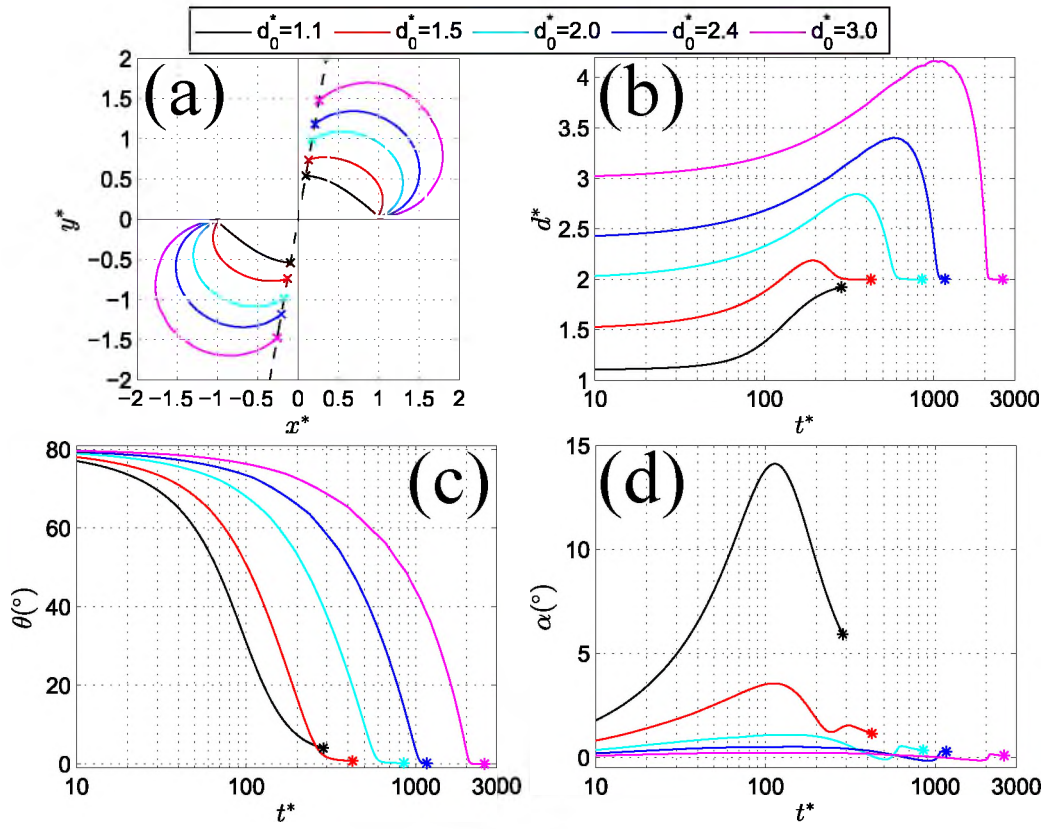

Figure 8. The effect of initial center-to-center distance on the particle-particle interaction. (a) Trajectories of particle centers, (b) center-to-center distance varying with dimensionless time, (c) the relative angle between the particles varying with dimensionless time, (d) the orientation angle of the particles varying with dimensionless time when $r_p = 2$ and $\theta_0 = 80°$. The cross and star dots represent the starting point and the ending point, respectively.

3.5.2. The Effect of Initial Center-to-Center Distance. Then, we investigate the effect of initial center-to-center distance between two particles, d_0^*, on the particle-particle interaction. Initially, the particles with aspect ratio $r_p = 2$ are placed at $(x^*, y^*) = [\pm d_0^* cos(80°), \pm d_0^* sin(80°)]$ when initial center-to-center distance, d_0^*, varies from 1.1 to

3.0 as shown as cross dots in Figure 8(a). As can be seen from Figure 8(a) and (b), the particles spend more time for the whole process and particle trajectory becomes longer when d_0^* increases from 1.1 to 3.0. There is a similar result for d_0^* as we discussed in Section 3.5.1: it first increases and then decreases with t^* when $d_0^* = 1.5$, 2.0, 2.4 or 3.0. The result is different for $d_0^* = 1.1$: it increases monotonously with t^*. The particle orientation angle varying with time shown as black line in Figure 8(b) demonstrates that the magnetic torque has much more influence on the particle-particle interaction when the two particles are so closer. In addition, the change rule for $d_0^* = 1.1$ is also different: it has just one increasing-and-decreasing circle, while other relative distances have the similar results as in Section 3.5.1: two increasing-and-decreasing circles happens. For the final relative orientation angle shown in Figure 8(c), it becomes smaller as the initial center-to-center distance becomes larger. Specifically, $\theta_f = 4.04°, 0.80°, 0.24°$, $0.20°$ and $0.06°$ for $d_0^* = 1.1$, 1.5, 2.0, 2.4 and 3.0, respectively. From Figure 8(d), the final particle rotation angle becomes smaller as as the initial center-to-center distance becomes larger.

3.5.3. The Effect of Particle Aspect Ratio. Here, we investigate the effect of particle aspect ratio, r_p, on the particle-particle interaction. To compare the effect of r_p on the particle-particle interaction, the particle trajectories and the center-to-center distance are dimensionless by its major semi-axis length a, where $a = \sqrt{r_p} * R_0$. Figure 9(a) and (b) show the particle trajectories and particle center-to-center distance for $r_p = 1$, 2 and 3. We can see that, as r_p becomes larger, the particle trajectory becomes longer and the particles spend more time for the whole process. What's more, the maximum of d^* becomes larger and the overall increasing rate from beginning to the maximum becomes smaller as r_p becomes larger. For the final relative orientation angle and particle orientation angle shown in Figure 9(c) and (d), they become larger as the initial orientation angle becomes larger. Specifically, $\theta_f = 0°, 0.06°, 0.30°$, and $\alpha_f = 0°, 0.09°, 0.22°$ for $r_p = 1$, 2, 3, respectively.

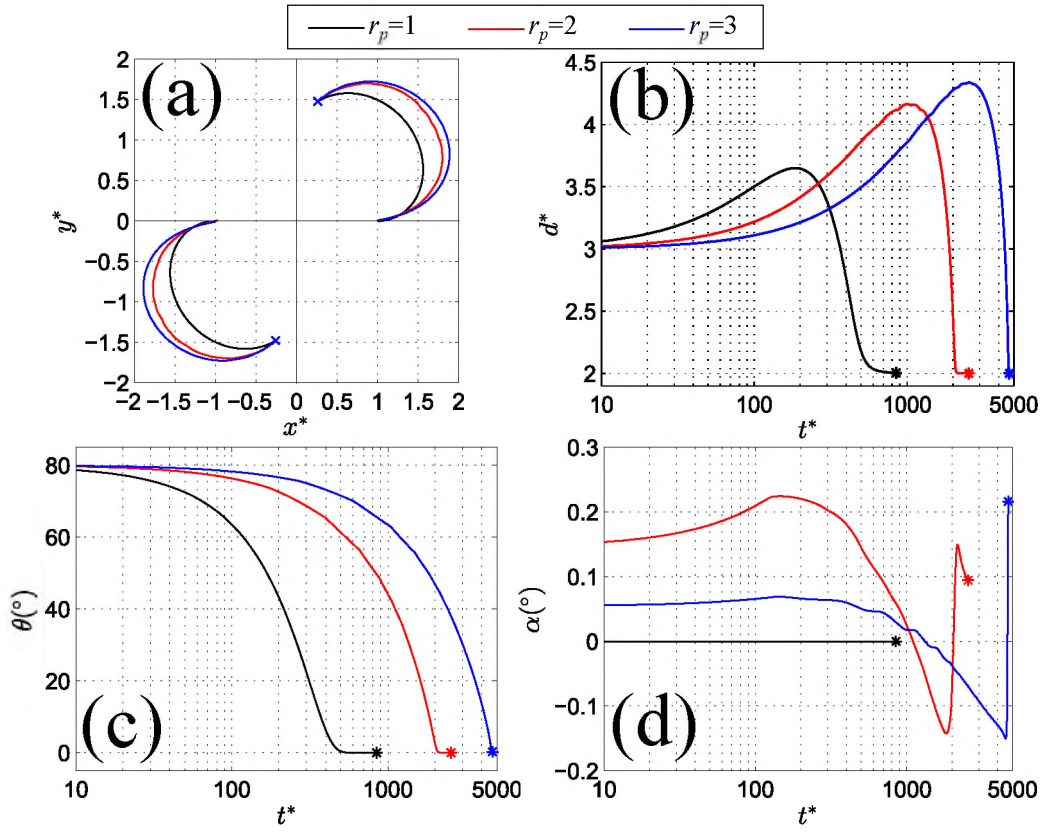

Figure 9. The effect of particle aspect ratio on the particle-particle interaction. (a) Trajectories of particle centers, (b) center-to-center distance varying with dimensionless time, (c) the relative angle between the particles varying with dimensionless time, (d) the orientation angle of the particles varying with dimensionless time when $d_0^* = 2.4$ and $\theta_0 = 80°$. The cross and star dots represent the starting point and the ending point, respectively.

4. CONCLUSION

The two-dimensional models of particle-particle interactions and relative motions of a pair of paramagnetic particles of elliptical shapes are numerically investigated using the direct numerical simulations based on the finite element method and arbitrary Lagrangian-Eulerian approach. The numerical modeling considers the particle-fluid-magnetic field interaction. By validating against previous numerical solutions for circular particles, our numerical model was shown to be able to accurately describe the dynamics of a pair of paramagnetic non-spherical particles under the uniform magnetic field. The rotational

dynamics of a single elliptical paramagnetic particle is first investigated. The simulation results are in qualitative agreement with the theory of Shine and Armstrong (Shine and Armstrong, 1987). By investigating the effect of the particle initial orientation angle on the local and global magneto-orientation of a pair of elliptical particles, it shows that the local orientation process is much faster than the global orientation. According to this finding, we focused our simulations on the relative motion of a pair of particles when the initial orientation angle is 0° (i.e. the initial major axis is parallel to the magnetic field). Based on this model, we investigated the influence of the initial relative angle and distance of the particles, aspect ratio on the particle-particle interactions and relative motions of two particles. The results show that the particles of larger initial relative angles and distances need more time to form a stable chain and smaller final particle and global relative orientation angles. For a larger particle aspect ratio, more time is required to form a chain, and the final particle and global relative orientation angles are larger. Therefore, this work provides useful information for the fundamental particle-particle interactions mechanism in the magnetic particle suspensions under a uniform magnetic field.

ACKNOWLEDGMENTS

The authors gratefully acknowledge the support from the Department of Mechanical and Aerospace Engineering (MAE) and the Center for Biomedical Research (CBR) at Missouri University of Science and Technology.

REFERENCES

Abbas, M. and Bossis, G., 'Separation of two attractive ferromagnetic ellipsoidal particles by hydrodynamic interactions under alternating magnetic field,' Physical Review E, 2017, **95**(6), p. 062611.

Ai, Y., Beskok, A., Gauthier, D. T., Joo, S. W., and Qian, S., 'Dc electrokinetic transport of cylindrical cells in straight microchannels,' Biomicrofluidics, 2009a, **3**(4), p. 044110.

Ai, Y., Joo, S. W., Jiang, Y., Xuan, X., and Qian, S., 'Pressure-driven transport of particles through a converging-diverging microchannel,' Biomicrofluidics, 2009b, **3**(2), p. 022404.

Ai, Y. and Qian, S., 'Dc dielectrophoretic particle–particle interactions and their relative motions,' Journal of colloid and interface science, 2010, **346**(2), pp. 448–454.

Ai, Y., Zeng, Z., and Qian, S., 'Direct numerical simulation of ac dielectrophoretic particle–particle interactive motions,' Journal of colloid and interface science, 2014, **417**, pp. 72–79.

Anupama, A., Kumaran, V., and Sahoo, B., 'Magnetorheological fluids containing rod-shaped lithium–zinc ferrite particles: the steady-state shear response,' Soft matter, 2018, **14**(26), pp. 5407–5419.

Bell, R., Karli, J., Vavreck, A., Zimmerman, D., Ngatu, G., and Wereley, N., 'Magnetorheology of submicron diameter iron microwires dispersed in silicone oil,' Smart Materials and Structures, 2008, **17**(1), p. 015028.

Bell, R., Miller, E., Karli, J., Vavreck, A., and Zimmerman, D., 'Influence of particle shape on the properties of magnetorheological fluids,' International Journal of Modern Physics B, 2007, **21**(28n29), pp. 5018–5025.

Bica, I., Liu, Y. D., and Choi, H. J., 'Physical characteristics of magnetorheological suspensions and their applications,' Journal of Industrial and Engineering Chemistry, 2013, **19**(2), pp. 394–406.

Bombard, A. J., Gonçalves, F. R., Morillas, J. R., and De Vicente, J., 'Magnetorheology of dimorphic magnetorheological fluids based on nanofibers,' Smart Materials and Structures, 2014, **23**(12), p. 125013.

Bossis, G., Marins, J. A., Kuzhir, P., Volkova, O., and Zubarev, A., 'Functionalized microfibers for field-responsive materials and biological applications,' Journal of Intelligent Material Systems and Structures, 2015, **26**(14), pp. 1871–1879.

De Vicente, J., Klingenberg, D. J., and Hidalgo-Alvarez, R., 'Magnetorheological fluids: a review,' Soft matter, 2011, **7**(8), pp. 3701–3710.

De Vicente, J., Segovia-Gutiérrez, J., Andablo-Reyes, E., Vereda, F., and Hidalgo-Álvarez, R., 'Dynamic rheology of sphere-and rod-based magnetorheological fluids,' The Journal of chemical physics, 2009, **131**(19), p. 194902.

de Vicente, J., Vereda, F., Segovia-Gutiérrez, J. P., del Puerto Morales, M., and Hidalgo-Álvarez, R., 'Effect of particle shape in magnetorheology,' Journal of Rheology, 2010, **54**(6), pp. 1337–1362.

Dong, X., Tong, Y., Ma, N., Qi, M., and Ou, J., 'Properties of cobalt nanofiber-based magnetorheological fluids,' RSC Advances, 2015, **5**(18), pp. 13958–13963.

Gao, Y., Hulsen, M., Kang, T., and Den Toonder, J., 'Numerical and experimental study of a rotating magnetic particle chain in a viscous fluid,' Physical Review E, 2012, **86**(4), p. 041503.

Gijs, M. A., 'Magnetic bead handling on-chip: new opportunities for analytical applications,' Microfluidics and Nanofluidics, 2004, **1**(1), pp. 22–40.

Gijs, M. A., Lacharme, F., and Lehmann, U., 'Microfluidic applications of magnetic particles for biological analysis and catalysis,' Chemical reviews, 2009, **110**(3), pp. 1518–1563.

Hejazian, M., Li, W., and Nguyen, N.-T., 'Lab on a chip for continuous-flow magnetic cell separation,' Lab on a Chip, 2015, **15**(4), pp. 959–970.

Hu, H. H., Patankar, N. A., and Zhu, M., 'Direct numerical simulations of fluid–solid systems using the arbitrary lagrangian–eulerian technique,' Journal of Computational Physics, 2001, **169**(2), pp. 427–462.

Jamshaid, T., Neto, E. T. T., Eissa, M. M., Zine, N., Kunita, M. H., El-Salhi, A. E., and Elaissari, A., 'Magnetic particles: From preparation to lab-on-a-chip, biosensors, microsystems and microfluidics applications,' TrAC Trends in Analytical Chemistry, 2016, **79**, pp. 344–362.

Jiang, W., Zhang, Y., Xuan, S., Guo, C., and Gong, X., 'Dimorphic magnetorheological fluid with improved rheological properties,' Journal of Magnetism and Magnetic Materials, 2011, **323**(24), pp. 3246–3250.

Kang, S. and Suh, Y., 'Direct simulation of flows with suspended paramagnetic particles using one-stage smoothed profile method,' Journal of Fluids and Structures, 2011, **27**(2), pp. 266–282.

Kang, T. G., Gao, Y., Hulsen, M. A., den Toonder, J. M., and Anderson, P. D., 'Direct simulation of the dynamics of two spherical particles actuated magnetically in a viscous fluid,' Computers & Fluids, 2013, **86**, pp. 569–581.

Kang, T. G., Hulsen, M. A., den Toonder, J. M., Anderson, P. D., and Meijer, H. E., 'A direct simulation method for flows with suspended paramagnetic particles,' Journal of Computational Physics, 2008, **227**(9), pp. 4441–4458.

Keaveny, E. E. and Maxey, M. R., 'Modeling the magnetic interactions between paramagnetic beads in magnetorheological fluids,' Journal of Computational Physics, 2008, **227**(22), pp. 9554–9571.

Kuzhir, P., López-López, M. T., and Bossis, G., 'Magnetorheology of fiber suspensions. ii. theory,' Journal of rheology, 2009, **53**(1), pp. 127–151.

López-López, M. T., Kuzhir, P., and Bossis, G., 'Magnetorheology of fiber suspensions. i. experimental,' Journal of Rheology, 2009, **53**(1), pp. 115–126.

López-López, M. T., Vertelov, G., Bossis, G., Kuzhir, P., and Durán, J. D., 'New magnetorheological fluids based on magnetic fibers,' Journal of Materials Chemistry, 2007, **17**(36), pp. 3839–3844.

Melle, S. and Martin, J. E., 'Chain model of a magnetorheological suspension in a rotating field,' The Journal of chemical physics, 2003, **118**(21), pp. 9875–9881.

Morillas, J. R., Carreón-González, E., and De Vicente, J., 'Effect of particle aspect ratio in magnetorheology,' Smart Materials and Structures, 2015, **24**(12), p. 125005.

Ngatu, G., Wereley, N., Karli, J., and Bell, R., 'Dimorphic magnetorheological fluids: exploiting partial substitution of microspheres by nanowires,' Smart Materials and Structures, 2008, **17**(4), p. 045022.

Petousis, I., Homburg, E., Derks, R., and Dietzel, A., 'Transient behaviour of magnetic micro-bead chains rotating in a fluid by external fields,' Lab on a Chip, 2007, **7**(12), pp. 1746–1751.

Rabinow, J., 'The magnetic fluid clutch,' Electrical Engineering, 1948, **67**(12), pp. 1167–1167.

Sedlacik, M., Pavlínek, V., Vyroubal, R., Peer, P., and Filip, P., 'A dimorphic magnetorheological fluid with improved oxidation and chemical stability under oscillatory shear,' Smart Materials and Structures, 2013, **22**(3), p. 035011.

Sheng, R., Flores, G., and Liu, J., 'In vitro investigation of a novel cancer therapeutic method using embolizing properties of magnetorheological fluids,' Journal of magnetism and magnetic materials, 1999, **194**(1-3), pp. 167–175.

Shine, A. and Armstrong, R., 'The rotation of a suspended axisymmetric ellipsoid in a magnetic field,' Rheologica Acta, 1987, **26**(2), pp. 152–161.

Stratton, J. A., *Electromagnetic theory*, John Wiley & Sons, 2007.

Stuart, D. C., Kleijn, C., and Kenjereš, S., 'An efficient and robust method for lagrangian magnetic particle tracking in fluid flow simulations on unstructured grids,' Computers & Fluids, 2011, **40**(1), pp. 188–194.

Suh, Y. K. and Kang, S., 'Motion of paramagnetic particles in a viscous fluid under a uniform magnetic field: benchmark solutions,' Journal of Engineering Mathematics, 2011, **69**(1), pp. 25–58.

Yamaguchi, M., Tanimoto, Y., and Yamaguchi, M., *Magneto-science: magnetic field effects on materials: fundamentals and applications*, volume 48, Springer, 2006.

Zhang, J., Sobecki, C. A., Zhang, Y., and Wang, C., 'Numerical investigation of dynamics of elliptical magnetic microparticles in shear flows,' Microfluidics and Nanofluidics, 2018, **22**(8), p. 83.

Zhang, J. and Wang, C., 'Numerical study of lateral migration of elliptical magnetic microparticles in microchannels in uniform magnetic fields,' Magnetochemistry, 2018, **4**(1), p. 16.

Zhou, R., Bai, F., and Wang, C., 'Magnetic separation of microparticles by shape,' Lab on a Chip, 2017a, **17**(3), pp. 401–406.

Zhou, R., Sobecki, C. A., Zhang, J., Zhang, Y., and Wang, C., 'Magnetic control of lateral migration of ellipsoidal microparticles in microscale flows,' Physical Review Applied, 2017b, **8**(2), p. 024019.

V. MIGRATION OF FERROFLUID DROPLETS IN SHEAR FLOW UNDER A UNIFORM MAGNETIC FIELD

Jie Zhang, Md. Rifat Hassan, Bhargav Rallabandi, and Cheng Wang

Department of Mechanical & Aerospace Engineering

Missouri University of Science and Technology

Rolla, Missouri 65409

Department of Mechanical Engineering

University of California, Riverside

Riverside, California 92521

Tel: 573–341–4636, Fax: 573–341–4607

Email: wancheng@mst.edu

ABSTRACT

Manipulation of droplets based on physical properties (e.g., size, interfacial tension, electrical, and mechanical properties) is a critical step in droplet microfluidics. Manipulations based on magnetic fields have several benefits compared to other active methods. While traditional magnetic manipulations require spatially inhomogeneous fields to apply forces, the fast spatial decay of magnetic field strength from the source make these techniques difficult to scale up. In this work, we report the observation of lateral migration of ferrofluid (or magnetic) droplets under the combined action of a uniform magnetic field and a pressure-driven flow in a microchannel. While the uniform magnetic field exerts negligible net force on the droplet, the Maxwell stresses deform the droplet into elongated shapes and modulate the orientation relative to the fluid flow. Hydrodynamic interactions between the droplets

and the channel walls results in a directional lateral migration. We experimentally study the effects of field strength and direction, and interfacial tension, and use analytical and numerical modeling to understand the lateral migration mechanism.

Keywords: convection

1. INTRODUCTION

Droplet microfluidics has emerged as a powerful technology on lab-on-a-chip platforms for high-throughput screening of chemical and biological assays (Du *et al.*, 2016; Guo *et al.*, 2012; Shembekar *et al.*, 2016). Dispersed in a continuous phase, individual droplets often encapsulate chemical or biological samples (e.g., cells, DNA, proteins, and bacteria), serve as miniaturized reactors, and allow biological and chemical reactions inside individual micro-droplets (Shang *et al.*, 2017). The large surface to volume ratio leads to significantly enhanced mass and heat transfer and bio-/chemical reactions. Furthermore, the high-throughput nature enables a vast number of assays in parallel, thereby drastically improving accuracy of the results.

Manipulation, e.g., sorting, of the droplets based on their contents or properties is a often a critical step in a chemical or biological assay. Droplets can be sorted by passive or active methods. Passive methods are based on hydrodynamic features, such as geometry and fluid properties, to manipulation the droplets (Bowman *et al.*, 2012; Hatch *et al.*, 2013; Kadivar *et al.*, 2013; Tan *et al.*, 2004, 2008; Tan and Lee, 2005). For passive methods to be effective, a complex geometry is usually employed or a particular fluid such as viscoelastic fluid is used as a buffer, which places some limitations on lab-on-a-chip applications. Active methods employ external fields (Xi *et al.*, 2017), such as electric (Agresti *et al.*, 2010; Ahn *et al.*, 2009, 2011, 2006; de Ruiter *et al.*, 2014; Eastburn *et al.*, 2015; Guo *et al.*, 2010; Link *et al.*, 2006; Niu *et al.*, 2007; Rao *et al.*, 2015a,b; Sciambi and Abate, 2014, 2015), acoustic (Lee *et al.*, 2012; Leibacher *et al.*, 2015; Li *et al.*, 2013; Nam *et al.*, 2012; Petersson *et al.*, 2005; Schmid *et al.*, 2014), or magnetic forces (Brouzes *et al.*, 2015; Kim *et al.*, 2014;

Li *et al.*, 2016; Lombardi and Dittrich, 2011; Nguyen *et al.*, 2006; Surenjav *et al.*, 2009; Teste *et al.*, 2015; Zhang *et al.*, 2011, 2009), to manipulate droplets. Among the various active methods, magnetic methods have several distinctive advantages such as low or no heat generation, simple implementation and contactless control, and thus, have received increasing attention over the last few years (Huang *et al.*, 2017).

Ferrofluids are colloidal suspensions consisting of superparamagnetic nanoparticles. Magnetic particles in a ferrofluid commonly have a size of around 10 nm and are coated with surfactant to stabilize and prevent agglomeration. Due to their ability to be controlled by external magnetic fields, ferrofluids have been widely used in applications of mechanical and biomedical fields (Gao *et al.*, 2009; Neuberger *et al.*, 2005; Torres-Díaz and Rinaldi, 2014). Some typical applications of ferrofluids in mircofluidics include microvalves (Oh and Ahn, 2006), micropumps (Laser and Santiago, 2004), magnetic drug targeting (Lübbe *et al.*, 2001) and magnetic separations of cells (Hejazian *et al.*, 2015). More recently in droplet microfluidics, ferrofluid droplets have been used to encapsulate cells for culturing and sorting (Sung *et al.*, 2017) purposes, owing to their bio-compability and ease of manipulation with magnetic fields.

Traditional magnetic manipulation of ferrofluid droplets mainly relies on magnetic forces acting on the droplets. Assuming small field variations over the droplet volume V_p, the magnetic force is (Inglis *et al.*, 2006) $\mathbf{F}_m = \mu_0 V_p[(\mathbf{M}_p - \mathbf{M}_f) \cdot \nabla]\mathbf{H}$, where μ_0 is the magnetic permeability of vacuum, $\mathbf{H}$ is the magnetic field, and $\mathbf{M}_p$, $\mathbf{M}_f$ denote the magnetization of the droplet and fluid respectively. Selective manipulation of droplets is possible based on the susceptibility contrast between the droplet and the surrounding phase, and droplet size (or volume). A number of groups have utilized the magnetic force approach for various applications, including sorting of microalgae encapsulated in ferrofluid droplets (Sung *et al.*, 2017), on-chip manipulation of ferrofluid droplets in water (Zhang *et al.*, 2009) or water droplets in ferrofluid (Zhang *et al.*, 2011), and selective distribution of water-in-magnetic-fluid droplets in curved channels (Kim *et al.*, 2014). However, due to

the fast decay of magnetic fields with distance from the source (Stratton, 2007), magnetic sources need to be placed in proximity to the droplets in order to exert sufficient influence on droplets. Often permanent magnets have to be placed nearby microfluidic channels (Kim *et al.*, 2014; Sung *et al.*, 2017; Zhang *et al.*, 2011, 2009), further making the scaling up of magnetic manipulation difficult.

In this work, we propose and demonstrate a simple and novel droplet manipulation technique by using a uniform magnetic field. In this method, while the uniform magnetic field does not directly exert magnetic forces on the droplets, it modulates the deformation of micro-droplets, which consequently leads to a net lift force and lateral migrations of droplets in shear flows. We explain the cross-stream migration using a hydrodynamic theory involving the interaction of the deformed droplet's stresslet field with the walls of the channel. We then also use numerical simulations, based on the level-set method, to better understand the magnetic and flow fields around the droplets and confirm the migration mechanism.

2. EXPERIMENT

Figure1(a) shows the microfluidic chip placed in a uniform magnetic field with strength H_0 and direction α, which is generated by a Halbach array (Raich and Blümler, 2004). The microfluidic chip was fabricated with polydimethylsiloxane (PDMS) using a previously reported soft-lithography method (Zhang *et al.*, 2015). The width, depth and length of main microchannel are w_c = 800 μm, d_c = 70 μm, and $L \approx$ 13,000 μm as shown in Figure 1(b). Three different sets of Halbach arrays were designed to generate the uniform magnetic fields, which consisted of 20 cuboid permanent 0.25" × 0.25" × 0.25", 0.25" × 0.25" × 0.5" or 0.25" × 0.25" × 1" magnets (K&J Magnetics, Inc.). The details of the design and test of the uniform magnetic field can be seen in the ESI of the previous reported work (Zhou *et al.*, 2017). The magnitudes of these magnetic fields within the central region were measured as $H_0 \approx$ 18,000, 35,000 and 60,000 A/m by a gaussmeter. The droplet is generated by a flow-focusing configuration at the upstream, as shown in Figure 1(b). Water-based

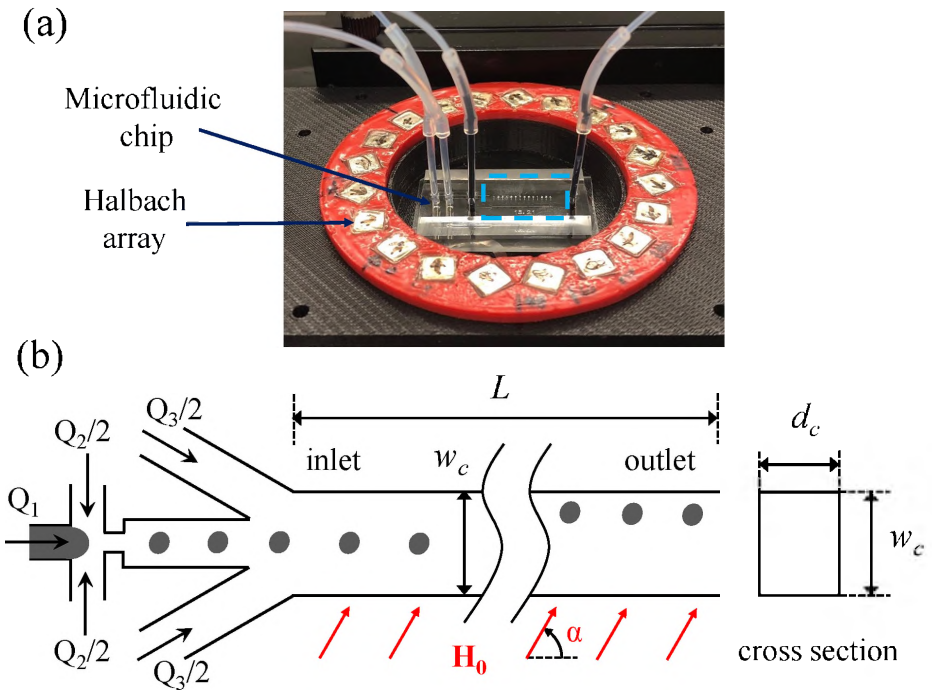

Figure 1. (a) Photo of the microfluidic chip located in a uniform magnetic field. (b) Schematic showing the dimensions of the microchannel.

ferrofluid (EMG 304, Ferrotec Corp.) is the dispersed phase, with the density $\rho_f = 1.24\times10^3$ kg/m^3, viscosity $\eta_f = 5 \times10^{-3}$ Pa·s and an initial magnetic susceptibility (i.e. at small field strength) $\chi_f = 5.03$. Olive oil is used as the continuous phase and buffer fluid, with a density $\rho_o = 0.92\times10^3$ kg/m^3, a viscosity $\eta_o = 78 \times10^{-3}$ Pa·s, and a magnetic susceptibility $\chi_o \approx 0$. Three different olive oil solutions were prepared by adding 0.125% wt, 0.25% wt, 0.375% wt of surfactant SPAN 80 (Sigma-Aldrich, USA) to vary the interfaical tension. The corresponding oil-ferrofluid interfacial tensions were measured as 5.86 ± 0.19, 4.31 ± 0.22 and 2.52 ± 0.22 mN/m using the pendant droplet method (Daerr and Mogne, 2016). Three syringe pumps (KDS Scientific) were used to control the flow rates of the inlets. The flow rates of the dispersed phase (i.e., ferrofluid), continuous phase and buffer flow are $Q_1 = 0.15$ μL/min, $Q_2 = 4$ μL/min and $Q_3 = 6$ μL/min. At these flow rates, the mean fluid speed is $\overline{u} \approx 3$ mm/s and the corresponding Reynolds number in the main channel is $Re \approx 0.028$. The trajectories of the ferrofluid droplets were recorded through an inverted microscope

(IX73, Olympus) with a high-speed CCD camera (Phantom Miro M310, Vision Research). Custom MATLAB codes were written to analyze the centroid position and shape (including deformation and orientation) of the droplets from the recorded videos.

3. RESULTS AND DISCUSSION

3.1. EFFECT OF DIRECTION OF MAGNETIC FIELD

Figure 2 shows the images of droplets at the inlet and outlet and the corresponding probability distributions of droplet centroid in the y direction. In this experiment, the oil-ferrofluid interfacial tension $\sigma = 4.31 \pm 0.22$ mN/m. The average radius of undeformed droplet is $R_0 = 60.76\,\mu$m. The droplets are generated upstream and enter along the centerline of the channel. As can be seen in Figure 2(a1)–(a3), there is a negligible deformation and almost zero net lateral migration in the cross-stream direction (i.e., y direction) when no magnetic field is applied ($H_0 = 0$). Since the Reynolds number is small ($Re \approx 0.028 \ll 1$), inertial effects are negligible. According to previous theoretical (Chan and Leal, 1979) and numerical (Mortazavi and Tryggvason, 2000) investigations, when the droplet is initially placed at the center-line of a channel flow in the absence of a magnetic field, the droplets will move only in the axial direction (i.e., x direction) for viscosity ratio between dispersed and continuous phases $\lambda \lesssim 0.5$ or $\lambda \gtrsim 10$. In this work, $\lambda = \eta_f/\eta_o = 0.064 < 0.5$, and indeed the droplets moving stably along the axial direction in Figure 2(a1)–(a3).

In the presence of a magnetic field, the droplet is deformed by the combination of shear and magnetic fields, the latter producing Maxwell stresses. The deformation due to shear is quantified by the capillary number $Ca = \overline{u}\eta_o/(\sigma w_c)$, while the deformation due to the magnetic field (assuming a linearly magnetizable material) is quantified by the magnetic bond number $Bo_m = \mu_0 H_0^2 R_0/(2\sigma)$. In our experiments, $Ca \approx 5 \cdot 10^{-3}$ and $Bo_m \approx 7$, suggesting that the deformation due to the magnetic field greatly dominates that due to shear.

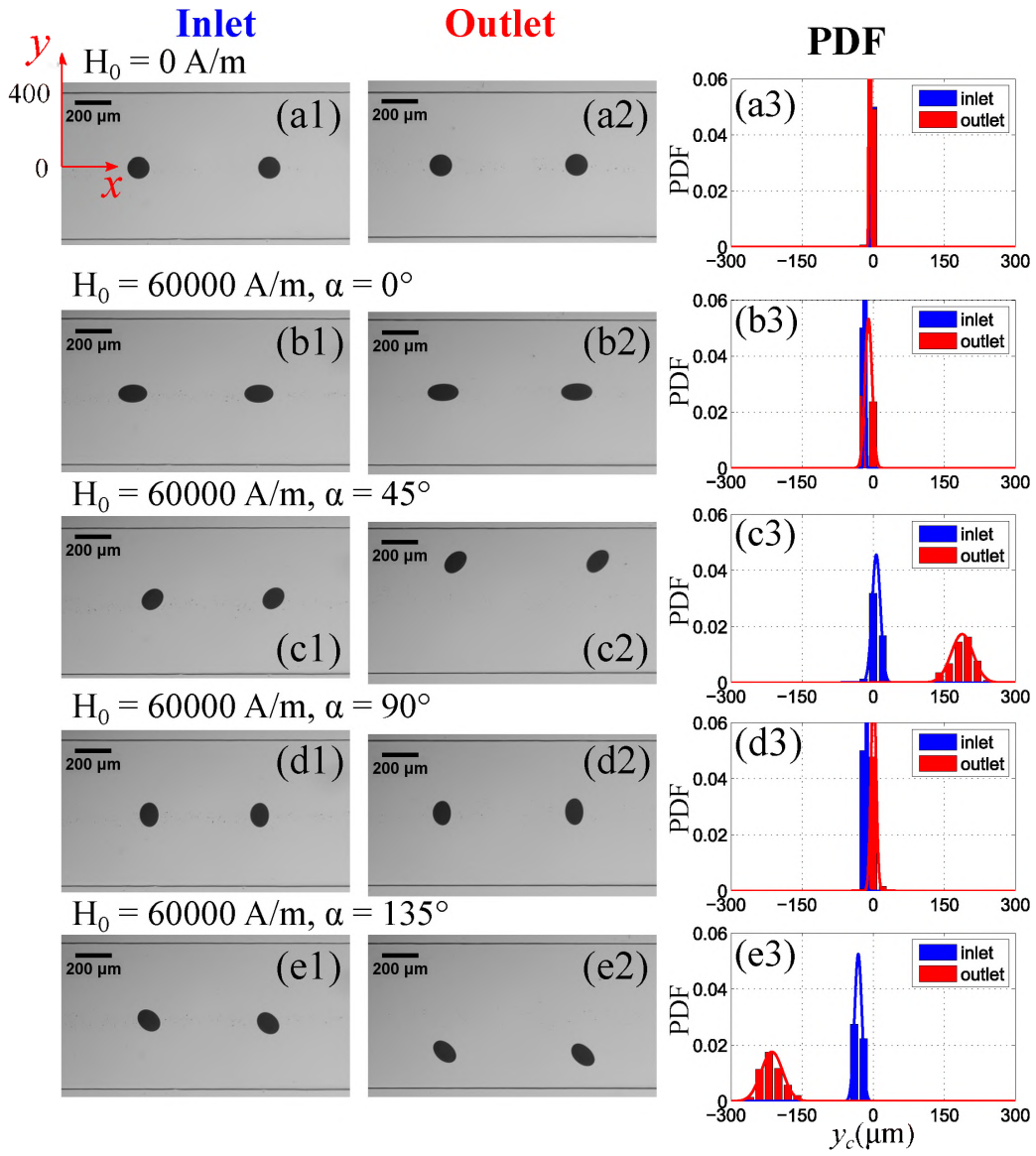

Figure 2. Images at the inlet and outlet, and the corresponding probability density function (PDF) of the centroid of the ferrofluid droplet in the y direction. (a1–a3) without a applied magnetic field (H_0 = 0 A/m); (b1–b3) $H_0 \approx$ 60,000 A/m, and $\alpha = 0°$; (c1–c3) $H_0 \approx$ 60,000 A/m, and $\alpha = 45°$; (d1–d3) $H_0 \approx$ 60,000 A/m, and $\alpha = 90°$; and (e1–e3) $H_0 \approx$ 60,000 A/m, $\alpha = 135°$. The flow rates are $Q_1 = 0.15$ μL/min, $Q_2 = 4.0$ μL/min and $Q_3 = 6.0$ μL/min for all the experiments. The oil-ferrofluid interfacial tension $\sigma = 4.31 \pm 0.22$ mN/m.

Indeed, this is borne out experimentally: when a uniform magnetic field ($H_0 \approx$ 60,000 A/m) is applied at various directions, as shown in Figure 2(b)–(e), the droplets become elongated in the direction of magnetic field independent of their position across

the channel width. Further, the direction of the magnetic field controls the direction of the cross-stream migration. When the magnetic field is parallel to the flow direction (i.e., $\alpha = 0°$) as shown in Figure 2(b1)–(b3), the droplets deform into an ellipsoidal shape with theirs major axis parallel to the flow direction, and there is only a slight net lateral migration in the cross-stream direction, which might be attributed to imperfection of the experimental conditions. As α increases to 45° as shown in Figure 2(c1)–(c3), a similar deformed shape is observed and the elongation axis is aligned to 45°, which results in the droplet migrating towards the upper channel wall. The average distance of the cross-stream migration between inlet and outlet is measured to be 181.16 μm. When α increases to 90° as shown in Figure 2(c1)–(c3), the elongation axis is perpendicular to the flow direction, and there is a slight net lateral migration in the cross-stream direction (again might be due to imperfect control of the experiments). At an inclination angle $\alpha = 135°$ shown in Figure 2(e1)–(e3), the elongation axis is aligned to 135°, which results in the droplets migrating towards the lower wall. The average distance of the cross-stream migration between the inlet and outlet is -182.17 μm.

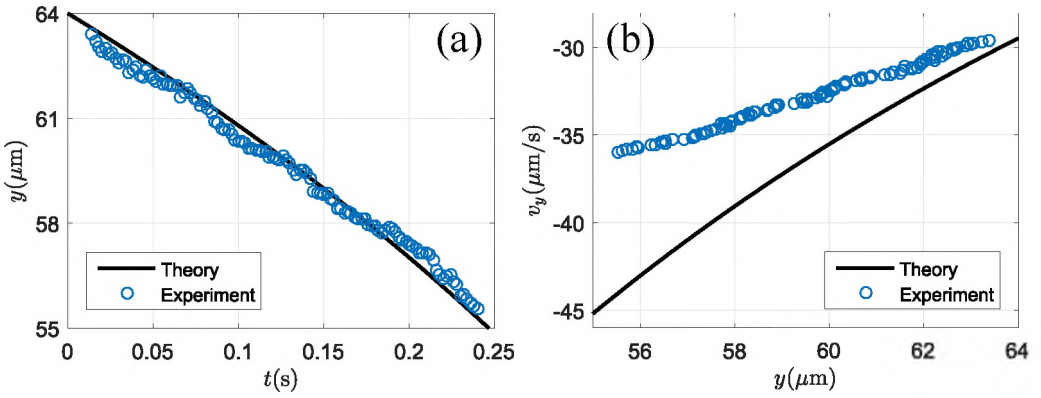

Figure 3. Comparison of the cross-stream migration of a droplet close to the lower wall between the theoretical prediction and experiment. (a) vertical position of the particle (y) as a function of time. (b) cross-stream velocity (v_y) a function of y. Here the magnetic field is applied at $\alpha = 135°$, and $D \approx 0.156$. Note that the channel width is 300 μm.

3.2. CROSS-STREAM MIGRATION MECHANISM

The cross-stream migration of the droplet can be understood by considering hydrodynamic interactions between the droplet and the upper and lower walls of the channel. It is well known for droplets in shear flow alone, the stresslet field around the deformed droplet, by hydrodynamic interactions with nearby boundaries, can result in a cross-stream migration of the droplet (Smart and Leighton Jr, 1989). A key observation is that the component of the stresslet responsible for lateral migration depends on the inclination of the droplet's long axis relative to the flow. In our experiments, the droplet's orientation is set largely by the magnetic field, independent of the flow.

We estimate the cross-stream migration velocity by modeling the droplet as a rigid particle with fixed orientation angle $\approx \alpha$ relative to the horizontal axis. Although this approximation neglects the influence of the interior flow of the droplet, it typically result in small errors for deformation due to shear alone (Aggarwal and Sarkar, 2007; Chan and Leal, 1979; Taylor, 1934). The stresslet of the droplet can then be approximated using the relations of (Kim and Karrila, 2013) for rigid ellipsoids. Next, we recognize that in the present experiments the droplet is centered between the channel walls in the depth direction, and therefore experiences shear gradients primarily in the width (y) direction. We introduce the Taylor deformation parameter $D = \frac{L-B}{L+B}$, where L and B are the semi-major and semi-minor axes, respectively, of the droplet; note that $0 \leq D < 1$. Then, the yy component of the hydrodynamic stresslet is $S_{yy} = \eta_o \pi L^3 \partial_y u_x \left\{ \left(\frac{5}{6} X^M - \frac{5}{6} Z^M - 2Y^H \right) \sin 2\alpha - \left(\frac{5}{4} X^M - \frac{5}{3} Y^M + \frac{5}{12} Z^M \right) \sin 4\alpha \right\}$, where X^M, Z^M, Z^M and Y^H are known functions of the deformation D (see Table 3.4 of (Kim and Karrila, 2013)). The term proportional to $\sin 4\alpha$ is numerically much smaller than the term proportional to $\sin 2\alpha$ for the deformations measured in experiments, and is therefore neglected in the following. Accounting only for the first reflection of the stresslet with the upper and lower walls ($y = 0$, $y = w_c$), the cross-stream migration velocity of a droplet whose center is at a position $y_d \gg R_0$ is (Matsunaga *et al.*, 2017; Smart and Leighton Jr,

1989)

$$v_y \approx -\frac{9}{64\pi\eta_o}\left(\frac{1}{y_d^2}-\frac{1}{(w_c-y_d)^2}\right)S_{yy}\Big|_{y_d}. \tag{1a}$$

$$\approx \frac{3R_0^3}{7}\frac{\partial u_x}{\partial y}\Big|_{y_d}\left(\frac{1}{y_d^2}-\frac{1}{(w-y_d)^2}\right)\frac{D}{1-D}\sin 2\alpha \quad \text{for} \quad D \ll 1, \tag{1b}$$

Note that (1b) is obtained as the leading term of a Taylor expansion of the (1a) for small deformations, although it remains accurate to within 10% even at $D = 0.5$. We note that to evaluate (1), we use the velocity field for a channel with a rectangular cross-section evaluated at the plane of symmetry in the z direction.

The theoretical prediction (1b) quantitatively reproduces the direction of the vertical drift observed in the experiments: the droplet drifts towards the upper wall ($y = w_c$) for α in the first and third quadrants, and towards the lower wall ($y = 0$) for α in the second and fourth quadrants. Figure 3 shows the comparison between the theory and experiment when a droplet was under a magnetic field at $\alpha = 135°$ and migrated towards the lower wall. Note that u_x is determined using the results for a rectangular channel (Mortensen *et al.*, 2005) and D in (1) is obtained from experimental measurements. According to the theory, the symmetry plane $y = 0$ is an unstable fixed point of the trajectory, so the droplet can drift across it. This behavior is similar to recent theoretical predictions for the migration of droplets in Poiseuille flow under uniform electric fields (Mandal *et al.*, 2016). Both the cases of magnetic and electric field are in contrast with the case of a droplet drifting due to deformation by shear alone, where the axis of the droplet follows the elongational axis of the local velocity gradient, which causes the droplet to migrate towards the centerline $y = w/2$, which in this case is a stable fixed point of the migration dynamics when $\lambda \lesssim 0.5$ or $\lambda \gtrsim 10$ (Chan and Leal, 1979).

To further confirm the cross-stream migration mechanism of the droplet, a two-dimensional (2D) numerical model was developed to investigate the ferrofluid droplet transport in the channel. By using commercial a finite element method solver (COMSOL

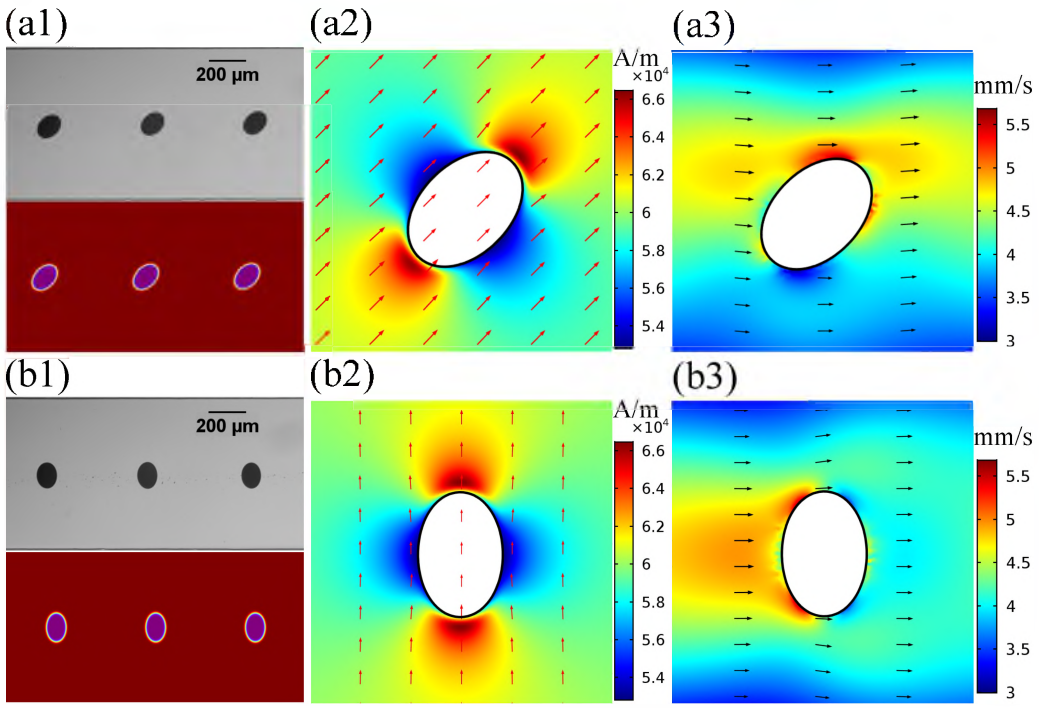

Figure 4. (a) Comparison of droplet trajectory between the experiments and simulation (a1), and numerical results of the magnetic field (a2) and velocity field (a3) for ferrofluid droplets when α = 45°.(b) Comparison of droplet trajectory between the experiments and numerical simulation (b1), and numerical results of the magnetic field (b2) and velocity field (b3) for ferrofluid droplets when α = 90°. The magnetic field strength H_0 = 60000 A/m and the oil-ferrofluid interfacial tension σ = 4.31 ± 0.22 mN/m.

Multiphysics), the numerical model employed the level-set method, and coupled the magnetic and flow fields. Briefly, the magnetic field is first determined by solving the magnetostatic equation, and the magnetic force term is then coupled to the Navier-Stokes equation. More details of the numerical modeling is available from our previous work (Hassan *et al.*, 2018). The magnetic field with strength of 60000 A/m and direction of 45° or 90° was used in the simulations.

Figure 4(a1) shows a comparison of experimental and numerical results when the magnetic field is applied at α = 45°. As we can see, the numerical results are in good agreement with the experiment. The magnetic field and velocity field around the droplet are shown in Figure 4(a2) and (a3). The magnetic force acting on the droplet is approximately

zero for an ellipsoidal droplet placed in a uniform field (Stratton, 2007), which is supported by numerical simulation of the magnetic field distribution (Figure 4(a2)). The presence of magnetic fields leads to the generation of Maxwell stresses at the interface between ferrofluid and olive oil, which cause the deformation of the droplet. Further, the direction of elongation (i.e., major axis) is aligned to the direction of magnetic field. As a result of the ellipsoidal shape and relative orientation of the droplet, the velocity profile around the droplet is asymmetric to the flow direction, as shown in Figure 4(a3). This asymmetric orientation of the deformed droplet with respect to the flow direction results in cross-stream migration towards the upper wall. Note at $\alpha = 135°$, the droplet will move towards the lower wall.

When applied at 90° to the flow direction, the magnetic field causes the droplet to deform into an ellipsoidal shape and the elongation direction is perpendicular to the flow direction. However, the velocity profile around the droplet is symmetric about the channel's centerline as can be seen in Figure 4(b). Similarly, for $\alpha = 0°$, the droplet will be elongated parallel to the flow direction, and no cross-stream migration will take place either due to symmetric flow field around the droplet. In both cases, the stresslet of the droplet is zero and therefore there are negligible hydrodynamic interactions with the walls.

3.3. EFFECTS OF MAGNETIC FIELD STRENGTH, INTERFACIAL TENSION AND FLOW RATE

As discussed earlier, the cross-stream migration depends on the deformation and relative orientation, which are expected to depend on the properties of the fluids, flow field and magnetic field. In a quiescent flow field, the deformation is related to the magnetic field strength, interfacial tension, and droplet size (Afkhami *et al.*, 2010). The droplet size depends on the flow rates used. So here, we focus on the effect of magnetic field strength, interfacial tension and flow rates on the drop migration by examining the case with a magnetic field applied at 45°, as shown in Figure 5(a,b). We used the Taylor deformation

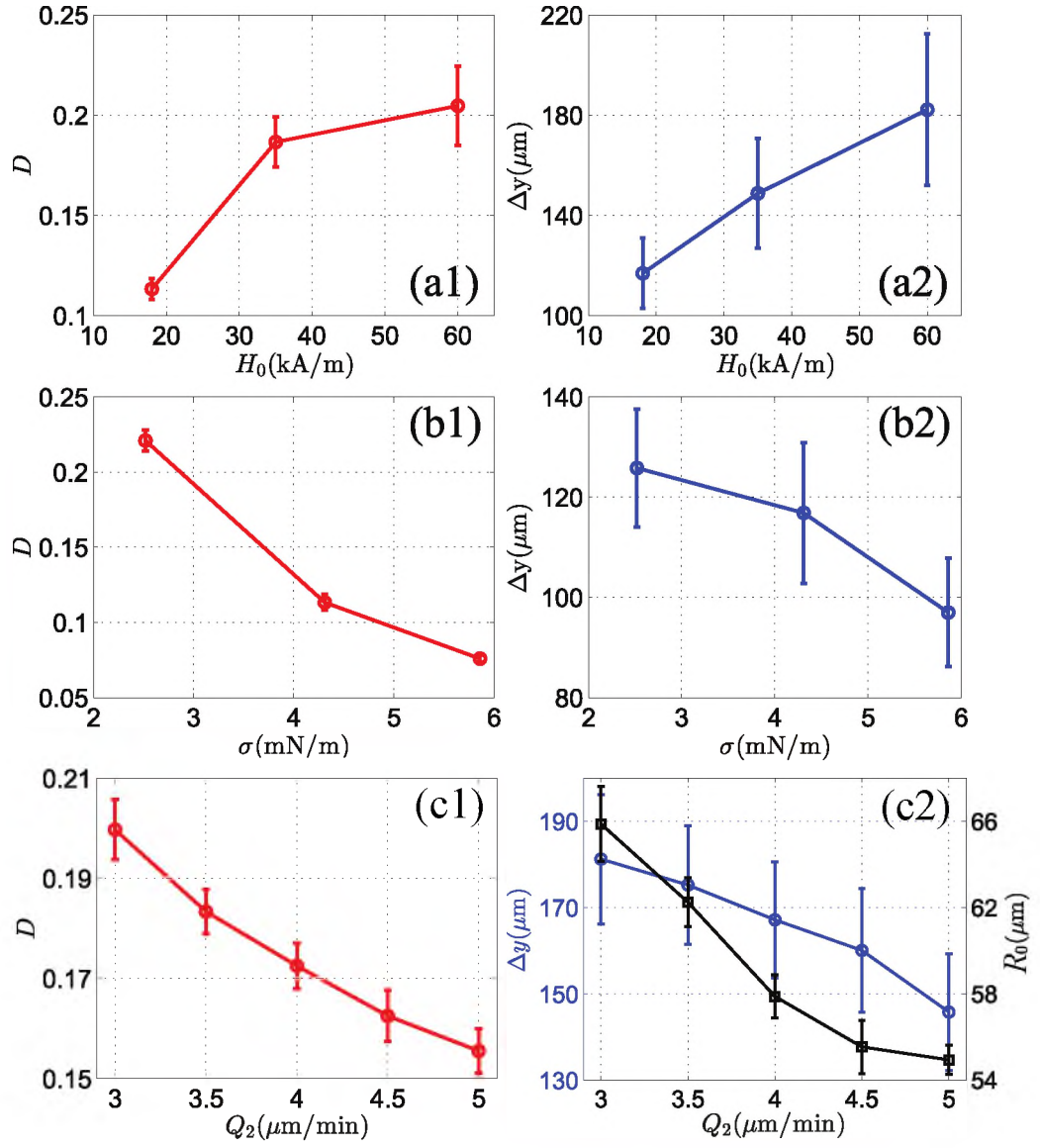

Figure 5. The effect of magnetic field strength, interfacial tension and flow rates on droplet migration. (a) Taylor deformation parameter, D, and the net lateral migration, Δy, vary with magnetic field strength, H_0, when $\sigma = 4.31 \pm 0.22$ mN/m. (b) Taylor deformation parameter, D, and the net lateral migration, Δy, vary with interfacial tension, σ, when $H_0 \approx 18000$ A/m. (c) Taylor deformation parameter, D, the net lateral migration, Δy, and equivalent sphere radius, R_0, vary with flow rate, Q_2, when $H_0 \approx 35000$ A/m.The magnetic field is applied at $\alpha = 45°$.

parameter D to characterize the droplet deformation. From Figure 5(a1), D increases with an increasing magnetic field, meaning the elongation of ferrofluid droplet increases. The larger deformation causes the a larger net lateral migration of droplet as shown in Figure

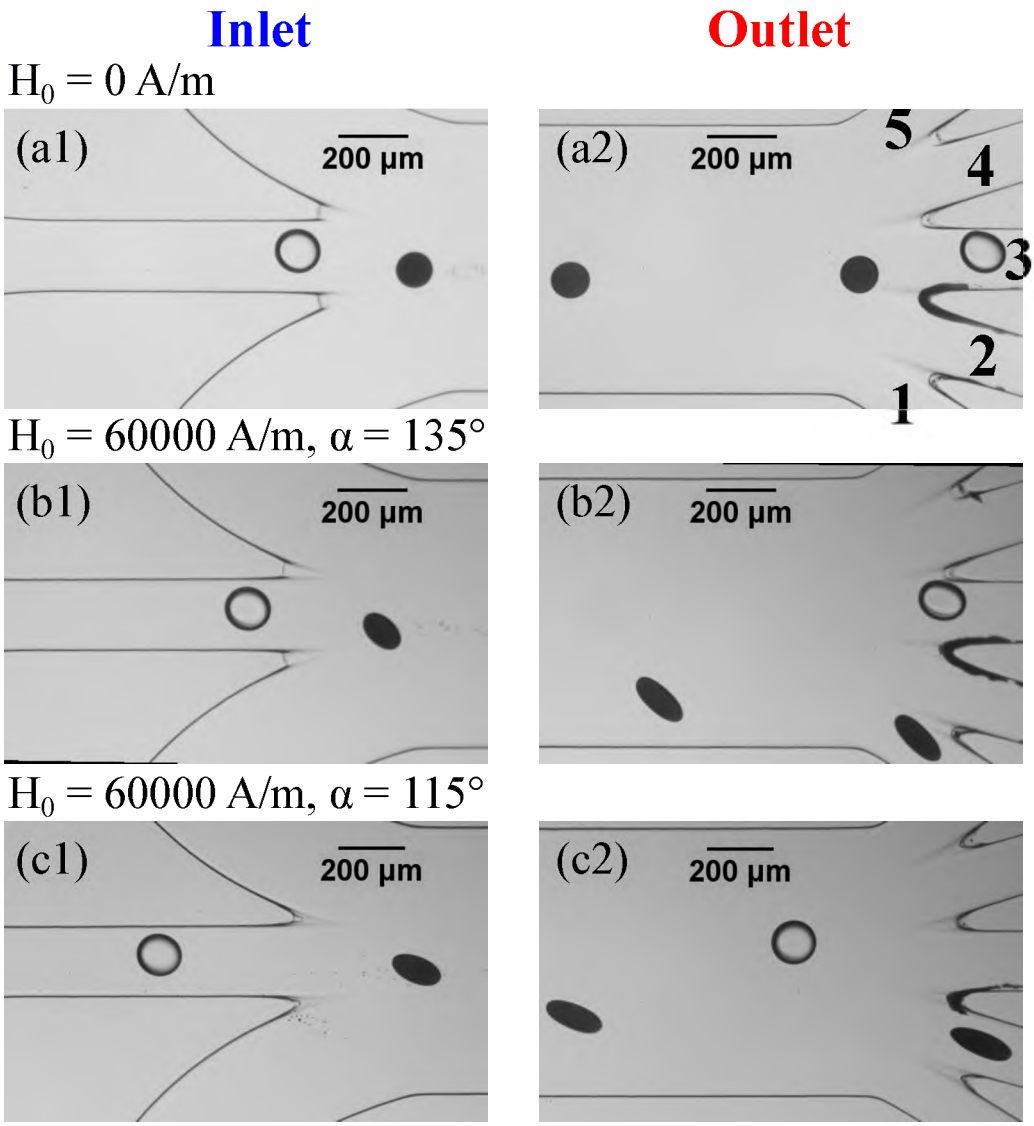

Figure 6. The separation of ferrofluid and water droplets by a uniform magnetic field. (a) Both ferrofluid and water droplets flow into the sub-microchannel 3 without a magnetic field; (b) The ferrofluid droplets flow into the sub-micrcahannel 1 when $H_0 \approx 60000$ A/m, $\alpha = 135°$; (c) The ferrofluid droplets flow into the sub-micrcahannel 2 when $H_0 \approx 60000$ A/m, $\alpha = 115°$. The oil-ferrofluid interfacial tension $\sigma = 2.52 \pm 0.22$ mN/m.

5(a2). Figure 5(b) shows the effect of oil-ferrofluid interfacial tension on the drop migration when magnetic field with $H_0 = 18000$ A/m is applied at 45°. As can be seen, D increases as the oil-ferrofluid interfacial tension decreases, resulting in the increasing the net lateral

migration of drop. By adjusting the flow rate Q_2, the droplet size can be changed. As can be seen in Figure 5(c2), equivalent sphere radius, R_0, decreases with an increasing magnetic field, resulting in the decreasing deformation and net lateral migration of drop.

Therefore, we can see that the magnetic field strength, interfacial tension and droplet size are three important factors for the migration of droplet. The droplet deformation measured in the experiments is much smaller than those predicted by existing theory (Afkhami *et al.*, 2010) for a ferrofluid droplet in an unbounded fluid, which could attributed to the confinement effect of the droplet.

3.4. SEPARATION OF FERROFLUID AND WATER DROPLETS

The deformation-dependent migration under a uniform magnetic field can be used for selectively separating droplets that exhibit different deformations, which could be due to differences in size, interfacial tension, or magnetic properties. As an illustration, Figure 6 shows the separation of ferrofluid droplets from water droplets by a uniform magnetic field. In this experiment, the ferrofluid and water droplets are all generated at the center of the channel. The oil-ferrofluid interfacial tension σ = 2.52 ± 0.22 mN/m. Without an applied magnetic field, both ferrofluid and water droplets flow into the center sub-microchannel 3 and there is no separation, as can be seen in Figure 6(a). When the magnetic field (H_0 = 60000 A/m) is applied at 135°, the water droplets remained at a similar initial position flowing into sub-microchannel 3, while the ferrofluid droplets moved to the lower wall and flow into the sub-microchannel 1. Thus, complete separation is achieved. This magnetic manipulation is also tunable due to the easy control of the direction of the magnetic field. When the magnetic field is set at 115°, the ferrofluid droplets can be diverted to flow into sub-microchannel 2.

4. CONCLUSIONS

In summary, we have demonstrated a unique approach to manipulate droplet migration in microfluidics by using a uniform magnetic field. In contrast to conventional magnetic manipulations, the current approach does not induce direct magnetic forces on the droplets. Instead, the Maxwell stresses arise at the droplet interface due to a change of magnetic susceptibility across the droplet interface, and consequently deform the droplet and affect its relative orientation to the flow. Due to the deformed shape and inclined angle to the shear flow, the droplet interacts hydrodynamically with the channel walls, and migrates in the cross-stream direction. We experimentally investigated various parameters that influence the droplet migration, including magnetic field strength, magnetic field direction and interfacial tension. It is found that the lateral migration speed increases with the droplet deformation, which in turn increases with the field strength and decreases with the interfacial tension. The magnetic field direction, on the other hand, controls the orientation of the drop and the direction of the lateral migration. The direction and speed of the lateral migration are well described by hydrodynamic theory that accounts for interactions of the droplet's stresslet flow with the walls of the channel. We have also developed two-dimensional numerical model that predicts the lateral migration and confirmed negligible magnetic force.

In comparison to conventional magnetic separation, the uniform magnetic field technique is simple to implement and is favorable for high-throughput parallelization. Multiple microfluidic channels can be conveniently integrated onto a single chip while being subjected to the same uniform magnetic field. The demonstrated technique thus provides a general mechanism for separation of micro-droplets, and has great potential for biological and biomedical applications that require sorting of droplets by their size, interfacial tension, or magnetic properties.

ACKNOWLEDGMENTS

The authors gratefully acknowledge the support from the Department of Mechanical and Aerospace Engineering (MAE) and the Center for Biomedical Research (CBR) at the Missouri University of Science and Technology. This work is partially supported by the National Science Foundation (Grant No. DMS-1818642). BR acknowledges the Department of Mechanical Engineering and the Bourns College of Engineering at the University of California, Riverside for support.

REFERENCES

Afkhami, S., Tyler, A., Renardy, Y., Renardy, M., St. Pierre, T., Woodward, R., and Riffle, J., 'Deformation of a hydrophobic ferrofluid droplet suspended in a viscous medium under uniform magnetic fields,' J. Fluid Mech., 2010, **663**, pp. 358–384, ISSN 00221120 14697645, doi:10.1017/S0022112010003551.

Aggarwal, N. and Sarkar, K., 'Deformation and breakup of a viscoelastic drop in a newtonian matrix under steady shear,' Journal of Fluid Mechanics, 2007, **584**, pp. 1–21.

Agresti, J. J., Antipov, E., Abate, A. R., Ahn, K., Rowat, A. C., Baret, J.-C., Marquez, M., Klibanov, A. M., Griffiths, A. D., and Weitz, D. A., 'Ultrahigh-throughput screening in drop-based microfluidics for directed evolution,' Proceedings of the National Academy of Sciences, 2010.

Ahn, B., Lee, K., Louge, R., and Oh, K. W., 'Concurrent droplet charging and sorting by electrostatic actuation,' Biomicrofluidics, 2009, **3**(4), p. 044102.

Ahn, B., Lee, K., Panchapakesan, R., and Oh, K. W., 'On-demand electrostatic droplet charging and sorting,' Biomicrofluidics, 2011, **5**(2), p. 024113.

Ahn, K., Kerbage, C., Hunt, T. P., Westervelt, R., Link, D. R., and Weitz, D. A., 'Di-electrophoretic manipulation of drops for high-speed microfluidic sorting devices,' Applied Physics Letters, 2006, **88**(2), p. 024104.

Bowman, T., Frechette, J., and Drazer, G., 'Force driven separation of drops by deterministic lateral displacement,' Lab on a Chip, 2012, **12**(16), pp. 2903–2908.

Brouzes, E., Kruse, T., Kimmerling, R., and Strey, H. H., 'Rapid and continuous magnetic separation in droplet microfluidic devices,' Lab on a Chip, 2015, **15**(3), pp. 908–919.

Chan, P.-H. and Leal, L., 'The motion of a deformable drop in a second-order fluid,' Journal of Fluid Mechanics, 1979, **92**(1), pp. 131–170.

Daerr, A. and Mogne, A., 'Pendent_drop: an imagej plugin to measure the surface tension from an image of a pendent drop,' Journal of Open Research Software, 2016, **4**(1).

de Ruiter, R., Pit, A. M., de Oliveira, V. M., Duits, M. H., van den Ende, D., and Mugele, F., 'Electrostatic potential wells for on-demand drop manipulation in microchannels,' Lab on a Chip, 2014, **14**(5), pp. 883–891.

Du, G., Fang, Q., and den Toonder, J. M., 'Microfluidics for cell-based high throughput screening platforms—a review,' Analytica chimica acta, 2016, **903**, pp. 36–50.

Eastburn, D. J., Huang, Y., Pellegrino, M., Sciambi, A., Ptáček, L. J., and Abate, A. R., 'Microfluidic droplet enrichment for targeted sequencing,' Nucleic acids research, 2015, **43**(13), pp. e86–e86.

Gao, J., Gu, H., and Xu, B., 'Multifunctional magnetic nanoparticles: design, synthesis, and biomedical applications,' Accounts of chemical research, 2009, **42**(8), pp. 1097–1107.

Guo, F., Ji, X.-H., Liu, K., He, R.-X., Zhao, L.-B., Guo, Z.-X., Liu, W., Guo, S.-S., and Zhao, X.-Z., 'Droplet electric separator microfluidic device for cell sorting,' Applied Physics Letters, 2010, **96**(19), p. 193701.

Guo, M. T., Rotem, A., Heyman, J. A., and Weitz, D. A., 'Droplet microfluidics for high-throughput biological assays,' Lab on a Chip, 2012, **12**(12), pp. 2146–2155.

Hassan, M. R., Zhang, J., and Wang, C., 'Deformation of a ferrofluid droplet in simple shear flows under uniform magnetic fields,' Phys. Fluids, 2018, **30**(9), p. 092002, ISSN 1070-6631, doi:10.1063/1.5047223.

Hatch, A. C., Patel, A., Beer, N. R., and Lee, A. P., 'Passive droplet sorting using viscoelastic flow focusing,' Lab on a Chip, 2013, **13**(7), pp. 1308–1315.

Hejazian, M., Li, W., and Nguyen, N.-T., 'Lab on a chip for continuous-flow magnetic cell separation,' Lab on a Chip, 2015, **15**(4), pp. 959–970.

Huang, G., Li, M., Yang, Q., Li, Y., Liu, H., Yang, H., and Xu, F., 'Magnetically actuated droplet manipulation and its potential biomedical applications,' ACS applied materials & interfaces, 2017, **9**(2), pp. 1155–1166.

Inglis, D. W., Riehn, R., Sturm, J. C., and Austin, R. H., 'Microfluidic high gradient magnetic cell separation,' Journal of Applied Physics, 2006, **99**(8), p. 08K101.

Kadivar, E., Herminghaus, S., and Brinkmann, M., 'Droplet sorting in a loop of flat microfluidic channels,' Journal of Physics: Condensed Matter, 2013, **25**(28), p. 285102.

Kim, J., Won, J., and Song, S., 'Dual-mode on-demand droplet routing in multiple microchannels using a magnetic fluid as carrier phase,' Biomicrofluidics, 2014, **8**(5), p. 054105.

Kim, S. and Karrila, S. J., *Microhydrodynamics: principles and selected applications*, Courier Corporation, 2013.

Laser, D. J. and Santiago, J. G., 'A review of micropumps,' Journal of micromechanics and microengineering, 2004, **14**(6), p. R35.

Lee, C., Lee, J., Kim, H. H., Teh, S.-Y., Lee, A., Chung, I.-Y., Park, J. Y., and Shung, K. K., 'Microfluidic droplet sorting with a high frequency ultrasound beam,' Lab on a Chip, 2012, **12**(15), pp. 2736–2742.

Leibacher, I., Reichert, P., and Dual, J., 'Microfluidic droplet handling by bulk acoustic wave (baw) acoustophoresis,' Lab on a Chip, 2015, **15**(13), pp. 2896–2905.

Li, H., Wu, Y., Wang, X., Zhu, C., Fu, T., and Ma, Y., 'Magnetofluidic control of the breakup of ferrofluid droplets in a microfluidic y-junction,' Rsc Advances, 2016, **6**(1), pp. 778–785.

Li, S., Ding, X., Guo, F., Chen, Y., Lapsley, M. I., Lin, S.-C. S., Wang, L., McCoy, J. P., Cameron, C. E., and Huang, T. J., 'An on-chip, multichannel droplet sorter using standing surface acoustic waves,' Analytical chemistry, 2013, **85**(11), pp. 5468–5474.

Link, D. R., Grasland-Mongrain, E., Duri, A., Sarrazin, F., Cheng, Z., Cristobal, G., Marquez, M., and Weitz, D. A., 'Electric control of droplets in microfluidic devices,' Angewandte Chemie International Edition, 2006, **45**(16), pp. 2556–2560.

Lombardi, D. and Dittrich, P. S., 'Droplet microfluidics with magnetic beads: a new tool to investigate drug–protein interactions,' Analytical and bioanalytical chemistry, 2011, **399**(1), pp. 347–352.

Lübbe, A. S., Alexiou, C., and Bergemann, C., 'Clinical applications of magnetic drug targeting,' Journal of Surgical Research, 2001, **95**(2), pp. 200–206.

Mandal, S., Bandopadhyay, A., and Chakraborty, S., 'The effect of uniform electric field on the cross-stream migration of a drop in plane poiseuille flow,' Journal of Fluid Mechanics, 2016, **809**, pp. 726–774.

Matsunaga, D., Meng, F., Zöttl, A., Golestanian, R., and Yeomans, J. M., 'Focusing and sorting of ellipsoidal magnetic particles in microchannels,' Phys. Rev. Lett., 2017, **119**, p. 198002, doi:10.1103/PhysRevLett.119.198002.

Mortazavi, S. and Tryggvason, G., 'A numerical study of the motion of drops in poiseuille flow. part 1. lateral migration of one drop,' Journal of Fluid Mechanics, 2000, **411**, pp. 325–350.

Mortensen, N. A., Okkels, F., and Bruus, H., 'Reexamination of hagen-poiseuille flow: Shape dependence of the hydraulic resistance in microchannels,' Physical Review E, 2005, **71**(5), p. 057301.

Nam, J., Lim, H., Kim, C., Yoon Kang, J., and Shin, S., 'Density-dependent separation of encapsulated cells in a microfluidic channel by using a standing surface acoustic wave,' Biomicrofluidics, 2012, **6**(2), p. 024120.

Neuberger, T., Schöpf, B., Hofmann, H., Hofmann, M., and Von Rechenberg, B., 'Superparamagnetic nanoparticles for biomedical applications: possibilities and limitations of a new drug delivery system,' Journal of Magnetism and Magnetic materials, 2005, **293**(1), pp. 483–496.

Nguyen, N.-T., Ng, K. M., and Huang, X., 'Manipulation of ferrofluid droplets using planar coils,' Applied Physics Letters, 2006, **89**(5), p. 052509.

Niu, X., Zhang, M., Peng, S., Wen, W., and Sheng, P., 'Real-time detection, control, and sorting of microfluidic droplets,' Biomicrofluidics, 2007, **1**(4), p. 044101.

Oh, K. W. and Ahn, C. H., 'A review of microvalves,' Journal of micromechanics and microengineering, 2006, **16**(5), p. R13.

Petersson, F., Nilsson, A., Holm, C., Jönsson, H., and Laurell, T., 'Continuous separation of lipid particles from erythrocytes by means of laminar flow and acoustic standing wave forces,' Lab on a Chip, 2005, **5**(1), pp. 20–22.

Raich, H. and Blümler, P., 'Design and construction of a dipolar halbach array with a homogeneous field from identical bar magnets: Nmr mandhalas,' Concepts in Magnetic Resonance Part B: Magnetic Resonance Engineering: An Educational Journal, 2004, **23**(1), pp. 16–25.

Rao, L., Cai, B., Wang, J., Meng, Q., Ma, C., He, Z., Xu, J., Huang, Q., Li, S., Cen, Y., *et al.*, 'A microfluidic electrostatic separator based on pre-charged droplets,' Sensors and Actuators B: Chemical, 2015a, **210**, pp. 328–335.

Rao, L., Cai, B., Yu, X.-L., Guo, S.-S., Liu, W., and Zhao, X.-Z., 'One-step fabrication of 3d silver paste electrodes into microfluidic devices for enhanced droplet-based cell sorting,' AIP Advances, 2015b, **5**(5), p. 057134.

Schmid, L., Weitz, D. A., and Franke, T., 'Sorting drops and cells with acoustics: acoustic microfluidic fluorescence-activated cell sorter,' Lab on a Chip, 2014, **14**(19), pp. 3710–3718.

Sciambi, A. and Abate, A. R., 'Generating electric fields in pdms microfluidic devices with salt water electrodes,' Lab on a Chip, 2014, **14**(15), pp. 2605–2609.

Sciambi, A. and Abate, A. R., 'Accurate microfluidic sorting of droplets at 30 khz,' Lab on a Chip, 2015, **15**(1), pp. 47–51.

Shang, L., Cheng, Y., and Zhao, Y., 'Emerging droplet microfluidics,' Chemical reviews, 2017, **117**(12), pp. 7964–8040.

Shembekar, N., Chaipan, C., Utharala, R., and Merten, C. A., 'Droplet-based microfluidics in drug discovery, transcriptomics and high-throughput molecular genetics,' Lab on a Chip, 2016, **16**(8), pp. 1314–1331.

Smart, J. R. and Leighton Jr, D. T., 'Measurement of the hydrodynamic surface roughness of noncolloidal spheres,' Physics of Fluids A: Fluid Dynamics, 1989, **1**(1), pp. 52–60.

Stratton, J. A., *Electromagnetic theory*, John Wiley & Sons, 2007.

Sung, Y. J., Kim, J. Y. H., Choi, H. I., Kwak, H. S., and Sim, S. J., 'Magnetophoretic sorting of microdroplets with different microalgal cell densities for rapid isolation of fast growing strains,' Scientific Reports, 2017, **7**(1), p. 10390.

Surenjav, E., Priest, C., Herminghaus, S., and Seemann, R., 'Manipulation of gel emulsions by variable microchannel geometry,' Lab on a Chip, 2009, **9**(2), pp. 325–330.

Tan, Y.-C., Fisher, J. S., Lee, A. I., Cristini, V., and Lee, A. P., 'Design of microfluidic channel geometries for the control of droplet volume, chemical concentration, and sorting,' Lab on a Chip, 2004, **4**(4), pp. 292–298.

Tan, Y.-C., Ho, Y. L., and Lee, A. P., 'Microfluidic sorting of droplets by size,' Microfluidics and Nanofluidics, 2008, **4**(4), p. 343.

Tan, Y.-C. and Lee, A. P., 'Microfluidic separation of satellite droplets as the basis of a monodispersed micron and submicron emulsification system,' Lab on a Chip, 2005, **5**(10), pp. 1178–1183.

Taylor, G. I., 'The formation of emulsions in definable fields of flow,' Proc. R. Soc. Lond. A, 1934, **146**(858), pp. 501–523.

Teste, B., Jamond, N., Ferraro, D., Viovy, J.-L., and Malaquin, L., 'Selective handling of droplets in a microfluidic device using magnetic rails,' Microfluidics and Nanofluidics, 2015, **19**(1), pp. 141–153.

Torres-Díaz, I. and Rinaldi, C., 'Recent progress in ferrofluids research: novel applications of magnetically controllable and tunable fluids,' Soft matter, 2014, **10**(43), pp. 8584–8602.

Xi, H.-D., Zheng, H., Guo, W., Gañán-Calvo, A. M., Ai, Y., Tsao, C.-W., Zhou, J., Li, W., Huang, Y., Nguyen, N.-T., *et al.*, 'Active droplet sorting in microfluidics: a review,' Lab on a Chip, 2017, **17**(5), pp. 751–771.

Zhang, K., Liang, Q., Ai, X., Hu, P., Wang, Y., and Luo, G., 'On-demand microfluidic droplet manipulation using hydrophobic ferrofluid as a continuous-phase,' Lab on a Chip, 2011, **11**(7), pp. 1271–1275.

Zhang, K., Liang, Q., Ma, S., Mu, X., Hu, P., Wang, Y., and Luo, G., 'On-chip manipulation of continuous picoliter-volume superparamagnetic droplets using a magnetic force,' Lab on a Chip, 2009, **9**(20), pp. 2992–2999.

Zhang, Z., Zhou, R., P Brames, D., and Wang, C., 'A low-cost fabrication system for manufacturing soft-lithography microfluidic master molds,' Micro and Nanosystems, 2015, **7**(1), pp. 4–12.

Zhou, R., Bai, F., and Wang, C., 'Magnetic separation of microparticles by shape,' Lab on a Chip, 2017, **17**(3), pp. 401–406.

SECTION

3. SUMMARY AND CONCLUSIONS

This dissertation has developed numerical and experimental methods to manipulate microparticles and microdroplets in the microfluidics by using a uniform magnetic field. This approach have many advantages over the traditional force-based techniques, including simple implementation, feasibility of scaling up, and large reach distance.

First, the fundamental mechanism of rotational dynamics of elliptical particles in a simple shear flow under a uniform magnetic field was fully numerically investigated. The numerical simulations revealed that the rotation of particle depends on the direction and strength of magnetic field, where the direction controls the symmetry of rotation and the strength controls the period of rotation and the degree of asymmetry of rotation.

Second, the lateral migration mechanism of elliptical paramagnetic particles in a plane Poiseuille flow under a uniform magnetic field was numerically investigated. The particle shown to exhibit negligible lateral migration in the absence of a magnetic field, while it migrates laterally in the presence of a magnetic field. The migration direction depends on the direction of magnetic field, which controls the symmetric property of the particle rotational velocity. The magnitude of lateral migration velocity over a π cycle increases with the magnetic field strength. By investigating a wide range of parameters, our direct numerical simulations yield a comprehensive understanding of the particle migration mechanism. An empirical scaling relationship is proposed to relate the lateral migration distance to the asymmetry of the rotational velocity and lateral oscillation amplitude.

Third, the comparison of rotational dynamics between paramagnetic and ferromagnetic elliptical particles in a simple shear flow under a uniform magnetic field was numerically investigated. In a weak field regime (below the critical magnetic field), the particle complete

a full rotation, and the symmetrical property of particle rotations depend on the direction of the magnetic field. For the same strength and direction of the magnetic field, paramagnetic and ferromagnetic particles exhibit different asymmetric rotational behaviors. In the strong field (above the critical strength), the particles are pinned at their respected steady angles, which depend on the direction of magnetic field. The steady angles of paramagnetic and ferromagnetic particles are different for the same magnetic field strength and direction. The numerical results have very good agreement with that of theoretical analysis. Based on these findings, the simulations on lateral migration of paramagnetic and ferromagnetic elliptical particles in a pressure-drive flow shown that these two kinds of particles can be separated, which suggested a useful strategy to manipulate non-spherical micro-particles in the microfluidic devices.

Fourth, the fundamental mechanism of the particle-particle interactions and relative motions of a pair of paramagnetic elliptical particles in a quiescent flow were numerically investigated. Numerical simulations revealed that the particles spend much more time for the global reorientation than for the local magneto-orientation. For a larger particle aspect ratio, more time is required to form a chain, and the final particle and global relative orientation angles are larger. Therefore, this work provides useful information for the fundamental particle-particle interactions mechanism in the magnetic particle suspensions under a uniform magnetic field.

Last, a unique approach to manipulate droplet migration in microfluidic devise by using a uniform magnetic field were proposed. This approach does not induce direct magnetic forces on the droplets, instead, the Maxwell stresses arise at the droplet interface due to a change of magnetic susceptibility across the droplet interface, and consequently deform the droplet and affect its relative orientation to the flow. Due to the deformed shape and inclined angle to the shear flow, the droplet interacts hydrodynamically with the channel walls, and migrates in the cross-stream direction. In comparison to conventional magnetic separation, the uniform magnetic field technique is simple to implement and is favorable

for high-throughput parallelization. Multiple microfluidic channels can be conveniently integrated onto a single chip while being subjected to the same uniform magnetic field. The demonstrated technique thus provides a general mechanism for separation of micro-droplets, and has great potential for biological and biomedical applications that require sorting of droplets by their size, interfacial tension, or magnetic properties.

REFERENCES

Abbas, M. and Bossis, G., 'Separation of two attractive ferromagnetic ellipsoidal particles by hydrodynamic interactions under alternating magnetic field,' Physical Review E, 2017, **95**(6), p. 062611.

Afkhami, S., Tyler, A., Renardy, Y., Renardy, M., St. Pierre, T., Woodward, R., and Riffle, J., 'Deformation of a hydrophobic ferrofluid droplet suspended in a viscous medium under uniform magnetic fields,' J. Fluid Mech., 2010, **663**, pp. 358–384, ISSN 00221120 14697645, doi:10.1017/S0022112010003551.

Aggarwal, N. and Sarkar, K., 'Deformation and breakup of a viscoelastic drop in a newtonian matrix under steady shear,' Journal of Fluid Mechanics, 2007, **584**, pp. 1–21.

Agresti, J. J., Antipov, E., Abate, A. R., Ahn, K., Rowat, A. C., Baret, J.-C., Marquez, M., Klibanov, A. M., Griffiths, A. D., and Weitz, D. A., 'Ultrahigh-throughput screening in drop-based microfluidics for directed evolution,' Proceedings of the National Academy of Sciences, 2010.

Ahn, B., Lee, K., Louge, R., and Oh, K. W., 'Concurrent droplet charging and sorting by electrostatic actuation,' Biomicrofluidics, 2009, **3**(4), p. 044102.

Ahn, B., Lee, K., Panchapakesan, R., and Oh, K. W., 'On-demand electrostatic droplet charging and sorting,' Biomicrofluidics, 2011, **5**(2), p. 024113.

Ahn, K., Kerbage, C., Hunt, T. P., Westervelt, R., Link, D. R., and Weitz, D. A., 'Di-electrophoretic manipulation of drops for high-speed microfluidic sorting devices,' Applied Physics Letters, 2006, **88**(2), p. 024104.

Ai, Y., Beskok, A., Gauthier, D. T., Joo, S. W., and Qian, S., 'Dc electrokinetic transport of cylindrical cells in straight microchannels,' Biomicrofluidics, 2009a, **3**(4), p. 044110.

Ai, Y., Joo, S. W., Jiang, Y., Xuan, X., and Qian, S., 'Pressure-driven transport of particles through a converging-diverging microchannel,' Biomicrofluidics, 2009b, **3**(2), p. 022404.

Ai, Y. and Qian, S., 'Dc dielectrophoretic particle–particle interactions and their relative motions,' Journal of colloid and interface science, 2010, **346**(2), pp. 448–454.

Ai, Y., Zeng, Z., and Qian, S., 'Direct numerical simulation of ac dielectrophoretic particle–particle interactive motions,' Journal of colloid and interface science, 2014, **417**, pp. 72–79.

Alava, M. and Niskanen, K., 'The physics of paper,' Reports on progress in physics, 2006, **69**(3), p. 669.

Allan, R. and Mason, S., 'Particle behaviour in shear and electric fields. ii. rigid rods and spherical doublets,' Proceedings of the Royal Society of London A: Mathematical, Physical and Engineering Sciences, 1962, **267**(1328), pp. 62–76.

Anstey, N. M., Russell, B., Yeo, T. W., and Price, R. N., 'The pathophysiology of vivax malaria,' Trends in parasitology, 2009, **25**(5), pp. 220–227.

Anupama, A., Kumaran, V., and Sahoo, B., 'Magnetorheological fluids containing rod-shaped lithium–zinc ferrite particles: the steady-state shear response,' Soft matter, 2018, **14**(26), pp. 5407–5419.

Arruebo, M., Fernández-Pacheco, R., Ibarra, M. R., and Santamaría, J., 'Magnetic nanoparticles for drug delivery,' Nano today, 2007, **2**(3), pp. 22–32.

Bell, R., Karli, J., Vavreck, A., Zimmerman, D., Ngatu, G., and Wereley, N., 'Magnetorheology of submicron diameter iron microwires dispersed in silicone oil,' Smart Materials and Structures, 2008, **17**(1), p. 015028.

Bell, R., Miller, E., Karli, J., Vavreck, A., and Zimmerman, D., 'Influence of particle shape on the properties of magnetorheological fluids,' International Journal of Modern Physics B, 2007, **21**(28n29), pp. 5018–5025.

Bica, I., Liu, Y. D., and Choi, H. J., 'Physical characteristics of magnetorheological suspensions and their applications,' Journal of Industrial and Engineering Chemistry, 2013, **19**(2), pp. 394–406.

Bombard, A. J., Gonçalves, F. R., Morillas, J. R., and De Vicente, J., 'Magnetorheology of dimorphic magnetorheological fluids based on nanofibers,' Smart Materials and Structures, 2014, **23**(12), p. 125013.

Bossis, G., Marins, J. A., Kuzhir, P., Volkova, O., and Zubarev, A., 'Functionalized microfibers for field-responsive materials and biological applications,' Journal of Intelligent Material Systems and Structures, 2015, **26**(14), pp. 1871–1879.

Bowman, T., Frechette, J., and Drazer, G., 'Force driven separation of drops by deterministic lateral displacement,' Lab on a Chip, 2012, **12**(16), pp. 2903–2908.

Brouzes, E., Kruse, T., Kimmerling, R., and Strey, H. H., 'Rapid and continuous magnetic separation in droplet microfluidic devices,' Lab on a Chip, 2015, **15**(3), pp. 908–919.

Bucak, S., Sharpe, S., Kuhn, S., and Hatton, T. A., 'Cell clarification and size separation using continuous countercurrent magnetophoresis,' Biotechnology progress, 2011, **27**(3), pp. 744–750.

Cao, Q., Li, Z., Wang, Z., and Han, X., 'Rotational motion and lateral migration of an elliptical magnetic particle in a microchannel under a uniform magnetic field,' Microfluidics and Nanofluidics, 2018, **22**(1), p. 3.

Chaffey, C. and Mason, S., 'Particle behavior in shear and electric fields. III. rigid spheroids and discs,' Journal of Colloid Science, 1964, **19**(6), pp. 525–548.

Champion, J. A., Katare, Y. K., and Mitragotri, S., 'Particle shape: a new design parameter for micro-and nanoscale drug delivery carriers,' Journal of controlled release, 2007, **121**(1-2), pp. 3–9.

Chan, P.-H. and Leal, L., 'The motion of a deformable drop in a second-order fluid,' Journal of Fluid Mechanics, 1979, **92**(1), pp. 131–170.

Chen, P., Huang, Y.-Y., Hoshino, K., and Zhang, J. X., 'Microscale magnetic field modulation for enhanced capture and distribution of rare circulating tumor cells,' Scientific reports, 2015, **5**, p. 8745.

Chen, Q., Li, D., Zielinski, J., Kozubowski, L., Lin, J., Wang, M., and Xuan, X., 'Yeast cell fractionation by morphology in dilute ferrofluids,' Biomicrofluidics, 2017, **11**(6), p. 064102.

Chen, S.-D., Pan, T.-W., and Chang, C.-C., 'The motion of a single and multiple neutrally buoyant elliptical cylinders in plane poiseuille flow,' Physics of Fluids, 2012, **24**(10), p. 103302.

Daerr, A. and Mogne, A., 'Pendent_drop: an imagej plugin to measure the surface tension from an image of a pendent drop,' Journal of Open Research Software, 2016, **4**(1).

de Ruiter, R., Pit, A. M., de Oliveira, V. M., Duits, M. H., van den Ende, D., and Mugele, F., 'Electrostatic potential wells for on-demand drop manipulation in microchannels,' Lab on a Chip, 2014, **14**(5), pp. 883–891.

De Vicente, J., Klingenberg, D. J., and Hidalgo-Alvarez, R., 'Magnetorheological fluids: a review,' Soft matter, 2011, **7**(8), pp. 3701–3710.

De Vicente, J., Segovia-Gutiérrez, J., Andablo-Reyes, E., Vereda, F., and Hidalgo-Álvarez, R., 'Dynamic rheology of sphere-and rod-based magnetorheological fluids,' The Journal of chemical physics, 2009, **131**(19), p. 194902.

de Vicente, J., Vereda, F., Segovia-Gutiérrez, J. P., del Puerto Morales, M., and Hidalgo-Álvarez, R., 'Effect of particle shape in magnetorheology,' Journal of Rheology, 2010, **54**(6), pp. 1337–1362.

Dong, X., Tong, Y., Ma, N., Qi, M., and Ou, J., 'Properties of cobalt nanofiber-based magnetorheological fluids,' RSC Advances, 2015, **5**(18), pp. 13958–13963.

Du, G., Fang, Q., and den Toonder, J. M., 'Microfluidics for cell-based high throughput screening platforms—a review,' Analytica chimica acta, 2016, **903**, pp. 36–50.

Eastburn, D. J., Huang, Y., Pellegrino, M., Sciambi, A., Ptáček, L. J., and Abate, A. R., 'Microfluidic droplet enrichment for targeted sequencing,' Nucleic acids research, 2015, **43**(13), pp. e86–e86.

Feng, J., Hu, H. H., and Joseph, D. D., 'Direct simulation of initial value problems for the motion of solid bodies in a newtonian fluid. part 2. couette and poiseuille flows,' Journal of fluid mechanics, 1994, **277**, pp. 271–301.

Gao, J., Gu, H., and Xu, B., 'Multifunctional magnetic nanoparticles: design, synthesis, and biomedical applications,' Accounts of chemical research, 2009, **42**(8), pp. 1097–1107.

Gao, Y., Hulsen, M., Kang, T., and Den Toonder, J., 'Numerical and experimental study of a rotating magnetic particle chain in a viscous fluid,' Physical Review E, 2012, **86**(4), p. 041503.

Gavze, E. and Shapiro, M., 'Particles in a shear flow near a solid wall: effect of nonsphericity on forces and velocities,' International Journal of Multiphase Flow, 1997, **23**(1), pp. 155–182.

Gijs, M. A., 'Magnetic bead handling on-chip: new opportunities for analytical applications,' Microfluidics and Nanofluidics, 2004, **1**(1), pp. 22–40.

Gijs, M. A., Lacharme, F., and Lehmann, U., 'Microfluidic applications of magnetic particles for biological analysis and catalysis,' Chemical reviews, 2009, **110**(3), pp. 1518–1563.

Goldsmith, H. and Mason, S., 'Axial migration of particles in poiseuille flow,' Nature, 1961, **190**(4781), pp. 1095–1096.

Guo, F., Ji, X.-H., Liu, K., He, R.-X., Zhao, L.-B., Guo, Z.-X., Liu, W., Guo, S.-S., and Zhao, X.-Z., 'Droplet electric separator microfluidic device for cell sorting,' Applied Physics Letters, 2010, **96**(19), p. 193701.

Guo, M. T., Rotem, A., Heyman, J. A., and Weitz, D. A., 'Droplet microfluidics for high-throughput biological assays,' Lab on a Chip, 2012, **12**(12), pp. 2146–2155.

Hassan, M. R., Zhang, J., and Wang, C., 'Deformation of a ferrofluid droplet in simple shear flows under uniform magnetic fields,' Phys. Fluids, 2018, **30**(9), p. 092002, ISSN 1070-6631, doi:10.1063/1.5047223.

Hatch, A. C., Patel, A., Beer, N. R., and Lee, A. P., 'Passive droplet sorting using viscoelastic flow focusing,' Lab on a Chip, 2013, **13**(7), pp. 1308–1315.

Hejazian, M., Li, W., and Nguyen, N.-T., 'Lab on a chip for continuous-flow magnetic cell separation,' Lab on a Chip, 2015, **15**(4), pp. 959–970.

Hsu, R. and Ganatos, P., 'Gravitational and zero-drag motion of a spheroid adjacent to an inclined plane at low reynolds number,' Journal of Fluid Mechanics, 1994, **268**, pp. 267–292.

Hu, H. H., Patankar, N. A., and Zhu, M., 'Direct numerical simulations of fluid–solid systems using the arbitrary lagrangian–eulerian technique,' Journal of Computational Physics, 2001, **169**(2), pp. 427–462.

Huang, G., Li, M., Yang, Q., Li, Y., Liu, H., Yang, H., and Xu, F., 'Magnetically actuated droplet manipulation and its potential biomedical applications,' ACS applied materials & interfaces, 2017, **9**(2), pp. 1155–1166.

Huang, S.-L., Chen, S.-D., Pan, T.-W., Chang, C.-C., and Chu, C.-C., 'The motion of a neutrally buoyant particle of an elliptic shape in two dimensional shear flow: A numerical study,' Physics of Fluids, 2015, **27**(8), p. 083303.

Inglis, D. W., Riehn, R., Sturm, J. C., and Austin, R. H., 'Microfluidic high gradient magnetic cell separation,' Journal of Applied Physics, 2006, **99**(8), p. 08K101.

Jamshaid, T., Neto, E. T. T., Eissa, M. M., Zine, N., Kunita, M. H., El-Salhi, A. E., and Elaissari, A., 'Magnetic particles: From preparation to lab-on-a-chip, biosensors, microsystems and microfluidics applications,' TrAC Trends in Analytical Chemistry, 2016, **79**, pp. 344–362.

Jeffery, G. B., 'The motion of ellipsoidal particles immersed in a viscous fluid,' Proceedings of the Royal Society of London A: Mathematical, Physical and Engineering Sciences, 1922, **102**(715), pp. 161–179.

Jiang, W., Zhang, Y., Xuan, S., Guo, C., and Gong, X., 'Dimorphic magnetorheological fluid with improved rheological properties,' Journal of Magnetism and Magnetic Materials, 2011, **323**(24), pp. 3246–3250.

Kadivar, E., Herminghaus, S., and Brinkmann, M., 'Droplet sorting in a loop of flat microfluidic channels,' Journal of Physics: Condensed Matter, 2013, **25**(28), p. 285102.

Kang, S. and Suh, Y., 'Direct simulation of flows with suspended paramagnetic particles using one-stage smoothed profile method,' Journal of Fluids and Structures, 2011, **27**(2), pp. 266–282.

Kang, T. G., Gao, Y., Hulsen, M. A., den Toonder, J. M., and Anderson, P. D., 'Direct simulation of the dynamics of two spherical particles actuated magnetically in a viscous fluid,' Computers & Fluids, 2013, **86**, pp. 569–581.

Kang, T. G., Hulsen, M. A., den Toonder, J. M., Anderson, P. D., and Meijer, H. E., 'A direct simulation method for flows with suspended paramagnetic particles,' Journal of Computational Physics, 2008, **227**(9), pp. 4441–4458.

Keaveny, E. E. and Maxey, M. R., 'Modeling the magnetic interactions between paramagnetic beads in magnetorheological fluids,' Journal of Computational Physics, 2008, **227**(22), pp. 9554–9571.

Kim, J., Won, J., and Song, S., 'Dual-mode on-demand droplet routing in multiple microchannels using a magnetic fluid as carrier phase,' Biomicrofluidics, 2014, **8**(5), p. 054105.

Kim, S. and Karrila, S. J., *Microhydrodynamics: principles and selected applications*, Courier Corporation, 2013.

Kuzhir, P., López-López, M. T., and Bossis, G., 'Magnetorheology of fiber suspensions. ii. theory,' Journal of rheology, 2009, **53**(1), pp. 127–151.

Larson, R. G., *The structure and rheology of complex fluids*, volume 150, Oxford university press New York, 1999.

Laser, D. J. and Santiago, J. G., 'A review of micropumps,' Journal of micromechanics and microengineering, 2004, **14**(6), p. R35.

Leal, L., 'Particle motions in a viscous fluid,' Annual Review of Fluid Mechanics, 1980, **12**(1), pp. 435–476.

Lee, C., Lee, J., Kim, H. H., Teh, S.-Y., Lee, A., Chung, I.-Y., Park, J. Y., and Shung, K. K., 'Microfluidic droplet sorting with a high frequency ultrasound beam,' Lab on a Chip, 2012, **12**(15), pp. 2736–2742.

Lee, S.-Y., Ferrari, M., and Decuzzi, P., 'Design of bio-mimetic particles with enhanced vascular interaction,' Journal of biomechanics, 2009a, **42**(12), pp. 1885–1890.

Lee, S.-Y., Ferrari, M., and Decuzzi, P., 'Shaping nano-/micro-particles for enhanced vascular interaction in laminar flows,' Nanotechnology, 2009b, **20**(49), p. 495101.

Leibacher, I., Reichert, P., and Dual, J., 'Microfluidic droplet handling by bulk acoustic wave (baw) acoustophoresis,' Lab on a Chip, 2015, **15**(13), pp. 2896–2905.

Li, H., Wu, Y., Wang, X., Zhu, C., Fu, T., and Ma, Y., 'Magnetofluidic control of the breakup of ferrofluid droplets in a microfluidic y-junction,' Rsc Advances, 2016, **6**(1), pp. 778–785.

Li, S., Ding, X., Guo, F., Chen, Y., Lapsley, M. I., Lin, S.-C. S., Wang, L., McCoy, J. P., Cameron, C. E., and Huang, T. J., 'An on-chip, multichannel droplet sorter using standing surface acoustic waves,' Analytical chemistry, 2013, **85**(11), pp. 5468–5474.

Link, D. R., Grasland-Mongrain, E., Duri, A., Sarrazin, F., Cheng, Z., Cristobal, G., Marquez, M., and Weitz, D. A., 'Electric control of droplets in microfluidic devices,' Angewandte Chemie International Edition, 2006, **45**(16), pp. 2556–2560.

Lombardi, D. and Dittrich, P. S., 'Droplet microfluidics with magnetic beads: a new tool to investigate drug–protein interactions,' Analytical and bioanalytical chemistry, 2011, **399**(1), pp. 347–352.

López-López, M. T., Kuzhir, P., and Bossis, G., 'Magnetorheology of fiber suspensions. i. experimental,' Journal of Rheology, 2009, **53**(1), pp. 115–126.

López-López, M. T., Vertelov, G., Bossis, G., Kuzhir, P., and Durán, J. D., 'New magnetorheological fluids based on magnetic fibers,' Journal of Materials Chemistry, 2007, **17**(36), pp. 3839–3844.

Lübbe, A. S., Alexiou, C., and Bergemann, C., 'Clinical applications of magnetic drug targeting,' Journal of Surgical Research, 2001, **95**(2), pp. 200–206.

Mandal, S., Bandopadhyay, A., and Chakraborty, S., 'The effect of uniform electric field on the cross-stream migration of a drop in plane poiseuille flow,' Journal of Fluid Mechanics, 2016, **809**, pp. 726–774.

Martinez, R., Roshchenko, A., Minev, P., and Finlay, W., 'Simulation of enhanced deposition due to magnetic field alignment of ellipsoidal particles in a lung bifurcation,' Journal of aerosol medicine and pulmonary drug delivery, 2013, **26**(1), pp. 31–40.

Matsunaga, D., Meng, F., Zöttl, A., Golestanian, R., and Yeomans, J. M., 'Focusing and sorting of ellipsoidal magnetic particles in microchannels,' Phys. Rev. Lett., 2017a, **119**, p. 198002, doi:10.1103/PhysRevLett.119.198002.

Matsunaga, D., Zöttl, A., Meng, F., Golestanian, R., and Yeomans, J. M., 'Far-field theory for trajectories of magnetic ellipsoids in rectangular and circular channels,' arXiv preprint arXiv:1711.00376, 2017b.

Melle, S. and Martin, J. E., 'Chain model of a magnetorheological suspension in a rotating field,' The Journal of chemical physics, 2003, **118**(21), pp. 9875–9881.

Mitragotri, S. and Lahann, J., 'Physical approaches to biomaterial design,' Nature materials, 2009, **8**(1), p. 15.

Morillas, J. R., Carreón-González, E., and De Vicente, J., 'Effect of particle aspect ratio in magnetorheology,' Smart Materials and Structures, 2015, **24**(12), p. 125005.

Mortazavi, S. and Tryggvason, G., 'A numerical study of the motion of drops in poiseuille flow. part 1. lateral migration of one drop,' Journal of Fluid Mechanics, 2000, **411**, pp. 325–350.

Mortensen, N. A., Okkels, F., and Bruus, H., 'Reexamination of hagen-poiseuille flow: Shape dependence of the hydraulic resistance in microchannels,' Physical Review E, 2005, **71**(5), p. 057301.

Nam, J., Lim, H., Kim, C., Yoon Kang, J., and Shin, S., 'Density-dependent separation of encapsulated cells in a microfluidic channel by using a standing surface acoustic wave,' Biomicrofluidics, 2012, **6**(2), p. 024120.

Neuberger, T., Schöpf, B., Hofmann, H., Hofmann, M., and Von Rechenberg, B., 'Super-paramagnetic nanoparticles for biomedical applications: possibilities and limitations of a new drug delivery system,' Journal of Magnetism and Magnetic materials, 2005, **293**(1), pp. 483–496.

Ngatu, G., Wereley, N., Karli, J., and Bell, R., 'Dimorphic magnetorheological fluids: exploiting partial substitution of microspheres by nanowires,' Smart Materials and Structures, 2008, **17**(4), p. 045022.

Nguyen, N.-T., Ng, K. M., and Huang, X., 'Manipulation of ferrofluid droplets using planar coils,' Applied Physics Letters, 2006, **89**(5), p. 052509.

Niu, X., Zhang, M., Peng, S., Wen, W., and Sheng, P., 'Real-time detection, control, and sorting of microfluidic droplets,' Biomicrofluidics, 2007, **1**(4), p. 044101.

Oh, K. W. and Ahn, C. H., 'A review of microvalves,' Journal of micromechanics and microengineering, 2006, **16**(5), p. R13.

Okagawa, A., Cox, R., and Mason, S., 'Particle behavior in shear and electric fields. VI. the microrheology of rigid spheroids,' Journal of Colloid and Interface Science, 1974, **47**(2), pp. 536–567.

Pamme, N., 'Magnetism and microfluidics,' Lab on a Chip, 2006, **6**(1), pp. 24–38.

Pamme, N., 'On-chip bioanalysis with magnetic particles,' Current opinion in chemical biology, 2012, **16**(3-4), pp. 436–443.

Pan, T.-W. and Glowinski, R., 'Direct simulation of the motion of neutrally buoyant circular cylinders in plane poiseuille flow,' Journal of Computational Physics, 2002, **181**(1), pp. 260–279.

Pan, T.-W., Huang, S.-L., Chen, S.-D., Chu, C.-C., and Chang, C.-C., 'A numerical study of the motion of a neutrally buoyant cylinder in two dimensional shear flow,' Computers & Fluids, 2013, **87**, pp. 57–66.

Pankhurst, Q. A., Connolly, J., Jones, S., and Dobson, J., 'Applications of magnetic nanoparticles in biomedicine,' Journal of physics D: Applied physics, 2003, **36**(13), p. R167.

Petersson, F., Nilsson, A., Holm, C., Jönsson, H., and Laurell, T., 'Continuous separation of lipid particles from erythrocytes by means of laminar flow and acoustic standing wave forces,' Lab on a Chip, 2005, **5**(1), pp. 20–22.

Petousis, I., Homburg, E., Derks, R., and Dietzel, A., 'Transient behaviour of magnetic micro-bead chains rotating in a fluid by external fields,' Lab on a Chip, 2007, **7**(12), pp. 1746–1751.

Rabinow, J., 'The magnetic fluid clutch,' Electrical Engineering, 1948, **67**(12), pp. 1167–1167.

Raich, H. and Blümler, P., 'Design and construction of a dipolar halbach array with a homogeneous field from identical bar magnets: Nmr mandhalas,' Concepts in Magnetic Resonance Part B: Magnetic Resonance Engineering: An Educational Journal, 2004, **23**(1), pp. 16–25.

Rao, L., Cai, B., Wang, J., Meng, Q., Ma, C., He, Z., Xu, J., Huang, Q., Li, S., Cen, Y., *et al.*, 'A microfluidic electrostatic separator based on pre-charged droplets,' Sensors and Actuators B: Chemical, 2015a, **210**, pp. 328–335.

Rao, L., Cai, B., Yu, X.-L., Guo, S.-S., Liu, W., and Zhao, X.-Z., 'One-step fabrication of 3d silver paste electrodes into microfluidic devices for enhanced droplet-based cell sorting,' AIP Advances, 2015b, **5**(5), p. 057134.

Saffman, P., 'On the motion of small spheroidal particles in a viscous liquid,' Journal of Fluid Mechanics, 1956, **1**(5), pp. 540–553.

Schmid, L., Weitz, D. A., and Franke, T., 'Sorting drops and cells with acoustics: acoustic microfluidic fluorescence-activated cell sorter,' Lab on a Chip, 2014, **14**(19), pp. 3710–3718.

Sciambi, A. and Abate, A. R., 'Generating electric fields in pdms microfluidic devices with salt water electrodes,' Lab on a Chip, 2014, **14**(15), pp. 2605–2609.

Sciambi, A. and Abate, A. R., 'Accurate microfluidic sorting of droplets at 30 khz,' Lab on a Chip, 2015, **15**(1), pp. 47–51.

Sedlacik, M., Pavlínek, V., Vyroubal, R., Peer, P., and Filip, P., 'A dimorphic magnetorheological fluid with improved oxidation and chemical stability under oscillatory shear,' Smart Materials and Structures, 2013, **22**(3), p. 035011.

Shang, L., Cheng, Y., and Zhao, Y., 'Emerging droplet microfluidics,' Chemical reviews, 2017, **117**(12), pp. 7964–8040.

Shembekar, N., Chaipan, C., Utharala, R., and Merten, C. A., 'Droplet-based microfluidics in drug discovery, transcriptomics and high-throughput molecular genetics,' Lab on a Chip, 2016, **16**(8), pp. 1314–1331.

Sheng, R., Flores, G., and Liu, J., 'In vitro investigation of a novel cancer therapeutic method using embolizing properties of magnetorheological fluids,' Journal of magnetism and magnetic materials, 1999, **194**(1-3), pp. 167–175.

Shine, A. and Armstrong, R., 'The rotation of a suspended axisymmetric ellipsoid in a magnetic field,' Rheologica Acta, 1987, **26**(2), pp. 152–161.

Sinha, A., Ganguly, R., De, A. K., and Puri, I. K., 'Single magnetic particle dynamics in a microchannel,' Physics of Fluids, 2007, **19**(11), p. 117102.

Smart, J. R. and Leighton Jr, D. T., 'Measurement of the hydrodynamic surface roughness of noncolloidal spheres,' Physics of Fluids A: Fluid Dynamics, 1989, **1**(1), pp. 52–60.

Smistrup, K., Hansen, O., Bruus, H., and Hansen, M. F., 'Magnetic separation in microfluidic systems using microfabricated electromagnets—experiments and simulations,' Journal of Magnetism and Magnetic Materials, 2005, **293**(1), pp. 597–604.

Sobecki, C. A., Zhang, J., Zhang, Y., and Wang, C., 'Dynamics of paramagnetic and ferromagnetic ellipsoidal particles in shear flow under a uniform magnetic field,' Physical Review Fluids, 2018, **3**(8), p. 084201.

Stratton, J. A., *Electromagnetic theory*, John Wiley & Sons, 2007.

Stuart, D. C., Kleijn, C., and Kenjereš, S., 'An efficient and robust method for lagrangian magnetic particle tracking in fluid flow simulations on unstructured grids,' Computers & Fluids, 2011, **40**(1), pp. 188–194.

Suh, Y. K. and Kang, S., 'Motion of paramagnetic particles in a viscous fluid under a uniform magnetic field: benchmark solutions,' Journal of Engineering Mathematics, 2011, **69**(1), pp. 25–58.

Sung, Y. J., Kim, J. Y. H., Choi, H. I., Kwak, H. S., and Sim, S. J., 'Magnetophoretic sorting of microdroplets with different microalgal cell densities for rapid isolation of fast growing strains,' Scientific Reports, 2017, **7**(1), p. 10390.

Surenjav, E., Priest, C., Herminghaus, S., and Seemann, R., 'Manipulation of gel emulsions by variable microchannel geometry,' Lab on a Chip, 2009, **9**(2), pp. 325–330.

Suwa, M. and Watarai, H., 'Magnetoanalysis of micro/nanoparticles: A review,' Analytica chimica acta, 2011, **690**(2), pp. 137–147.

Tan, Y.-C., Fisher, J. S., Lee, A. I., Cristini, V., and Lee, A. P., 'Design of microfluidic channel geometries for the control of droplet volume, chemical concentration, and sorting,' Lab on a Chip, 2004, **4**(4), pp. 292–298.

Tan, Y.-C., Ho, Y. L., and Lee, A. P., 'Microfluidic sorting of droplets by size,' Microfluidics and Nanofluidics, 2008, **4**(4), p. 343.

Tan, Y.-C. and Lee, A. P., 'Microfluidic separation of satellite droplets as the basis of a monodispersed micron and submicron emulsification system,' Lab on a Chip, 2005, **5**(10), pp. 1178–1183.

Taylor, G. I., 'The motion of ellipsoidal particles in a viscous fluid,' Proceedings of the Royal Society of London. Series A, Containing Papers of a Mathematical and Physical Character, 1923, **103**(720), pp. 58–61.

Taylor, G. I., 'The formation of emulsions in definable fields of flow,' Proc. R. Soc. Lond. A, 1934, **146**(858), pp. 501–523.

Teste, B., Jamond, N., Ferraro, D., Viovy, J.-L., and Malaquin, L., 'Selective handling of droplets in a microfluidic device using magnetic rails,' Microfluidics and Nanofluidics, 2015, **19**(1), pp. 141–153.

Torres-Díaz, I. and Rinaldi, C., 'Recent progress in ferrofluids research: novel applications of magnetically controllable and tunable fluids,' Soft matter, 2014, **10**(43), pp. 8584–8602.

Trevelyan, B. and Mason, S., 'Particle motions in sheared suspensions. i. rotations,' Journal of Colloid Science, 1951, **6**(4), pp. 354–367.

Valero, A., Braschler, T., Rauch, A., Demierre, N., Barral, Y., and Renaud, P., 'Tracking and synchronization of the yeast cell cycle using dielectrophoretic opacity,' Lab on a Chip, 2011, **11**(10), pp. 1754–1760.

Winkleman, A., Perez-Castillejos, R., Gudiksen, K. L., Phillips, S. T., Prentiss, M., and Whitesides, G. M., 'Density-based diamagnetic separation: devices for detecting binding events and for collecting unlabeled diamagnetic particles in paramagnetic solutions,' Analytical chemistry, 2007, **79**(17), pp. 6542–6550.

Xi, H.-D., Zheng, H., Guo, W., Gañán-Calvo, A. M., Ai, Y., Tsao, C.-W., Zhou, J., Li, W., Huang, Y., Nguyen, N.-T., *et al.*, 'Active droplet sorting in microfluidics: a review,' Lab on a Chip, 2017, **17**(5), pp. 751–771.

Yamaguchi, M., Tanimoto, Y., and Yamaguchi, M., *Magneto-science: magnetic field effects on materials: fundamentals and applications*, volume 48, Springer, 2006.

Yang, B. H., Wang, J., Joseph, D. D., Hu, H. H., Pan, T.-W., and Glowinski, R., 'Migration of a sphere in tube flow,' Journal of Fluid Mechanics, 2005, **540**, pp. 109–131.

Yavuz, C. T., Prakash, A., Mayo, J., and Colvin, V. L., 'Magnetic separations: from steel plants to biotechnology,' Chemical Engineering Science, 2009, **64**(10), pp. 2510–2521.

Young, K. D., 'The selective value of bacterial shape,' Microbiol. Mol. Biol. Rev., 2006, **70**(3), pp. 660–703.

Zborowski, M., Sun, L., Moore, L. R., Williams, P. S., and Chalmers, J. J., 'Continuous cell separation using novel magnetic quadrupole flow sorter,' Journal of Magnetism and Magnetic Materials, 1999, **194**(1-3), pp. 224–230.

Zhang, J., Sobecki, C. A., Zhang, Y., and Wang, C., 'Numerical investigation of dynamics of elliptical magnetic microparticles in shear flows,' Microfluidics and Nanofluidics, 2018, **22**(8), p. 83.

Zhang, J. and Wang, C., 'Study of rotation of ellipsoidal particles in combined simple shear flow and magnetic fields,' COMSOL Conference 2017 Boston, 2017.

Zhang, J. and Wang, C., 'Numerical study of lateral migration of elliptical magnetic microparticles in microchannels in uniform magnetic fields,' Magnetochemistry, 2018a, **4**(1), p. 16.

Zhang, J. and Wang, C., 'Numerical study of lateral migration of elliptical magnetic microparticles in microchannels in uniform magnetic fields,' Magnetochemistry, 2018b, **4**(1), p. 16.

Zhang, K., Liang, Q., Ai, X., Hu, P., Wang, Y., and Luo, G., 'On-demand microfluidic droplet manipulation using hydrophobic ferrofluid as a continuous-phase,' Lab on a Chip, 2011, **11**(7), pp. 1271–1275.

Zhang, K., Liang, Q., Ma, S., Mu, X., Hu, P., Wang, Y., and Luo, G., 'On-chip manipulation of continuous picoliter-volume superparamagnetic droplets using a magnetic force,' Lab on a Chip, 2009, **9**(20), pp. 2992–2999.

Zhang, Z., Zhou, R., P Brames, D., and Wang, C., 'A low-cost fabrication system for manufacturing soft-lithography microfluidic master molds,' Micro and Nanosystems, 2015, **7**(1), pp. 4–12.

Zhou, R., Bai, F., and Wang, C., 'Magnetic separation of microparticles by shape,' Lab on a Chip, 2017a, **17**(3), pp. 401–406.

Zhou, R., Sobecki, C. A., Zhang, J., Zhang, Y., and Wang, C., 'Magnetic control of lateral migration of ellipsoidal microparticles in microscale flows,' Physical Review Applied, 2017b, **8**(2), p. 024019.

Zhou, Y., Song, L., Yu, L., and Xuan, X., 'Continuous-flow sheathless diamagnetic particle separation in ferrofluids,' Journal of Magnetism and Magnetic Materials, 2016, **412**, pp. 114–122.

Zhou, Y. and Xuan, X., 'Diamagnetic particle separation by shape in ferrofluids,' Applied Physics Letters, 2016, **109**(10), p. 102405.

VITA

Jie Zhang was born in Lu'an, Anhui, China. He received his Bachelor of Science degree in Thermal Energy and Power Engineering in June 2013 from University of Shanghai for Science and Technology, Shanghai, China. In June 2016, he received his Master of Science degree in Power Machinery and Engineering from University of Shanghai for Science and Technology, Shanghai, China. In August 2020, he received his Doctor of Philosophy degree in Mechanical Engineering from Missouri University of Science and Technology, Rolla, Missouri, USA. His research interests included fluid mechanics, computational fluid dynamics, finite element method, microfluidics, particle suspensions, and droplet dynamics at the microscale scale. During this Ph.D period, Jie worked as a graduate assistant and took charge of the course of Senior Engineering Design and Fluid Mechanics Lab. He authored and co-authored 11 journal papers and 8 conference abstracts/papers/presentations.